NASA Contractor Report 191572

# Shock Tunnel Studies of Scramjet Phenomena

*Supplement 7*

R. J. Bakos, R. G. Morgan, S. L. Tuttle, G. M. Kelly,
A. Paull, J. M. Simmons, R. J. Stalker, M. V. Pulsonetti,
D. Buttsworth, G. A. Allen, Jr., N. Ward, K. Skinner,
A. J. Neely, and R. M. Krek

*University of Queensland*
*St. Lucia, Queensland*
*Australia*

Grant NAGW-674
December 1993



National Aeronautics and
Space Administration

**Langley Research Center**
Hampton, Virginia 23681-0001

# REPORT ON SHOCK TUNNEL STUDIES OF SCRAMJET PHENOMENA

## NASA GRANT NAGW-674-Supplement 7, 1991

This report follows the arrangement of previous ones, with a series of reports on specific project areas, and a brief general introduction commenting on each report in the order in which they are presented.

The commentary begins with a brief statement of the program of work planned for 1991.

## PLANNED PROGRAM FOR 1991

During 1991, work proceeded under two programs, A and B.

- **Program A** involved comparison of duct static pressure distribution in T4 and Hypulse, wall orifice injection with hot hydrogen, direct measurement of thrust on a nozzle using a thrust balance, and skin friction measurements on a flat plate and in a combustion duct.

  A series of measurements for the T4-Hypulse comparison was taken, wall orifice injection with hot hydrogen was initiated (and was described in the report for 1990), the direct measurement of thrust was studied numerically, in order to resolve problems arising from flexural waves, and skin friction measurements on a flat plate were advanced.

- **Program B** involved continuation of combustion scaling studies, measurements of specific impulse increment with hypersonic combustion, continuation of development of laser induced fluorescence and mass spectrometric methods of measuring species concentration, and the study of wave effects in two dimensional ducts.

  The combustion scaling studies in a large duct revealed the existence of combustion at unexpectedly low pressures, the measurements of specific impulse were delayed by experiments to improve the quality of duct pressure measurements in the shock tunnel, and the development of species concentration measurements continued, together with the study of wave effects.

  Studies of shock induced combustion were initiated. Facility studies included further work on expansion tube operation, and a flight to wind tunnel comparison using a model of the space shuttle orbiter.

## PROJECT REPORTS

Scramjet Testing - Ground Facility Comparisons R.G. Morgan, R.J. Stalker, R.J. Bakos, J. Tamagno and J.I. Erdos

This is a continuation of work done in 1990 on the effect of free stream atomic oxygen on combustion simulation in impulse facilities, and addresses the

problem of matching combustion pressure rise in T4 and Hypulse by oxygen depletion of the T4 free stream. The experiments indicate that this is a viable approach to combustion simulation, although considerable attention must be given to the effect of oxygen depletion on other flow variables.

Comparison Studies of Scramjet Combustion in Hypulse and T4 R.J. Bakos and R.G. Morgan

Analysis indicates that, at a given Mach number and temperature, the effect on the combustion pressure rise of enhanced heat release due to the presence of atomic oxygen in the free stream tends to be balanced by the higher sensible enthalpy associated with free stream dissociation. For combustion at high Mach number, the ratio of combustion heat release to sensible enthalpy determines the combustion pressure rise.

Experiments in T4 have tentatively indicated that, with attention to the requirements of the theory, nearly identical combustion pressure distributions can be obtained in T4 and Hypulse, although some further measurements are desirable in order to clarify the Hypulse test conditions.

Numerical Simulation of a Scramjet Thrust Balance S.L. Tuttle

Early experiments indicated that the measurement of axial force on an asymmetric model, such as a typical thrust nozzle, was more difficult than with an axially symmetric model. The difficulty was associated with the large flexural stress waves attendant on model asymmetry. Numerical studies of this effect were conducted, and indicated that it could be overcome by using a twisted sting configuration.

Skin-Friction Gauge for Use in Hypervelocity Impulse Facilities G.M. Kelly, J.M. Simmons, A. Paull – See: AIAA Journal, V30, No.3, March 92 pp 844-845

Skin friction measurements have been made in a laminar boundary layer on a flat plate in the small free piston shock tunnel TQ. The gauge rise time was approximately 20 $\mu$ sec, and results agreed satisfactorily with laminar boundary layer predictions. In later tests, an improved gauge was constructed, and the time history of skin friction was compared with that of heat transfer at the same station. As shown in Figure A following the report, similar records for the two measurements were obtained, providing further confirmation that skin friction was indeed being measured.

Pressure Scaling in a Scramjet Engine M.V. Pulsonetti

As a first step in this study, experiments were conducted on combustion in a 48mm x 100 mm constant area duct 1.3 m long. Paying particular attention to ignition phenomena, it was observed that ignition delay generally decreased with increase in static temperature. However, probably the most interesting observation was that vigorous combustion occurred in the duct at initial pressures as low as 0.07 atm.

Shock Wave Impingement on Mixing Regions D. Buttsworth

The possibility that shock induced combustion may offer a means of improving the performance of scramjets at the high end of the speed range has generated interest in the interaction between a combustible wake and an oblique shock wave. These experiments represent a first investigation of the interaction between an oblique shock wave and a mixing wake.

Progress with Analysis of Thrust Generation G.A. Allen Jr.

A numerical model of thrust generation by expansion wave - combustion wake interaction, which was developed in earlier work, requires knowledge of combustion wake Mach number profiles. Experiments have been performed to determine these profiles.

A Study of Shock Induced Heat Release N. Ward

This is a continuation of studies in which the recombination of dissociated $N_2$ is used to simulate interactions between wave phenomena and heat release in a two dimensional scramjet configuration.

Mass Spectrometry in Shock Tunnels K.A. Skinner

This report recounts early failures with attempts to operate a time of flight mass spectrometer in the test section of shock tunnel T4, and the measures taken to ensure future success.

The Effect on an Acoustic Wave as it traverses an Unsteady Expansion A. Paull and R.J. Stalker - See Physics Fluid A v3, No4, April 1991 pp 717-719

The test section disturbances which occur in an expansion tube have been observed to exhibit a dominant frequency when large expansion ratios across the unsteady expansion take place. It is shown that if these disturbances are lateral acoustic waves, then this "focussing" of disturbances to a single frequency would indeed occur. Furthermore, the frequencies observed in experiments correspond to the expected values, indicating that lateral acoustic waves are a major source of expansion tube test flow disturbances.

Comparative Features of Free Piston Shock Tunnel and Expansion Tube Facilities R.J. Stalker, A. Paull and A.J. Neely

This paper was presented at the 10th NASP Technology Symposium. It notes that there are three impulse facilities which may be operated with a free piston driver namely, the reflected shock tunnel, the non-reflected shock tunnel and the expansion tube. The paper outlines the particular advantages of each type of operation, paying particular attention to the limitations placed on the expansion tube by the need to avoid lateral acoustic waves in the test flow.

Experiments on Space Shuttle Orbiter Models in a Free Piston Shock Tunnel
R.M. Krek and R.J. Stalker

One of the tests of the worth of a ground facility is its ability to simulate flight flow fields. Since a substantial body of flight data exists for the Shuttle Orbiter, it was worthwhile testing orbiter models in T4 in order to compare tunnel data with flight data. It was found that, although high enthalpy effects could be important, Reynolds' number effects played a dominant role in determining the flow in both the laminar and turbulent regimes. Transition occurred in T4 at a lower Reynolds' number than in flight, although the difference between flight and tunnel transition 'Reynolds' numbers was not as great as in other shock tunnel or blowdown facilities.

Paper No. ISABE 91-194(L)

X ISABE

Nottingham, UK September 1991

# SCRAMJET TESTING - GROUND FACILITY COMPARISONS

R.G. Morgan and R.J. Stalker
University of Queensland
St. Lucia, Queensland, Australia

R.J. Bakos, J. Tamagno and J.I. Erdos
General Applied Science Laboratories, Inc. (GASL)
77 Raynor Avenue
Ronkonkoma, New York, USA

# SCRAMJET TESTING - GROUND FACILITY COMPARISONS

R. G. Morgan*, R. J. Bakos**, J. Tamagno**, R.J. Stalker*, J. I. Erdos**

## Abstract

The results of a preliminary series of tests to compare the effect of test gas composition on hypersonic combustion are presented. Parallel experiments were performed in the HYPULSE shock expansion tunnel and in the T4 reflected shock tunnel using identical axisymmetric models with wall injection. Test conditions were established at the same stagnation enthalpy and static pressure, with the reflected shock tunnel having approximately 50% by mass of the oxygen in a dissociated form either as atomic oxygen or as NO radicals. The expansion tunnel test gas contained less than 3% of non-molecular oxygen, and therefore closely represented the composition which might be found in flight. The static pressure rise upon combustion was found to be significantly greater when dissociated oxygen was present, and this is attributed principally to the heat of formation of the oxygen adding to the combustion heat release of the fuel at these test conditions. By reducing the total oxygen content of the reflected shock tunnel test gas it was possible to approximately compensate for this effect. The criteria for calculating the appropriate oxygen depletion are discussed, and the results are interpreted in the light of premixed one-dimensional computations.

## NOTATION

| | |
|---|---|
| $\alpha$ | mass fraction of total oxygen in the form of O atoms |
| $\alpha_n$ | mass fraction of total oxygen in the form of NO molecules |
| $\phi$ | fuel/oxygen equivalence ratio |
| $\phi_a$ | equivalence ratio referenced to ideal air oxygen content |
| $\phi^*$ | $=\phi$ for $\phi_a X_a/X < 1$, $=1$ for $\phi_a X_a/X > 1$ |
| d | combustor internal diameter |
| $h_c$ | heat of combustion of $H_2$ from $O_2$ (90 MJ/kg $H_2$) |
| $h_f$ | heat of formation of O atoms from $O_2$ (15.7 MJ/kg) |
| $h_n$ | heat of formation of NO molecules from $N_2 + O_2$ (2.93 MJ/kg) |
| $h_m$ | heat release per mole of combustion products |
| $O_2$ | mass fraction $O_2$ |
| $N_2$ | mass fraction $N_2$ |
| NO | mass fraction NO |
| Ar | mass fraction Argon |
| x | combustor model axial location |
| X | mass fraction of total O content |
| $X_a$ | mass fraction of total O content in "ideal" air |
| P | static pressure |
| u | velocity |
| $\rho$ | density |
| T | static temperature |
| M | Mach number |
| $H_s$ | stagnation enthalpy |
| $T_s$ | stagnation Temperature |

Subscripts:

| | |
|---|---|
| C | data from a hydrogen combustion test |
| M | data from a hydrogen into nitrogen mixing test |
| Tare | data from a fuel-off test |
| In | property at facility exit or combustor inlet condition |

## Introduction

Test facilities for the upper envelope of scramjet flight are currently restricted to reflected shock tunnels and shock expansion tunnels, (References 1 and 2). Both devices have limitations in their simulation capabilities. The reflected shock tunnel, by creating a stagnant high energy reservoir, has test gas with significant residual dissociated species content. The shock expansion tunnel avoids this problem by never stagnating the test gas, but the unsteady wave processes used to generate high energy flow restrict the useful test time, which in turn limits the length scale of models which may be used. The two test facility concepts complement each other and, if the differences between them can be satisfactorily explained in a quantitative way, then they form a powerful base for scramjet testing and evaluation.

Both facility types have been successfully used for scramjet combustor testing. Figures 1 and 2 show sample axial pressure profiles for constant area ducts with hydrogen injection for the T4 free-piston reflected shock tunnel, from Reference 1, and the HYPULSE shock expansion tunnel, from Reference 2.

The results are encouraging in that steady hypersonic flows with mixing and combustion have been demonstrated in pulsed facilities. However, the model geometries and injector configurations were sufficiently different in each case that a direct comparison of the two facilities is not possible. The data from Figure 1 was obtained using a rectangular section duct with a parallel central injector. The model used for the Figure 2 data was an axisymmetric duct with wall injection from around the whole circumference. For the comparisons reported here, an identical axisymmetric model to that tested previously in the expansion tunnel, was tested in a reflected shock tunnel at nearly identical conditions of stagnation enthalpy, static

* Department of Mechanical Engineering, University of Queensland, Brisbane AUSTRALIA

** General Applied Science Laboratories, Inc., Ronkonkoma, NY USA

pressure and temperature.

The test flow in a reflected shock tunnel is created by means of a steady expansion from the stagnation region occurring behind the reflected shock at the end of the shock tube. The gas in the stagnation region is approximately in a condition of equilibrium composition due to the high density levels and low particle velocity. At the stagnation enthalpies corresponding to flight speeds, the stagnation temperatures are such that significant dissociation occurs to the oxygen and nitrogen molecules. As the flow travels down the expansion nozzle, the temperature drops and the composition shifts toward a reduced dissociation content. However, due to the high particle velocities and low density in the nozzle, reaction rates may in some circumstances be insufficient to maintain equilibrium composition. The test gas at the nozzle exit will therefore have a residual content of the dissociated radicals created in the stagnation region. The higher the stagnation enthalpy, the higher will be the concentration of dissociated gas.

Processing of the test gas in an expansion tunnel is different in several important aspects. The test gas is shock heated in the shock tube portion of the facility where only a fraction of the final flow stagnation enthalpy is added. After shock passage the test flow is expanded in a constant area acceleration tube by means of an unsteady expansion wave. This expansion accelerates the flow from a low supersonic Mach number to hypersonic velocity while increasing the stagnation enthalpy. Because the test gas is never stagnated while at large stagnation enthalpies, it does not experience the high temperatures necessary for dissociation, and is thus delivered with a composition close to equilibrium.

The presence of non-equilibrium levels of dissociated species may affect the flow in several ways. Perhaps most important is that some of the stagnation enthalpy will be stored as atomic heat of formation, and will not be converted directly to thermal or kinetic energy. It is necessary, when comparing the results of reflected shock tunnel tests with real flight, or with other tunnels which do not produce dissociated air, to match the stagnation enthalpy including thermal, chemical and kinetic energy components.

For combustion testing, the presence of free-stream oxygen atoms may have other significant effects, which must be examined closely. There are three main mechanisms by which the free oxygen atoms may be seen to enhance combustion, and influence comparisons made between reflected shock tunnel experiments and real flight.

(i) Combustion heat release When combustion is from atomic oxygen form, the atomic oxygen heat of formation is added to the combustion heat release. This increases the net heat release from approximately 90 MJ to 215 MJ per kg of hydrogen burned. This is clearly a substantial increase and relatively small oxygen dissociation fractions may be significant.

(ii) Ignition delay times Forming of oxygen radicals is a necessary step in the combustion of hydrogen, and the pre-dissociated shock tunnel flow may be expected to react faster than ordinary air.

(iii) Mixing Effects In some circumstances a scramjet may be considered to be a pure diffusion flame, where reaction rates are so fast that heat release is mixing controlled. Oxygen molecules have different diffusion rates than atoms, and the local chemical composition will affect the rate of heat release. Furthermore, the macroscopic development of the fuel-air mixing layer is dependent on the local flow properties such as Reynolds number, and this may also be influenced by the dissociated oxygen content.

In summary, for a given static pressure, dissociated oxygen increases the partial pressure of the oxygen components, effectively enhancing mixing and combustion.

This paper reports on preliminary experiments and associated analytical work aimed at using the differences between the two facilities to resolve facility-induced effects, developing methods to quantify and compensate for them, so that the results may be related to flight conditions. Only the first mechanism will be addressed, that of predicting, and compensating for, the enhanced heat release due to the chemical enthalpy of the dissociated oxygen. Adjustment of the reflected shock tunnel oxygen content is examined as a way to match the net heat release of combustion, when compared to tests in undissociated air. In this way it is possible to produce pressure profiles which are approximately decoupled from the effects of differing levels of free stream dissociation and allow a direct comparison between reflected shock tunnel experiments and tests using undissociated air.

## Analytical Approach

Analysis of the reflected shock tunnel nozzle flow using a one-dimensional, non-equilibrium, chemical kinetics code (Reference 3) indicates that there are two significant dissociation products present (as far as hydrogen combustion is concerned), namely NO and O, in the range of stagnation enthalpies from about 12 to 20 MJ/kg. Similar analysis of the unsteady expansion system in the shock expansion tunnel reveal substantially lower concentration of these species at comparable enthalpies.

The effects of dissociation on hydrogen combustion heat release are quantified in the following manner: Combustion to water from the 3 oxygen-bearing constituents of the test gas proceeds with heat release as indicated below:

$$H_2 + 1/2\ O_2 = H_2O + 120.6\ MJ/kg\ H_2 \quad (1)$$
$$H_2 + O = H_2O + 246\ MJ/kg\ H_2 \quad (2)$$
$$H_2 + NO = H_2O + 1/2\ N_2 + 164.6\ MJ/kg\ H_2 \quad (3)$$

(NOTE: These equations are not intended to represent reaction schemes, but are used to calculate differences in heat release for varying reactant compositions.)

Combustion of undissociated air involves only reaction from oxygen molecules, and may be seen to give significantly less heat release than the two other main combustion paths. An approach to matching heat release is to apply a correction to the free stream oxygen concentration as was done in Reference 4. In other words, the reflected shock tunnel tests could be performed with a reduced oxygen concentration intended to reproduce the results of combustion in an expansion tunnel or atmospheric air with the same fluid dynamic properties.

The primary measured experimental parameter in scramjet testing is duct static pressure distribution. Corrections made to oxygen levels should be calculated to produce identical pressure/distance profiles in the two facilities. To match these exactly, a numerical simulation is required which fully evaluates the changes in combustion species composition produced by changing the free stream oxygen level. However, a first-order correction based on the three reaction mechanism identified above has been made and numerical simulations and experimental data used to assess the validity of the approach.

In Reference 4, a chemical equation was constructed from the three reaction mechanism as a function of test gas composition and fuel/oxygen equivalence ratio. This was used to calculate the appropriate oxygen depletion level by conserving heat release per unit mole of combustion products. To first order, this should lead to the same pressure rise, and should create the same wave pattern and flowfield in the two cases. This is considered to be of fundamental importance for scramjet ducts, which can only be analyzed correctly in light of a full wave capturing treatment, Reference 5.

The heat release per unit mole of combustion products is given by

$$h_m = \frac{\varphi^* h_c \left(1 + 8\alpha \frac{h_f}{h_c} + 15\alpha_n \frac{h_n}{h_c}\right)}{\frac{1}{4}\left(2\phi_a \frac{X_a}{X} - \phi^* + \alpha(1-\phi^*) - \frac{4}{28}\right) + \frac{8}{28X}} \quad (4)$$

From this the modified oxygen mass fraction for the reflected shock tunnel test gas is computed (by equating heat release from (4) to that for the undissociated case) to be:

$$X = \frac{\frac{8}{7} + 2X_a\phi_a}{B\left(A + \frac{32}{28X_a}\right) - A - \alpha(1-\phi^*) + 2\phi_a} \quad (5)$$

Where

$$A = 2\phi - \phi^* - \frac{4}{28}$$

$$B = 1 + 8\alpha\frac{h_f}{h_c} + 15\alpha_n\frac{h_n}{h_c}$$

The two terms involving $\phi_a$ have been added to the original equation for X (as found in Reference 4) to account for matching of fuel mass flow rates in the comparison experiments as opposed to matching of actual fuel/oxygen equivalence ratio which was assumed in the original derivation. Conserving fuel mass flow rate is important for hypersonic combustion comparisons due to its significant influence on mixing. The effect of these terms will be discussed below.

It should be clear that the mass fraction X includes the total oxygen content in all its forms. It is sensitive to O and NO concentrations, which are functions of flow enthalpy, and also equivalence ratio. Note also that the heat release of 120.6 MJ/kg from equation (1), combustion from oxygen molecules, is based on combustion to water alone. The equilibrium composition of a hydrogen flame contains dissociated radicals, and the full heat release is not achieved. A heat release of 90 MJ/kg $H_2$ is more representative of that developed in a real combustion chamber and is chosen for $h_c$.

## Experimental Conditions and Apparatus

It is not possible to conserve all the flow parameters when choosing test conditions in the two facilities. For example, the molecular weights of the test gases are different, and therefore if flow velocity and temperature are matched then the Mach number will have to be different. The approach taken for comparison was to conserve static temperature and static pressure so as to match combustion conditions as closely as possible. Then matching stagnation enthalpy prescribes velocity, and it is not possible to then simultaneously match pitot pressure.

The test conditions chosen for these tests are given in Table 1 and are based on the nominal Mach 17 stagnation enthalpy (15.3 MJ/kg) operating point of the HYPULSE expansion tunnel. A contoured Mach 5 nozzle was used to obtain the quoted test conditions for the reflected shock tunnel. For the expansion tunnel operating at 15.3 MJ/kg, the test gas diffuser described in Reference 6 is necessary to compress the flow to the static pressures required to support hydrogen/air combustion.

As described previously, the operating principles of the facilities are quite different and therefore so are the time histories of the facility start-up and subsequent flow establishment in the model. For the reflected shock tunnel, a nozzle plenum pressure trace is shown in Figure 3. Operation of the tunnel to achieve 15.7 MJ/kg stagnation enthalpy is at a condition only slightly under tailored, and therefore the stagnation pressure is held approximately constant over a period of 1 msec. A corresponding static pressure history, as measured in the model, is shown in Figure 4, from which a corresponding steady pressure period of 0.75 msec. can be seen.

An expansion tunnel Mach number trace, as derived from pitot and static pressure data measured in a calibration test, is shown in Figure 5 for comparison. It is clear that the steady test period is significantly shorter than for the shock tunnel. To insure flow establishment in the model, heat transfer data are examined for relaxation to steady state.

Figure 6 shows a heat flux trace measured in the model for a fuel-off run. This time history is typical of a laminar heat flux trace, and shows relaxation well within the available steady flow period.

The tests were run with the axisymmetric combustor model shown in Figure 7. Its overall length to diameter ratio is 24, and fuel is injected via a single annular slot located 4.67 model diameters downstream of the inlet. Fuel is injected at Mach 1.9 and radially inward at an angle of 15° from the model axis. The injector throat area to model capture area is 0.062. This choice was made to permit the injected fuel to be pressure matched to the duct inlet pressure at stoichiometric fuel mass flow. Higher equivalence ratios are obtained by raising the fuel plenum pressure accordingly. The model was positioned for both facilities in a free jet configuration, capturing the central uniform core of the facility exit flows.

Model instrumentation includes 13 high frequency, high sensitivity pressure transducers. One was located upstream, and 12 downstream of the injector. An additional transducer was located at the end of the model for the shock tunnel tests. All were positioned at the same azimuthal angle. Thin-film resistance gages were used to measure wall heat transfer. These were located at the same axial locations but diametrically opposed to the pressure transducers. Frequency response for both types of instrumentation is 500 MHz.

## Comparison Test Results

As previously noted the reflected shock tunnel experiments were configured around results from HYPULSE tests at a condition equivalent to flight Mach number 17 (as reported in Reference 6). An equivalence ratio of 3 was targeted as it had been shown to give good mixing and combustion in the HYPULSE tests. The corresponding T4 condition, shown in Table 1A, is seen to have a large dissociated radical content.

Results of fuel-off tare runs in the two facilities are shown in Figure 8. Although nominal facility exit pressures were matched, it is clear that a higher average static pressure is achieved in the expansion tunnel tests. A complete explanation for this discrepancy is not available at this time; however, results of calibration tests for the HYPULSE test gas diffuser, as discussed in Reference 6, suggest that the diffuser is producing a weak conical shock system which is captured by the model. It is postulated that this wave system results in a lower average combustor entrance Mach number and a higher average static pressure than would be inferred from the last wall pressure measurement in the diffuser (at x/d=-1.0 in Figure 8). Unfortunately, because the diffuser exit pressure was taken as representative of the expansion tunnel average exit pressure (and chosen to be matched in the tests), the reflected shock tunnel tests resulted in the lower duct pressures.

Because duct pressure level is the primary diagnostic used to gauge combustion heat release, it is necessary to remove systematic variations in pressure level between the two experiments. The tare run pressure distributions were therefore averaged to obtain a scale factor to relate the results of other tests. The success of this method can be seen in Figure 9 which compares the scaled pressure distributions for hydrogen-into-nitrogen mixing runs in the two facilities. It may be seen that the pressure distributions agree quite well.

Figure 10 shows the scaled pressure/distance development for the two cases using air as the test gas. Enhanced combustion in the reflected shock tunnel is clearly evident.

An alternative method of displaying this result is shown in Figure 11. Here the difference between measured combustion run and mixing run pressures are normalized by the average tare pressures and plotted against distance along the duct. The plotted curves are logarithmic regressions of the form $a + b \log cx$, fit to the data from the injection station to the end of the duct in both cases. There is considerable scatter of the data about the fit curves which is primarily a result of the actual two-dimensional nature of the flowfields. However, the pressure level increase, due to combustion, is more easily quantified by this procedure.

In attempting to match the expansion tunnel results in the reflected shock tunnel, it was decided first to maintain the actual fuel/oxygen equivalence ratio at 3, and use the procedure outlined above (equation (5) without the modifying terms) to compute a required test gas oxygen content. This leads to a total oxygen content of 0.0675, by mass, for the reflected shock tunnel. The computed test gas composition for this case is shown in Table 1B.

In arriving at this oxygen content a new problem becomes apparent. The reduced oxygen partial pressure in the expansion nozzle leads to increased dissociation, and a further shift in the heat release balance, required by equation (5), toward even lower oxygen content. Furthermore, the requirement of conserving stagnation enthalpy requires stagnation temperature to increase. This is because when the total oxygen content is reduced, less stagnation enthalpy per unit mass of test gas mixture is available in the nitrogen molecules than in the dissociated oxygen atoms which they replace. This again leads to more dissociation. The test gas composition which satisfies the heat release requirement is found through a series of iterations.

The solution for test gas composition now determines what fuel injection conditions are required to achieve the equivalence ratio of 3. The models were designed with identical geometry for both tunnels so that required injector plenum pressures (and thus mass flows) scale approximately with the free stream oxygen mass fraction. This meant that the T4 tests were to be performed with approximately 1/3 the plenum pressure of the HYPULSE tests. This injection pressure corresponds to an equivalence ratio of 1 for the HYPULSE combustion tests, which showed little signs of combustion, mainly due to mixing limitations, Reference 7. Results of tests at this same injection pressure in T4, which are not shown, again confirmed the absence of combustion, even with the elevated dissociation levels.

Fuel/oxygen equivalence ratio had initially been

considered to be a primary parameter to be matched when comparing facilities. However, the mixing process is so sensitive to injection pressure, and it has such an influence on macroscopic flow properties in hypersonic ducted flow, Reference 7, that it is now evident that the injection parameters must be conserved in order to reproduce the same basic flow features in both facilities. This implies that a compromise must be made on equivalence ratio by conserving fuel mass flow rate.

A test with the test gas composition given in Table 1B was subsequently made with the fuel plenum pressure and resultant fuel flow rate matched to the HYPULSE runs at equivalence ratio of 3. The pressure difference results are shown in Figure 12 from which it is seen that combustion takes place, but the heat release is lower than for the HYPULSE condition shown previously in Figure 11. This is because the fuel/oxygen equivalence ratio is approximately 9 for this test and the excess unburnt fuel reduces the heat release per mole of combustion products.

Working from this result, the oxygen content was recomputed by equation (5), this time conserving fuel flow rate. This is accomplished by specifying the fuel-to-ideal-air equivalence ratio, $\phi_a$, to be constant at 3 and including the modified terms in (5). The resultant test gas composition is shown in Table 1C where an oxygen content of 0.128 was converged upon. Although no data were taken at this level of depletion, a linear interpolation in X of the T4 regressions has been plotted in Figure 12 to show the anticipated result. This curve is seen to be quite similar in level to the HYPULSE regression curve.

Analyses were performed using a one-dimensional, fully mixed, chemical kinetics code to predict rate limited and equilibrium pressure levels using the hydrogen/air reaction scheme given in Reference 8. The fuel and test gas were mixed in a chemically frozen, constant area process to define start-line conditions for the combustion calculation. The parameter plotted is computed combustion pressure minus the mixing pressure normalized by the nominal facility exit pressure. This parameter is sensitive to combustion heat release, and approximately equivalent to that plotted for the data. The equilibrium levels were computed by allowing the calculation to run for sufficient distance to allow axial gradients to vanish.

Figure 13 shows computed pressure parameter distributions for the T4 and HYPULSE air conditions as given in Tables 1A and 1D. More rapid ignition and enhanced combustion for the T4 air are seen. Comparing these distributions with the data in Figure 11, very similar pressure distributions are noted. In this regard, the analysis of Reference 7 indicated substantial mixing at $\phi_a = 3$ for this injector configuration. Also, by plotting differences between combustion and mixing run pressure distributions, effects due to wall shear, wall heat transfer, and finite rate mixing are approximately canceled. Therefore, the close agreement of experiment with the computations is not surprising, even considering the simplicity of the analysis. And thus, the predicted trend toward greater heat release with increased oxygen dissociation is regarded as confirmation of cause for a similar trend seen in the data.

Similar calculations were done for the oxygen depleted conditions (Table 1B, with $\phi_a$ = 3), and the modified conditions (Table 1C, with $\phi_a$ = 3). These results are shown in Figure 14. The extremely suppressed pressure rise, which was observed experimentally for case 1B, is well predicted. In comparing case 1C with the HYPULSE prediction, a more rapid ignition is seen for the reflected shock tunnel. However, the down stream behavior and equilibrium pressure levels agree fairly well. Considering the strong agreement already demonstrated, between the predictions and the data, it is clear that an experiment run with the modified oxygen content of X=0.128 should match the HYPULSE pressure data.

## Conclusions

A series of experiments have been conducted to compare the effects of oxygen dissociation on hypersonic combustion at conditions simulating flight Mach number 17. It has been demonstrated that the effect of differences in test gas composition on combustion heat release can, to a significant extent, be accounted for by adjusting the oxygen content of the test gas.

These parallel experiments were run in the HYPULSE shock expansion tunnel and the T4 reflected shock tunnel using identical scramjet models at nearly matched levels of stagnation enthalpy, static temperature and static pressure. Despite the nominally identical intake flow conditions, a substantial difference in the duct flow pressures was observed for the two facilities. However, appropriate normalization of the data enabled meaningful comparisons to be made between the two data sets.

Pressure rise due to combustion was found to be clearly greater for the reflected shock tunnel tests run with real air. This difference was shown to be consistent with chemical kinetics calculations which accounted for the dissociated oxygen resident in the test gas.

A first-order correction to the reflected shock tunnel oxygen content to account for enhanced heat release was described and implemented experimentally. It was found that such a correction must be done by conserving fuel flow rate, rather than fuel/oxygen equivalence ratio. This is primarily a result of the large influence that injectant stagnation pressure (hence, mass flow rate) has on the mixing process for ducted hypersonic flow. An initial experiment was run at matched fuel flow rate; however, the oxygen depletion had not been optimized for this fuel flow and the resulting pressure level fell below the expansion tunnel level. Chemical kinetic and equilibrium computations for this test gas, and for an appropriately optimized test gas, indicate that the correct depletion will yield the approximately correct pressure rise.

There remain several aspects of these comparisons which require further investigation. This initial set of experiments addressed only the issue of dissociated oxygen effects on heat release. The influence on ignition, although clearly evident in some of the calculations, was not considered nor were the effects on fuel/air mixing. These issues will require more detailed comparison tests and correlation with more complete CFD simulations.

Additional experiments and numerical simulations are planned for the continuation of this work.

Acknowledgements

The portion of this work conducted at General Applied Science Laboratories was sponsored by the National AeroSpace Plane Joint Program Office, Mr. Curtis D. Snyder was the Task Manager. The work done at the University of Queensland was funded by a grant from the NASA Langley Research Center, Hypersonic Propulsion Branch, Griffin Y. Anderson - Branch Head. Their support and encouragement are gratefully acknowledged.

## REFERENCES

1. Stalker, R.J., Morgan, R.G., Paull, A., and Brescianni, C.P., "Scramjet Experiments in Free Piston Shock Tunnels," Paper No. 28, 8th National AeroSpace Plane Technology Symposium, March 26-30, 1990.

2. Tamagno, J., Bakos, R.J., Pulsonetti, M.V., and Erdos, J.I., "Hypervelocity Real Gas Capabilities of GASL's Expansion Tube (HYPULSE) Facility," Paper 90-1390, AIAA 16th Aerodynamic Ground Testing Conference, Seattle, WA, June 1990.

3. Lordi, J.A., Mates, R.E., and Moselle, J.R., "Computer Program for the Numerical Solution of Nonequilibrium Expansions of Reacting Gas Mixtures," NASA CR-472, 1966.

4. Morgan, R.G., "Dissociated Test Gas, Effects on Scramjet Combustors," NASA CR-182096, October 1990.

5. Stalker, R.J., Morgan, R.G., and Netterfield, M.P., "Wave Processes in Scramjet Thrust Generation," Combustion and Flame, Vol. 71, pp 63-77, 1988.

6. Bakos, R.J., Tamagno, J., Rizkalla, O., Pulsonetti, M.V., Chinitz, W., and Erdos, J.I., "Hypersonic Mixing and Combustion Studies in the GASL HYPULSE Facility," Paper 90-2095, AIAA 26th Joint Propulsion Conference, Orlando, Fl., July 1990.

7. Morgan, R.G., Bakos, R.J., and Tamagno, J., "Bulk Parameter Analysis of Hypersonic Combustion Experiments," GASL TR-321, August 1990.

8. "Hypersonic Combustion Kinetics - Status Report of the Rate Constant Committee, NASP High-Speed Propulsion Technology Team," Oldenborg, R. - Chmn, NASP Technical Memorandum 1107, May 1990.

TABLE 1 NOMINAL TEST FLOW CONDITIONS

| | Table 1 A T4 real air | Table 1 B T4 6.75% Oxy | Table 1 C T4 12.8% Oxy | Table 1 D HYPULSE |
|---|---|---|---|---|
| $H_s$ (MJ/kg) | 15.70 | 15.70 | 15.70 | 15.30 |
| $T_s$ (K) | 7880 | 8350 | 8180 | 8355 |
| T (K) | 2065 | 2120 | 2037 | 2088 |
| $P/P_{HYPULSE}$ | 0.927 | 0.885 | 0.885 | 1.000 |
| u (m/s) | 4710 | 4910 | 4819 | 5078 |
| M | 5.17 | 5.31 | 5.30 | 5.75 |
| $N_2$ | .7320 | .9150 | .8470 | .7507 |
| $O_2$ | .1080 | .0063 | .0328 | .2253 |
| Ar | .0129 | .0131 | .0131 | .0129 |
| N | 2.20E-6 | 3.30E-6 | 2.20E-6 | 3.00E-9 |
| O | 9.70E-2 | 5.43E-2 | 7.90E-2 | 7.82E-4 |
| NO | .0508 | .0114 | .0281 | .0103 |
| X | .2320 | .0675 | .1280 | .2320 |
| $\alpha$ | .4180 | .8100 | .6200 | .0034 |
| $\alpha_n$ | .1168 | .0900 | .1200 | .0238 |

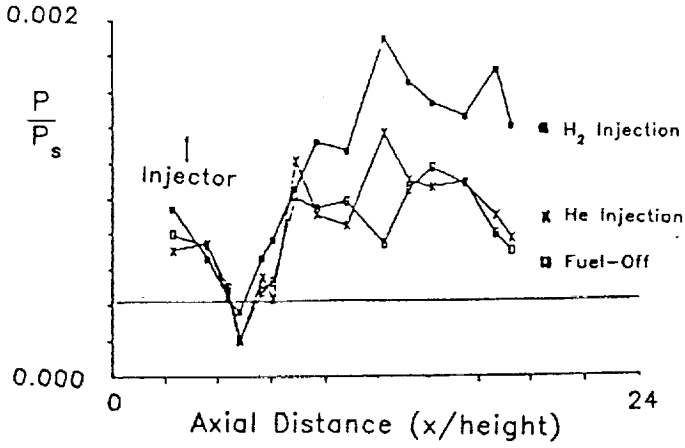


Figure 1. Rectangular scramjet combustor data, $H_s$ =8.39 MJ/kg - T4 Reflected Shock Tunnel Facility.

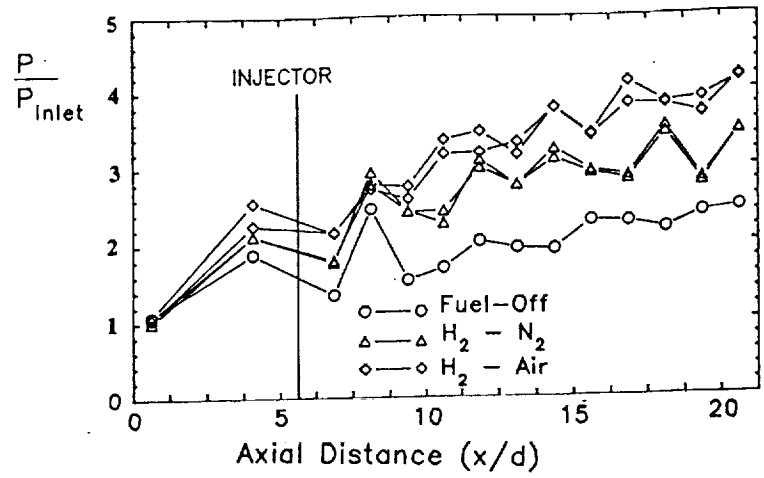


Figure 2. Axisymmetric scramjet combustor data, $H_s$ = 15.3 MJ/kg - HYPULSE Shock Expansion Tunnel. Facility.

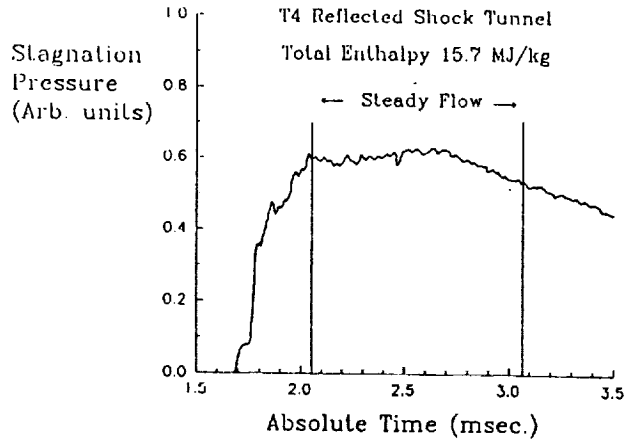


Figure 3. Reflected shock tunnel stagnation pressure trace, $H_s$ = 15.7 MJ/kg.

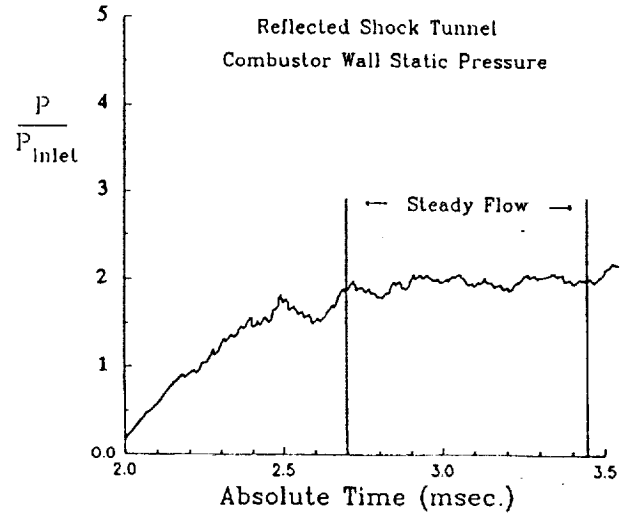


Figure 4. Reflected shock tunnel static pressure trace measured in the combustor model, $H_s$ = 15.7 MJ/kg.

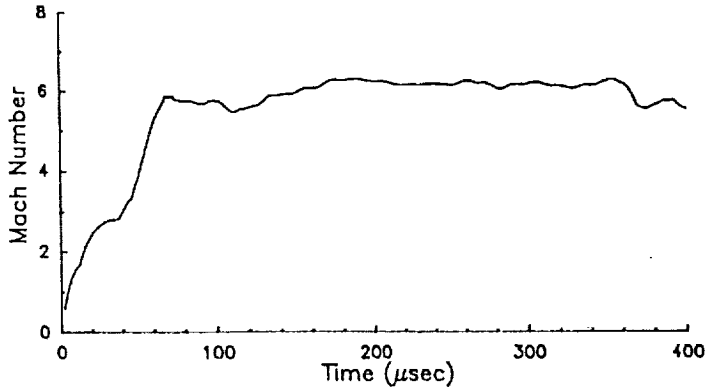


Figure 5. Expansion tunnel diffuser exit Mach number trace, $H_s$ = 15.3 MJ/kg.

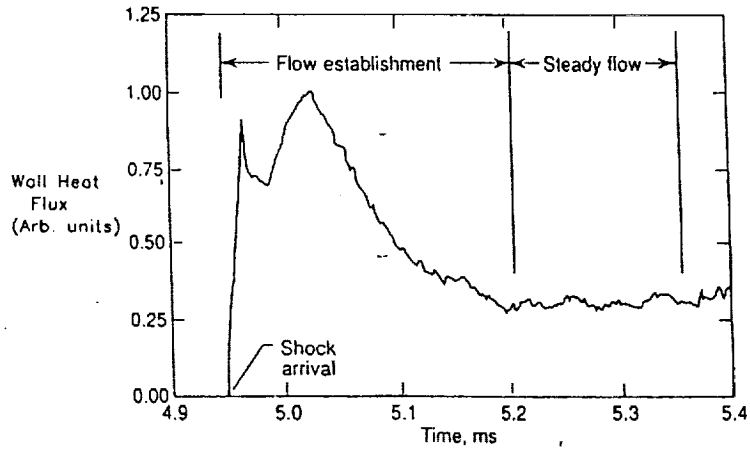


Figure 6. Expansion tunnel combustor wall heat flux trace showing flow establishment and steady flow periods, $H_s$ = 15.3 MJ/kg.

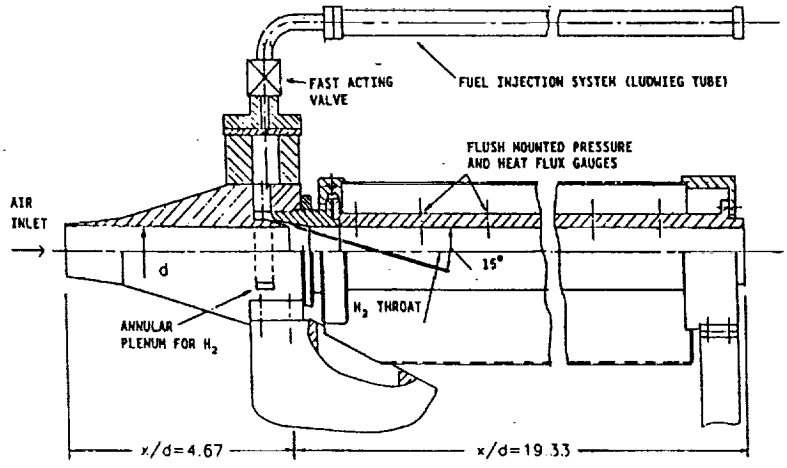


Figure 7. Schematic of axisymmetric combustor model.

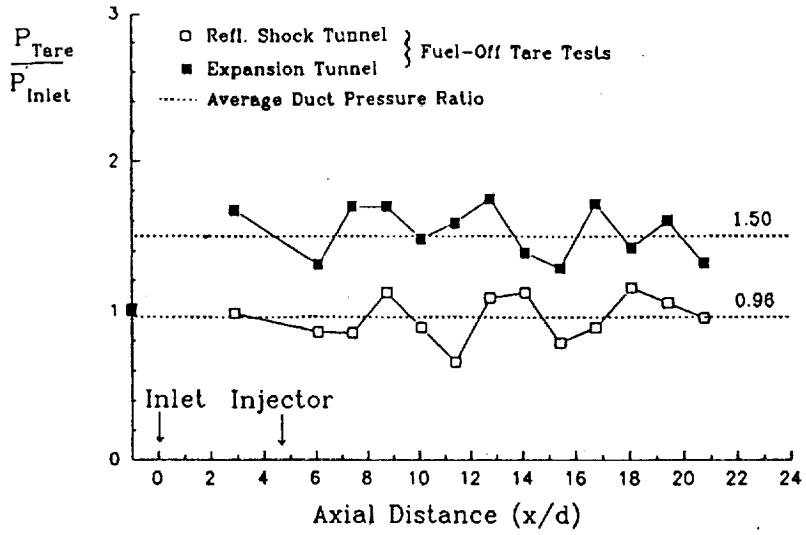


Figure 8. Measured static pressure distributions for fuel-off tare tests in both facilities.

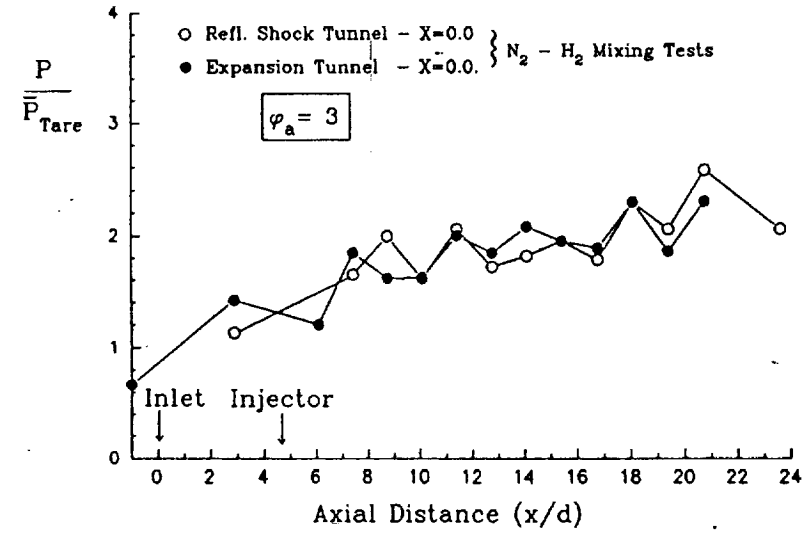


Figure 9. Measured mixing test static pressure distributions shown normalized by the average tare pressure for each facility.

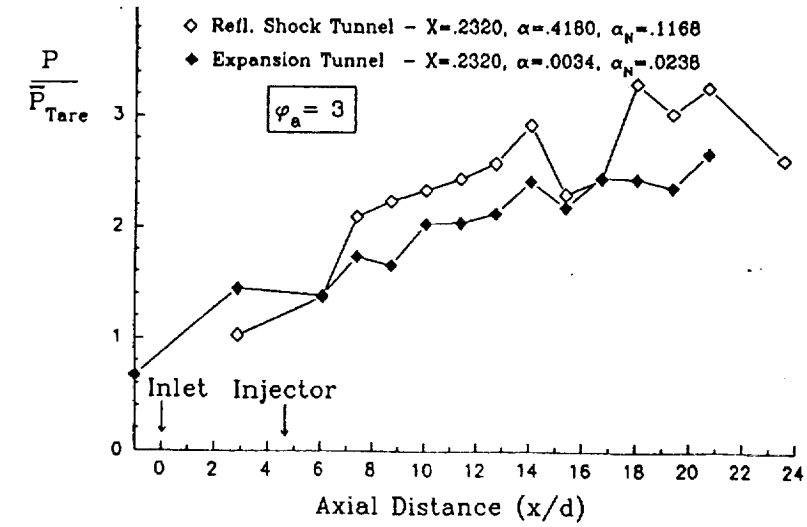


Figure 10. Measured real air combustion test static pressure distributions shown normalized by the average tare pressure for each facility.

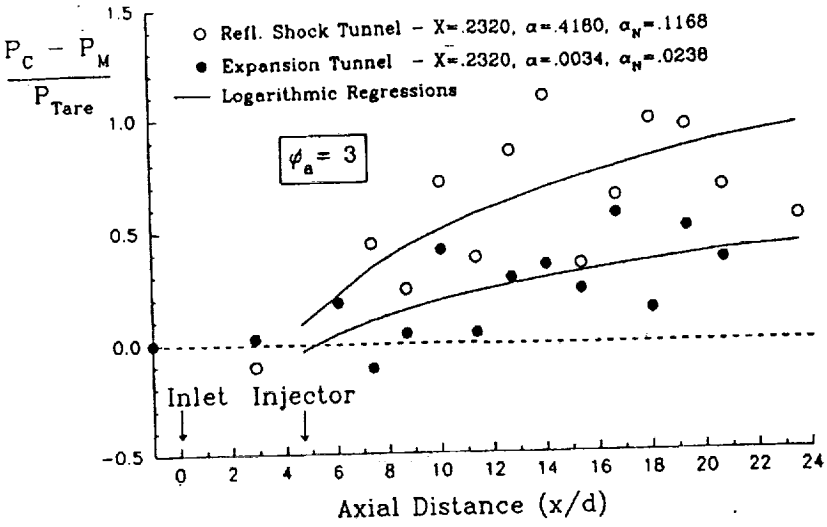


Figure 11. Difference in normalized combustion and mixing run pressures for real air as measured in both facilities.

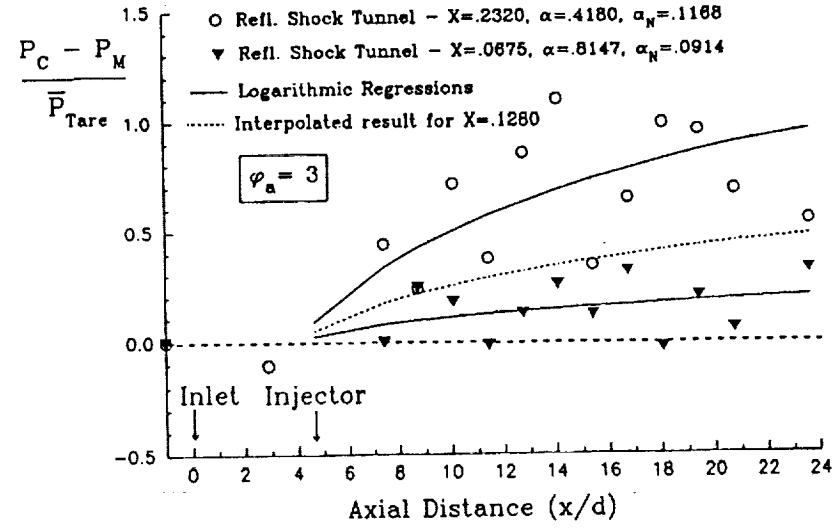


Figure 12. Difference in normalized combustion and mixing run pressures. Comparing reflected shock tunnel real air result with reflected shock tunnel depleted oxygen results.

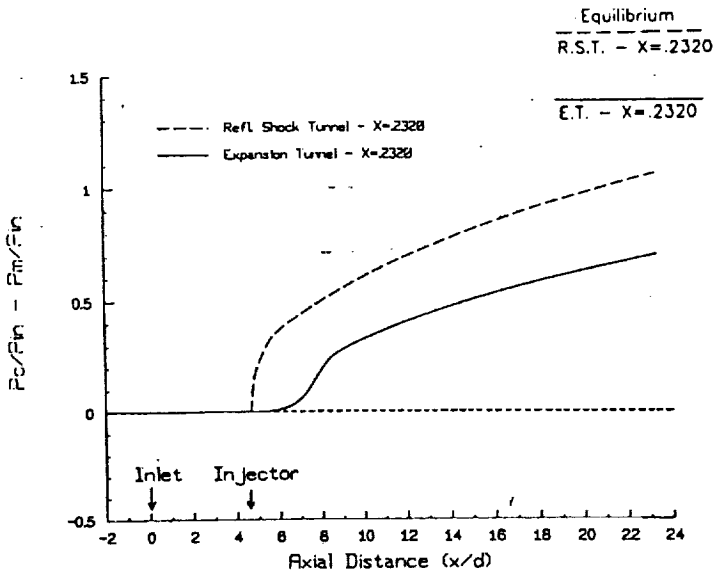


Figure 13. Computed chemical kinetic distributions and equilibrium levels of combustion pressure rise for real air in both facilities.

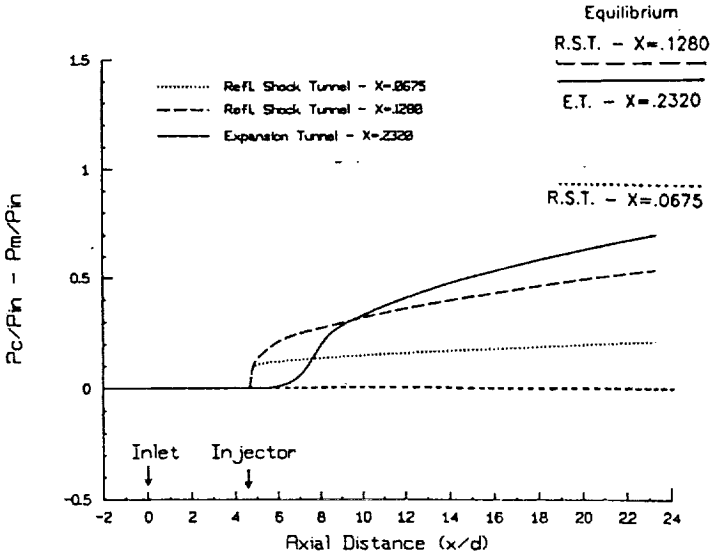


Figure 14. Computed chemical kinetic distributions and equilibrium levels of combustion pressure rise. Comparing reflected shock tunnel using depleted oxygen with expansion tunnel.

# Comparison Studies of Scramjet Combustion in HYPULSE and T4 - Progress Summary

March 1992

R.J. Bakos and R.G. Morgan

Summary (1991-92)

New scramjet combustion data have been obtained in the T4 reflected shock tunnel for comparison to existing HYPULSE expansion tunnel data using two different injector configurations in a cylindrical combustor model. Tests conditions have been established in T4 which targeted the Mach 13 and 17 conditions in HYPULSE attempting to match the test gas pressure, temperature, and Mach number. A rationale has been developed for this choice of matched flow parameters such that if enhanced heat release due to excess atomic oxygen content occurs in T4, it will be unambiguously detected by duct pressure rise. However, at the available HYPULSE test conditions, an inherent stability of the duct pressure to variations in test gas atomic oxygen content has been predicted with a two-stream equilibrium combustion analysis. This prediction has been confirmed experimentally at Mach 13 enthalpy where measured combustion pressure data from the two facilities is similar. The experimental results at Mach 17 are not yet conclusive due to persistent minor differences in test flow parameters. Specific progress is as follows.

## Test Program Methodology

Comparison of data obtained in T4 and HYPULSE at a given simulated flight condition is expected to show differences in measured performance, this being caused by the high atomic oxygen content in the T4 test gas enhancing combustion heat release (Reference 1). But, the presence of atomic oxygen alters the test gas molecular weight as well as its chemical energy content. So in addition to adding to the combustion heat release, atomic oxygen changes the oxidiser sound speed at a given temperature. Thus, for matched oxidiser Mach number and temperature a

different velocity is achieved in the two facilities and precise duplication of all flow parameters is therefore impossible.

For simulating chemically reacting flows behind strong shock waves, hypersonic Mach number independence has lead to adopting stagnation enthalpy as the primary simulation parameter to be matched when relating reflected shock tunnel data to ideal air. It is instructive to examine the implications of matching stagnation enthalpy for the present case of a flow where no strong shock waves occur.

There are three components of the stagnation enthalpy in a dissociated test gas,

$$H_{STAG}=h_c+h_s+\frac{u^2}{2}$$

which are defined as follows.

$h_c=\sum_i Y_i h^\circ_{f,i}$ chemical contribution

$h_s=\sum_i \int_0^T Y_i C_{p,i} dT$ sensible or thermal contribution

$\frac{u^2}{2}$ kinetic energy contribution

For a test gas composed of only elemental species, the chemical enthalpy is zero.

Consider two air flows, A and B, at equal stagnation enthalpy, static temperature, and static pressure. Flow A is in equilibrium at this condition which is such that no dissociation occurs. This is approximately the case for air temperatures near or below 2000 K where the fraction of oxygen in atomic form and in nitric oxide is below 5%. Flow B is far from equilibrium and contains significant fractions of atomic oxygen and nitric oxide and therefore its chemical enthalpy is non-zero and may be of the order

of the sensible enthalpy. Because B has positive chemical enthalpy, the sum of its sensible and kinetic contributions will be less than for A. However, because the dissociated gas will have lower molecular weight, there will also be more moles of B in a given mass and thus at the same temperature it will have greater sensible enthalpy per unit mass. This leaves B necessarily having a lower mass motion kinetic energy and thus a lower velocity than A. Thus at matched stagnation enthalpy the dissociated gas will have lower velocity and higher sensible enthalpy and hence a significantly lower Mach number than the non-dissociated gas. This comparison of stagnation enthalpy is shown schematically in Figures 1a and 1b. It will be convenient in what follows to make reference to the total sensible enthalpy, defined as $h_0 = h_s + u^2/2$. This is not to be confused with the stagnation enthalpy, the difference being clear from the foregoing discussion.

Beyond these fundamental limitations for test condition duplication, there are practical bounds to the degree of accuracy with which test conditions can be contrived in each facility so that they are matched. It is therefore of interest to know the sensitivities of measured quantities to variations in test conditions. To this end an analytical study was conducted to investigate which oxidiser flow parameters need to be matched such that the measured wall pressure distributions in a constant area duct would indicate atomic oxygen enhanced heat release, and not other coincidental fluid dynamic effects caused by test condition mismatch. It is assumed fuel conditions including injector geometry, pressure, and mass flow can be duplicated.

The combustion process in a constant area scramjet duct can be approximated by a one-dimensional flow with heat addition and composition change. A thermally and calorically perfect gas is assumed, and no change of $\gamma$ with reaction, although a change in specific heats is permitted between end states. These approximations are necessary to achieve analytical closure and the physical understanding given to the process justifies them. Their validity is evaluated later in a more complete numerical procedure.

From the conservation equations and the equation of state the duct pressure, enthalpy, and total enthalpy ratios are functions of the reactant, $M_r$, and product, $M_p$,

Mach numbers alone as given by the following,

$$\frac{p_p}{p_r} = \frac{(1+\gamma M_r^2)}{(1+\gamma M_p^2)} \tag{1}$$

$$\frac{h_{s,p}}{h_{s,r}} = \left(\frac{1+\gamma M_r^2}{1+\gamma M_p^2}\right)^2 \left(\frac{M_p^2}{M_r^2}\right) \tag{2}$$

$$\frac{h_{0,p}}{h_{0,r}} = \left(\frac{1+\gamma M_r^2}{1+\gamma M_p^2}\right)^2 \left(\frac{M_p^2}{M_r^2}\right) \left(\frac{1+\frac{\gamma-1}{2}M_p^2}{1+\frac{\gamma-1}{2}M_r^2}\right) \tag{3}$$

where,

$$h_0 = h_s\left(1+\frac{\gamma-1}{2}M^2\right)$$

has been used which is appropriate for a calorically perfect gas. The product Mach number is determined from (3) after evaluating the total sensible enthalpy ratio from the energy conservation equation,

$$\frac{h_{0,p}}{h_{0,r}} = \frac{\Delta h_{C,NET}}{h_{0,r}} + 1 \tag{4}$$

with $h_{C,NET}$ being the net heat release from combustion and equalling the difference in standard state heats of formation between the products and reactants. Denoting $D_2$ as the ratio of net heat release to total sensible enthalpy of the reactants (Damkohler's second number), equation (4) is rewritten as,

$$D_2 = \frac{h_{0,p}}{h_{0,r}} - 1 \tag{4a}$$

From this equation with (3), it is seen that for a fixed value of $D_2$ and $M_r$, the product

Mach number is uniquely determined as are duct pressure and temperature ratios from (1) and (2). In the context of the comparison experiments, increasing the reactant dissociated oxygen fraction will increase the net heat release, altering $D_2$ and thus the measured pressure rise. This change in pressure rise will only be purely a result of modified heat release if $h_0$ is matched between facilities.

Because the reactant Mach number contributes to $h_0$, $D_2$ will change with Mach number for constant heat release. An alternative way of writing (3) is to move all of the Mach number contributions to the right side giving a different non-dimensional heat release parameter,

$$\frac{\Delta h_{C,NET}}{h_{s,r}} = \left(1 + \frac{\gamma - 1}{2} M_r^2\right) \left(\frac{h_{0,p}}{h_{0,r}} - 1\right) \qquad (4b)$$

Figure 2 shows duct pressure ratio plotted against reactant Mach number (being the mach number of the fuel plus oxidiser mixture) for constant $D_2$ and constant $h_{C,NET}/h_s$. The significance of this plot is that for two experiments with the same level of heat release and matched total sensible enthalpy (and thus $D_2$), but however, a Mach number difference, a different pressure rise will be measured. Alternatively, by matching the sensible enthalpy, and thus $h_{C,NET}/h_s$, a pressure mismatch still occurs but to a lesser extent than the in the first case. For this parameter, as the reactant mixture approaches hypersonic conditions, Mach number independence is seen to apply.

Therefore, when targeting test conditions between experiments, which are expected to give different levels of heat release, it is desirable to match Mach number and sensible enthalpy of the reactant test gases so that duct pressure is only sensitive to heat release. If an error in Mach number is unavoidable, its significance can be minimised by matching of the sensible enthalpy by itself rather than the total sensible enthalpy. It is also desirable to match the static temperature between facilities such that differing chemistry results from composition differences alone. With sensible enthalpy duplicated, temperature will differ only because of specific heat and its dependence on composition. For the composition differences of interest, $C_p$

variations will be small, on the order of 5%, and in the following matching of temperature will imply matching of sensible enthalpy.

Referring to Figure 1c it is seen that the stagnation enthalpy for the reflected shock tunnel, test gas B, needs to be modified such that the above criteria for matching ideal air conditions can be met. At equal values of sensible enthalpy and Mach number, the stagnation enthalpy of B is greater both because of its chemical contribution and the additional velocity necessary to match the Mach numbers. For a perfect gas and using

$$a^2 = (\gamma - 1)\, h_s$$

the required velocity ratio is calculated as,

$$\frac{u_B}{u_A} = \sqrt{\frac{\gamma_B - 1}{\gamma_A - 1}}$$

An Engineering Model for Performance Analysis

A more realistic engineering model of scramjet combustion (from here on referred to as NTRAIN) has been developed to verify the above approximate analytical results and to do pre-experiment simulations for particular conditions. The fuel and oxidiser are each modelled as quasi-one-dimensional stream tubes. Startline conditions are calculated by pressure and direction matching the fuel and oxidiser streams. This process is not necessarily isentropic and a total pressure loss coefficient must be specified for one stream, with conditions for the other stream then determined by conservation of streamwise momentum. The oxidiser stream is held frozen at the inlet composition whether dissociated or not. At each streamwise step through the combustor an increment of oxidiser mass is entrained into the fuel stream (mixing stream) where it is assumed to mix completely and react to equilibrium. The rate of entrainment is prescribed by a mixing schedule which is chosen, along with the injection total pressure loss coefficient, to model the pressure distribution developed in a "mixing" test where hydrogen is injected into nitrogen. Pressure is assumed

laterally uniform and is chosen along with the area of the two streams such that the conservation equations are satisfied for both streams at each step. Wall boundary layer effects are computed from, and act upon, the mixing stream using specified skin friction and Stanton number coefficients. This assumes that only the mixing stream is in contact with the duct wall.

This model is based upon the entrainment model developed by Morgan, Reference 2, to examine the mixing and combustion process in the present cylindrical scramjet with an annular slot injector. The justification for the uniform mixing stream assumption came from the observation that at and near the point of injection the fuel layer is thin, typically occupying 2% to 5% of the duct radius. Entrained oxygen needs only to diffuse across a layer 1mm thick, and the approximation of a uniform composition mixing layer is therefore thought to be good. As the mixing layer develops, significant species concentration gradients must exist across the mixing layer, and the approximation becomes less valid. However, in Reference 2 this type of model was shown to be insensitive to species concentration profiles in the mixing layer for constant area duct configurations. This approximate model which now incorporates equilibrium chemistry in the mixing layer is considered to incorporate the major macroscopic fluid dynamic effects adequately, and within the limits of the chemistry assumption, to provide a useful basis for evaluating the effects of dissociated oxygen on ducted flows.

Mach 13 Condition - Test Results

Testing in T4 of the cylindrical combustor with 4 discrete orifice injectors was conducted at test conditions shown in Table 1. The dissociation fraction, $\alpha_T$=0.538, is defined as the mass fraction of total oxygen in the form of both atomic oxygen and nitric oxide. The Mach number and temperature are nearly identical to those obtained in the undissociated HYPULSE test flow, however, the stagnation enthalpy is unavoidably different because of the chemical energy content and lower molecular weight of the T4 test gas. Due to experimental constraints, the test section pressure was approximately 20% greater in T4. Fuel injection pressures were chosen to approximately conserve fuel total pressure to duct static pressure ratio.

Figures 3a and 3b show that near the duct exit the measured and NTRAIN predicted pressures are in good agreement. These and all subsequent simulations were run with the actual fuel and test gas conditions calculated for each run and using a constant entrainment rate (linear mixing) to a fully mixed condition at the combustor exit. Boundary layer properties of $C_f$=.003 and St=.0015 were used for all calculations. As such NTRAIN is being used as a predictive tool. The adequacy of the mixing and boundary layer parameter choice can be judged by the agreement between the predictions and the mixing data.

Both measurements and predictions suggest no strong effect of oxygen dissociation level on combustion pressure rise. Examining the NTRAIN calculation the reason becomes clear. Although atomic oxygen adds to the heat release achieved in T4, the thermal energy yield is small because of the high static temperature of the test condition. Physically, this means that the flame is sufficiently hot ( 3000 K) that the extra energy from dissociated test gas, goes primarily to dissociated combustion products and produces a small increase in the temperature, and hence pressure. Calculated combustor exit temperatures are 2865 K in HYPULSE vs. 3093 K in T4. In addition, the higher velocity of the T4 test gas, inhibits an increase in $D_2$, so that although the net heat release is 1.22 MJ/kg in HYPULSE vs 1.41 MJ/kg in T4 a difference of 15.6%, the values for $D_2$ are 0.127 and 0.138 a difference of only 9.2%. Referring back to Figure 2 (and noting the small inlet Mach number mismatch which implies a similar mismatch in reactant Mach number) it is clear that this change in $D_2$ produces a change in pressure ratio that is experimentally negligible.

To further investigate the influence of test gas oxygen dissociation, the total oxygen content of the oxidiser was varied. Three different values of the test gas total oxygen mass fraction, $X_a$, were run with the fuel plenum pressure and mass flow rate kept constant. The dissociation fraction varies with $X_a$ because it changes the oxygen partial pressure and therefore the rate of recombination in the facility nozzle. Both predictions and data in Figure 4 show little difference in duct exit pressure. The explanation for this constancy of pressure rise is again the high temperature limiting net heat release, but also, the facility nozzle exit Mach number is altered by the different recombination rates with oxygen content, which tends to further offset the

heat release variation. An adjunct experiment was run at a lower stagnation enthalpy with standard air where measured data in Figure 4 are clearly higher near the duct exit as is the predicted pressure. A sensitivity study of pressure rise to oxygen content at the lower enthalpy was not performed.

Summary of Mach 13 Results

- There is no strong effect of dissociation on the pressure rise at the Mach 13 condition.

- The effect of changing the total oxygen content, at levels of 63% to 186% of standard air and at constant fuel flow rate, is also not significant. Lowering the test gas enthalpy is seen to raise the duct exit pressure.

- The trends and absolute values of exit pressure are well predicted by the equilibrium combustion model.

Mach 17 Condition - Test Results

Results reported in Reference 3 from preliminary tests run in 1990 with the cylindrical model and annular slot injection suggested a difference in performance due to oxygen dissociation in T4. However, the test gas pressures were not well matched for these tests and it was necessary to normalise results by mean fuel-off pressure to form this conclusion.

An objective of the 1991 test series was to raise the T4 test pressure to that of HYPULSE. This was done by using thicker, 5mm, diaphragms for the new T4 tests. As such, this condition is at the maximum pressure limit for T4 using mild steel diaphragms. The calculated T4 pressure at this condition is 18 kPa, slightly higher than HYPULSE. However, this inlet pressure was still not sufficient to bring the fuel-off pressures into agreement.

Measured fuel-off pressures from the two facilities are compared in Figure 5 to simulations run by R. Bittner at NASA LaRC using a PNS code and two different boundary layer treatments. In both cases the assumed inlet pressure was taken as 16.5 kPa, the quoted HYPULSE value. The good agreement of the laminar case and the T4 data is evident. There is also reasonable agreement near the duct exit between the HY-1991 data and the turbulent calculation. However, transition to turbulence for this case, as evidenced by heat transfer measurements, occurs at 300mm from the duct inlet. Sketching in a laminar distribution from this transition point, back to the inlet as shown, suggests that better agreement with the HYPULSE results would be achieved with a higher assumed inlet pressure.

A further investigation into this pressure mismatch was done by running fuel-off tests in T4 with a 50x25mm rectangular duct for comparison with existing HYPULSE data. In these comparisons (Figure 6), HYPULSE yielded 25% higher mean duct pressure. Back in Figure 5, this 25% value also brings the T4 data in line with the HY-1990 data for which a purely laminar boundary layer was observed experimentally.

The possibility of such an uncertainty in the HYPULSE diffuser exit pressure has been investigated by reanalysing the most recent HYPULSE facility and diffuser calibration data. Reference 4 shows that in the absence of reliable instream static pressure measurement, the measured pitot pressure distributions at the diffuser exit are not sufficient to preclude a shock system and some total pressure loss in the diffuser. Depending on the magnitude of this total pressure loss, the stream tube captured by the combustor will have significantly higher pressure and temperature than predicted for the ideal isentropic diffuser operation which is currently assumed. From this analysis and consistent with the diffuser calibration data, the HYPULSE diffuser exit conditions were calculated postulating a total pressure loss which yields the 25% higher combustor inlet pressure needed to make HYPULSE data consistent with the T4 measurements and the CFD calculations. Along with this pressure increase, and more important from the combustion standpoint, is a static temperature increase of 13%. These conditions are shown in Table 2 under "modified" HYPULSE conditions. The currently accepted HYPULSE diffuser exit conditions are shown under "ideal" and the T4 conditions which were established for the comparison tests

under "T4".

At Mach 17, tests were run in T4 with both the discrete orifice and slot injectors. No significant difference in performance was observed between the two injectors and conclusions drawn for the discrete injectors carry over directly to the slot.

NTRAIN simulations and T4 measurements of combustor exit pressures (Figure 7), for the discrete orifice injector, were found to be consistent in trend if not absolute value. The same constant entrainment rate and boundary layer parameters were used as for Mach 13. For the HYPULSE data (Figure 8), the "modified" diffuser exit conditions were required to bring the simulations nearer the measurements, giving further evidence that this may be a better estimate of the actual HYPULSE test condition.

Comparison of combustion heat release is best done in terms of the combustion to mixing run pressure ratio which is approximately equivalent to the premixed duct pressure ratio shown in Figure 2. Previously, it was shown that this parameter is sensitive to normalised heat release as well as to Mach number. In Figure 9 NTRAIN calculations also show the effect of increasing Mach number or temperature is to reduce the pressure ratio. The simulations are seen to agree quite well with both T4 and HYPULSE data, and if they are to be believed, the difference between measurements in each facility is not because of dissociation, but rather, because of Mach number and temperature mismatch.

Of additional significance in Figure 9 is that the predicted pressure ratio for the "ideal" HYPULSE conditions are not very different from T4, so that when test conditions are adequately matched, the dissociation effects measured between the facilities are expected to be small.

Mach 17 - Finite Rate Chemistry Effects

In Reference 5, Jachimowski has analysed the Mach 17 slot injection comparison experiments reported in Reference 3. Using a three-stream model, which accounts

for mixing and wall friction by contracting the duct area profile, both finite rate and equilibrium chemistry calculations were made to predict the effects of oxygen dissociation on pressure rise. From Figure 10 of Reference 5, the combustion to mixing pressure ratio can be inferred, and although not exactly equivalent because of the different injection geometries, can be compared to the NTRAIN predictions and the current data set. With equilibrium chemistry a pressure ratio of 0.43 was predicted for T4 and. 0.40 for HYPULSE. (The HYPULSE "ideal" test conditions were used for these calculations.) With finite rate chemistry, the T4 value was 0.30 vs. 0.26 for HYPULSE.

Clearly, the equilibrium values are consistent with those shown in Figure 8, and predict a very small influence of atomic oxygen content. The pressures predicted for finite rate chemistry are lower, but the difference between facilities is still not large. Without knowledge of the possible mismatch in test conditions, particularly in static temperature, it was concluded in Reference 5 that the difference measured between facilities was verification of atomic oxygen enhanced combustion. However, it now seems evident that this conclusion must await further data with better test condition duplication.

Summary of Mach 17 Results

- No significant difference has been found in T4 with orifice injection as compared to annular slot injection.

- Differences in HYPULSE and T4 fuel-off pressures show that an inlet pressure mismatch of 25% to 50% persists. Direct comparison of combustion data at this condition is inconclusive considering that a temperature mismatch may be coincident as indicated by an approximate analysis of the HYPULSE diffuser where a postulated shock system accounts for the pressure mismatch.

- Equilibrium predictions for the combustor agree reasonably well with the T4 data and with the HYPULSE data when the inlet flow is

modified by the assumed shock system. These same simulations predict a small effect of dissociation at this test condition.

Thrust Measurement

The analytical approach developed to quantify the effect of heat release on ducted pressure rise shows that duct exit Mach number will itself be matched for equal oxidiser Mach number and achieved Damkohler number. If the duct is subsequently attached to a thrust nozzle, then for one-dimensional flow, the matching of pressure and Mach number at the nozzle inlet will ensure equal thrust and $I_{sp}$ would be developed in each facility in the absence of finite rate chemical effects in the nozzle. For 2- and 3-dimensional flows the situation is more complex, and requires the matching of profiles at the duct exit. It is of fundamental importance to determine if the test criteria presented here which result in near duplication of the duct exit pressure in a constant area duct also lead to the development of the same $I_{sp}$ in a thrust producing situation.

The axisymmetry of the cylindrical combustor with the annular slot injector was therefore identified as in ideal geometry to obtain thrust data for comparison in the two facilities and to evaluate reasonably simple (2-D) computational models. For this purpose a 9:1 area ratio conical nozzle was added to the combustor exit and surface pressures monitored by 10 transducers spaced at 25 mm intervals along its surface. Successful pressure measurements were obtained at Mach 17 however, vibrational noise corrupted all of the Mach 13 data in the nozzle. Measured pressures in the nozzle showed good delineation between fuel-off, hydrogen into nitrogen and hydrogen into air, Figure 10. Also summarised are calculated values of $I_{sp}$.

Conclusions and Recommendations for Further Work

The results of facility comparison tests run in T4 to date have shown that similar although not identical pressure data can be achieved in the two facilities. More refined instrumentation techniques and calibration should reduce measurement uncertainty and hopefully bring the data into agreement, or provide data of sufficient

quality to allow the differences to be explained. Several issues have been shown to require further experimental and analytical investigation.
Specifically, further theoretical work is underway to determine the flight envelope over which the insensitivity of test facilities will apply.

The uncertainty in the HYPULSE diffuser exit conditions has made comparison of the Mach 17 data obtained inconclusive, and some means to refine the diffuser calibration is required. In T4 this uncertainty can be examined by perturbing the test condition to approximately match the HYPULSE fuel-off and mixing results. However, ultimately an instream pressure measurement must be made in HYPULSE.

The equilibrium chemistry model being used oversimplifies the physics, however, it has been useful for doing quick analyses of data and has been quite successful for predicting data trends. This model suggests that at the comparable operating conditions achievable in the facilities, the effect of oxygen dissociation is small and will require very refined experimental technique to detect. It is likely that if the experimental conditions can be sufficiently defined, then by examining different enthalpy levels and test gas compositions, a more refined computational model can be calibrated such that extrapolations to regimes where the effects of dissociation are not minor can be made. Naturally, this has implications for future, large scale reflected shock tunnels and expansion tunnels. The premixed analytical model has proven very useful in understanding the preliminary experimental results and in defining the flow parameters which must be matched when setting up flow conditions for comparative tests.

The thrust nozzle measurements have yielded clean pressure distributions which will be valuable when compared between facilities and to a proper computation. To use this nozzle in HYPULSE, the combustor must be truncated to keep the overall model length within the flow start-up limit. In addition, detailed combustor exit pitot surveys are required to both refine combustor analysis and start a nozzle computation.

References

1. Morgan, R.G.,"Dissociated Test Gas, Effects on Scramjet Combustors", NASA CR-182096, Supplement 5, October 1990.

2. Morgan, R.G., Bakos, R.J. and Tamagno, J., "Bulk Parameter Analysis of Hypersonic Combustion Experiments," GASL TR-321, August 1990.

3. Morgan, R.G., et al, "Scramjet Testing - Ground Facility Comparisons," ISABE Paper 91-194(L), September 1991.

4. Bakos, R.J. "HYPULSE Diffuser Calibration - Analysis Supplement," Private Communication to GASL, February 1992.

5. Jachimowski, C.J., "An Analysis of Combustion Studies in Shock Expansion Tunnels and Reflected Shock Tunnels," NASA TP-3224, July 1992.

Table 1. Mach 13 air test conditions in T4 and HYPULSE

| Flow Parameters | T4 | HYPULSE |
|---|---|---|
| p (kPa) | 27.96 | 23.50 |
| T (K) | 2363 | 2350 |
| Mach No. | 4.01 | 4.10 |
| U (m/s) | 3966 | 3840 |
| $H_{STAG}$ (MJ/kg) | 12.3 | 10.2 |
| $\alpha_T$ | .538 | .049 |
| $h_s$ (MJ/kg) | 2.77 | 2.70 |
| $\gamma$ | 1.323 | 1.293 |
| u ($kg/m^2$-s) | 150.2 | 133.4 |

Table 2. Mach 17 air test conditions in T4 and HYPULSE

| Flow Parameters | T4 | Ideal HYPULSE | Modified HYPULSE |
|---|---|---|---|
| p (kPa) | 18.1 | 16.4 | 20.2 |
| T (K) | 2040 | 2100 | 2370 |
| Mach No. | 5.13 | 5.75 | 5.35 |
| U (m/s) | 4680 | 5090 | 5030 |
| $H_{STAG}$ (MJ/kg) | 14.7 | 15.4 | 15.5 |
| $\alpha_T$ | .467 | .027 | .061 |
| $h_s$ | 2.35 | 2.38 | 2.72 |
| $\gamma$ | 1.322 | 1.296 | 1.293 |
| u ($kg/m^2$-s) | 134.7 | 138.4 | 148.8 |

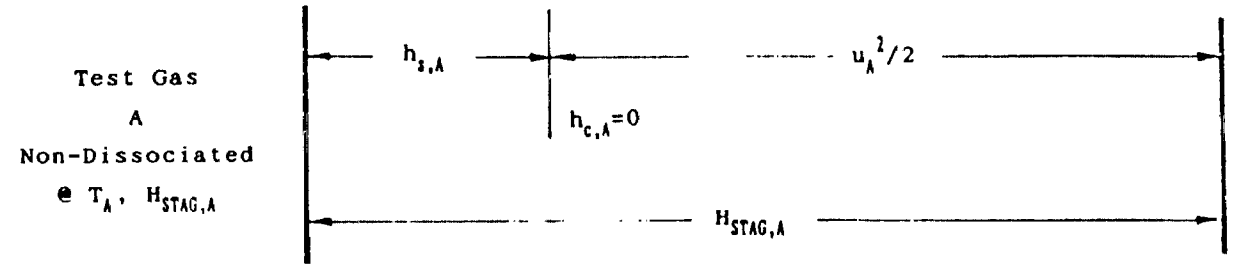


Figure 1a.

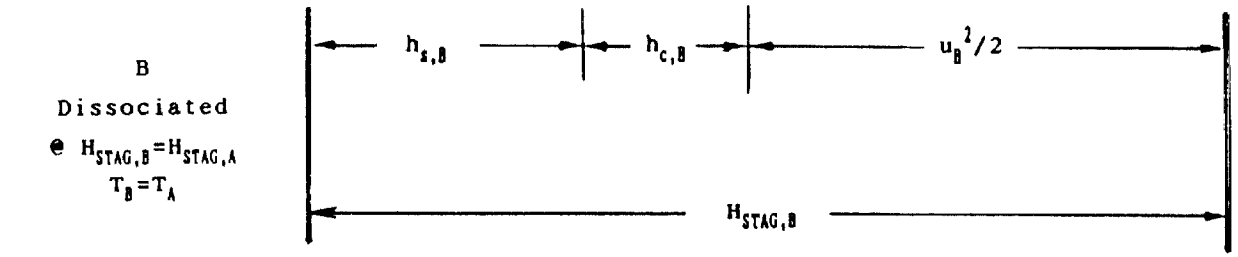


Figure 1b.

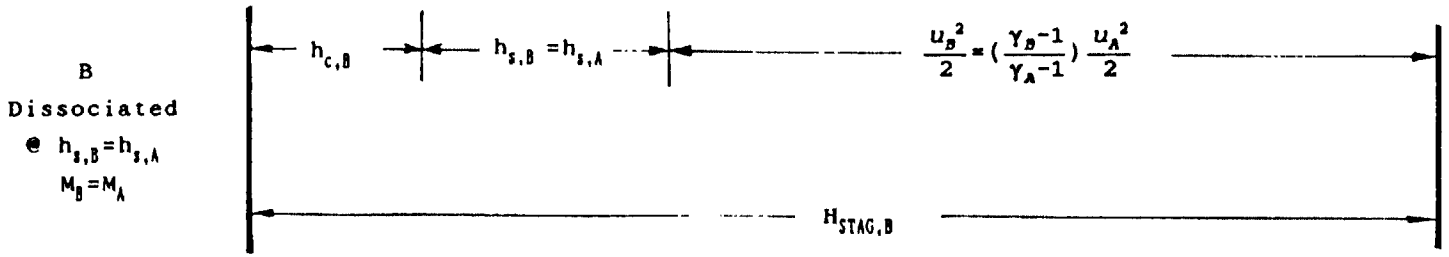


Figure 1c.

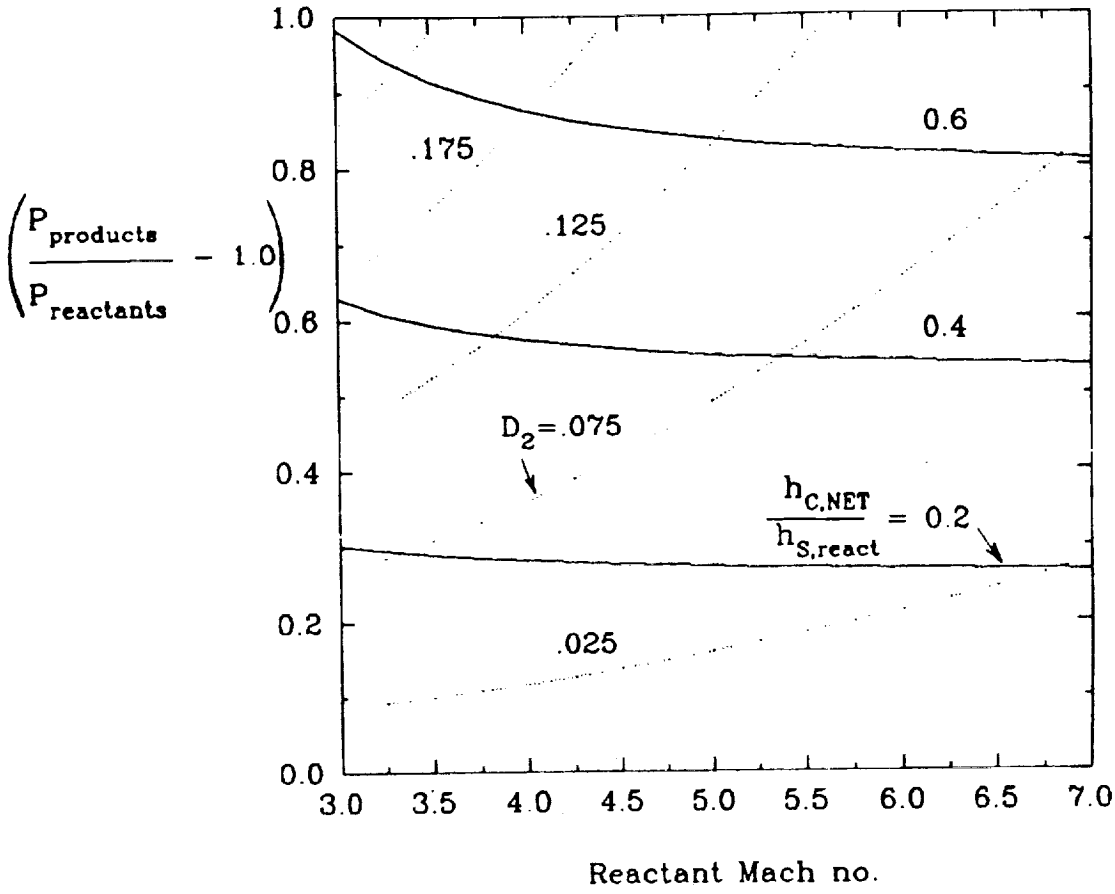


Figure 2. Theoretical combustor pressure ratio for different non-dimensional heat release parameters vs. reactant Mach number.

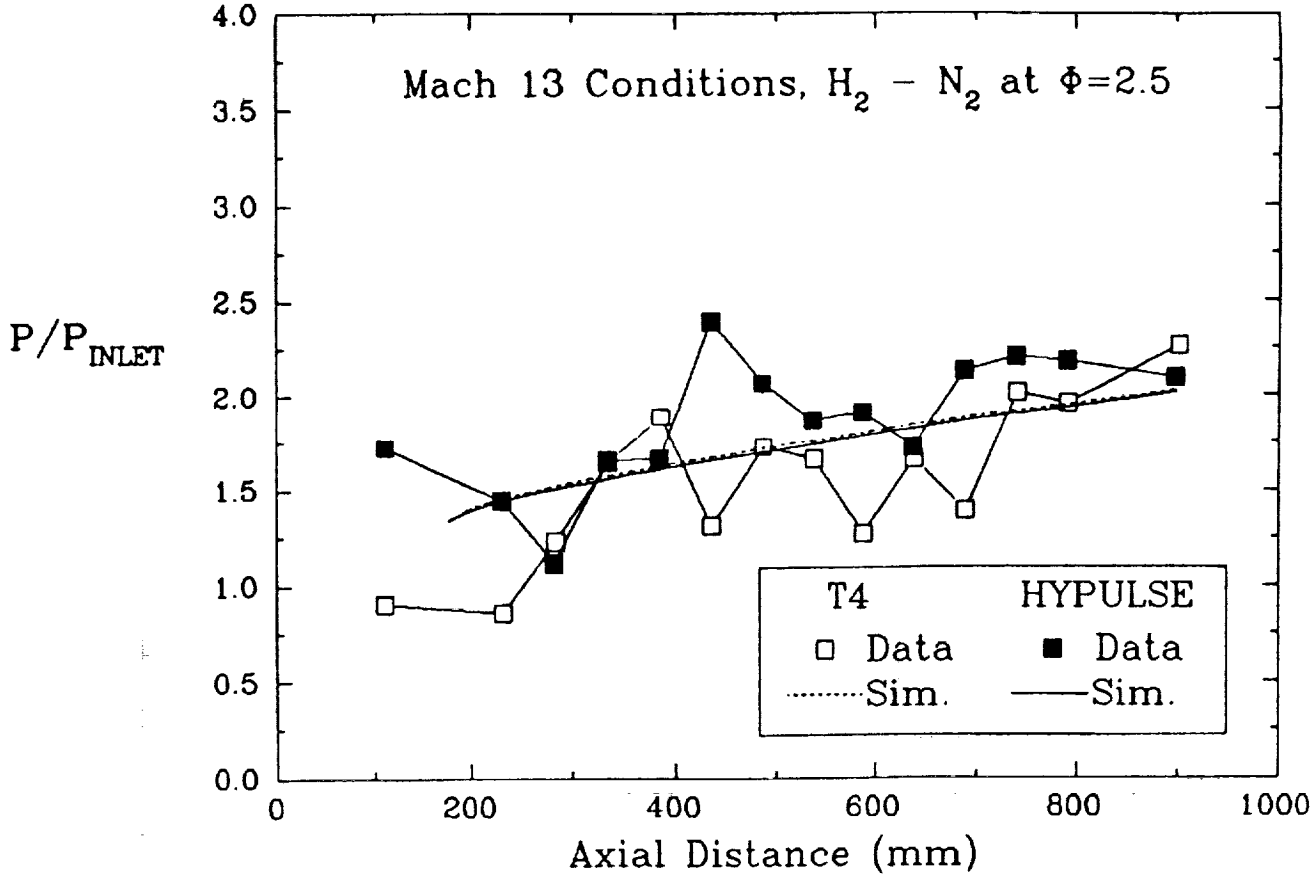


Figure 3a. Facility comparisons of mixing data and NTRAIN predictions at Mach 13 stagnation enthalpy.

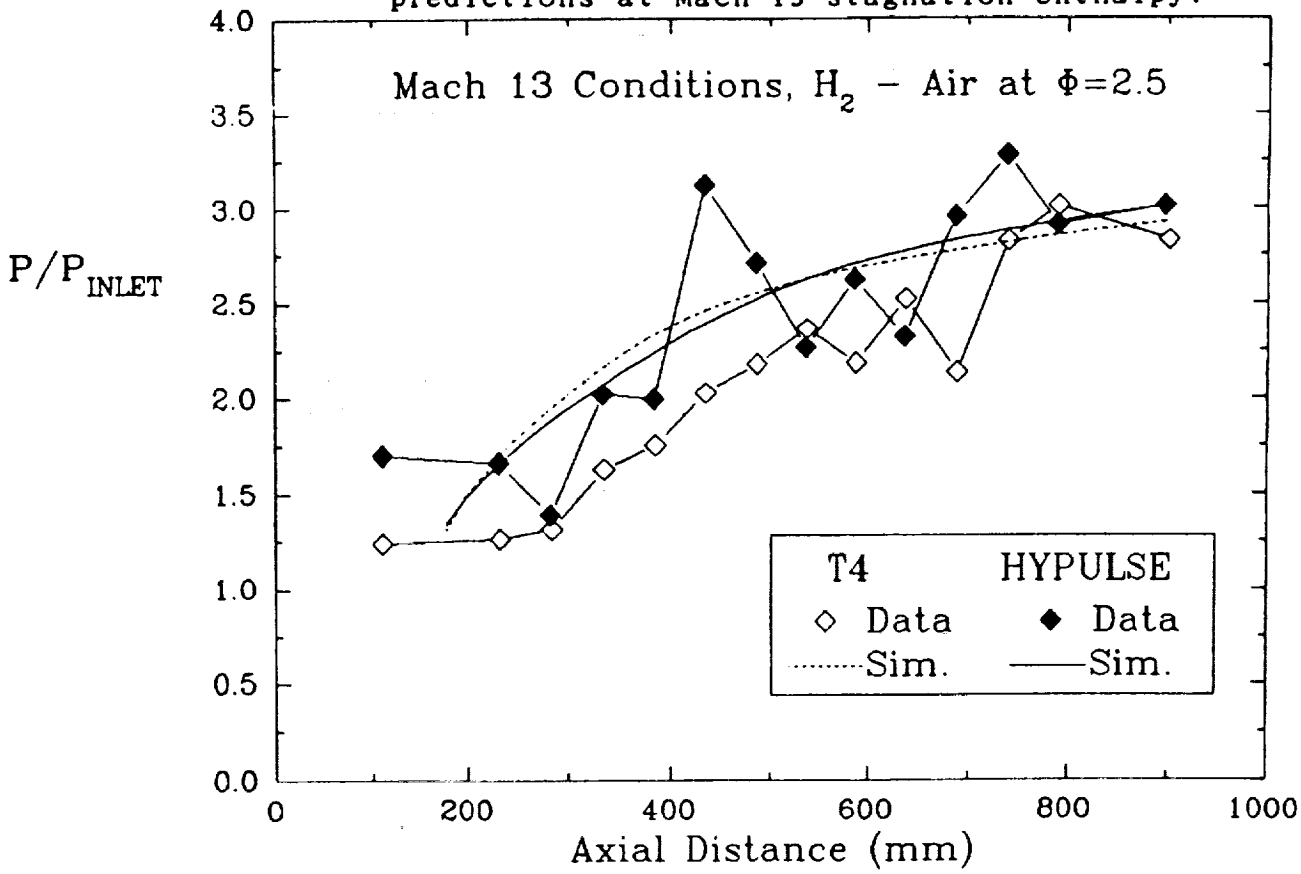


Figure 3b. Facility comparisons of combustion data and NTRAIN predictions at Mach 13 stagnation enthalpy.

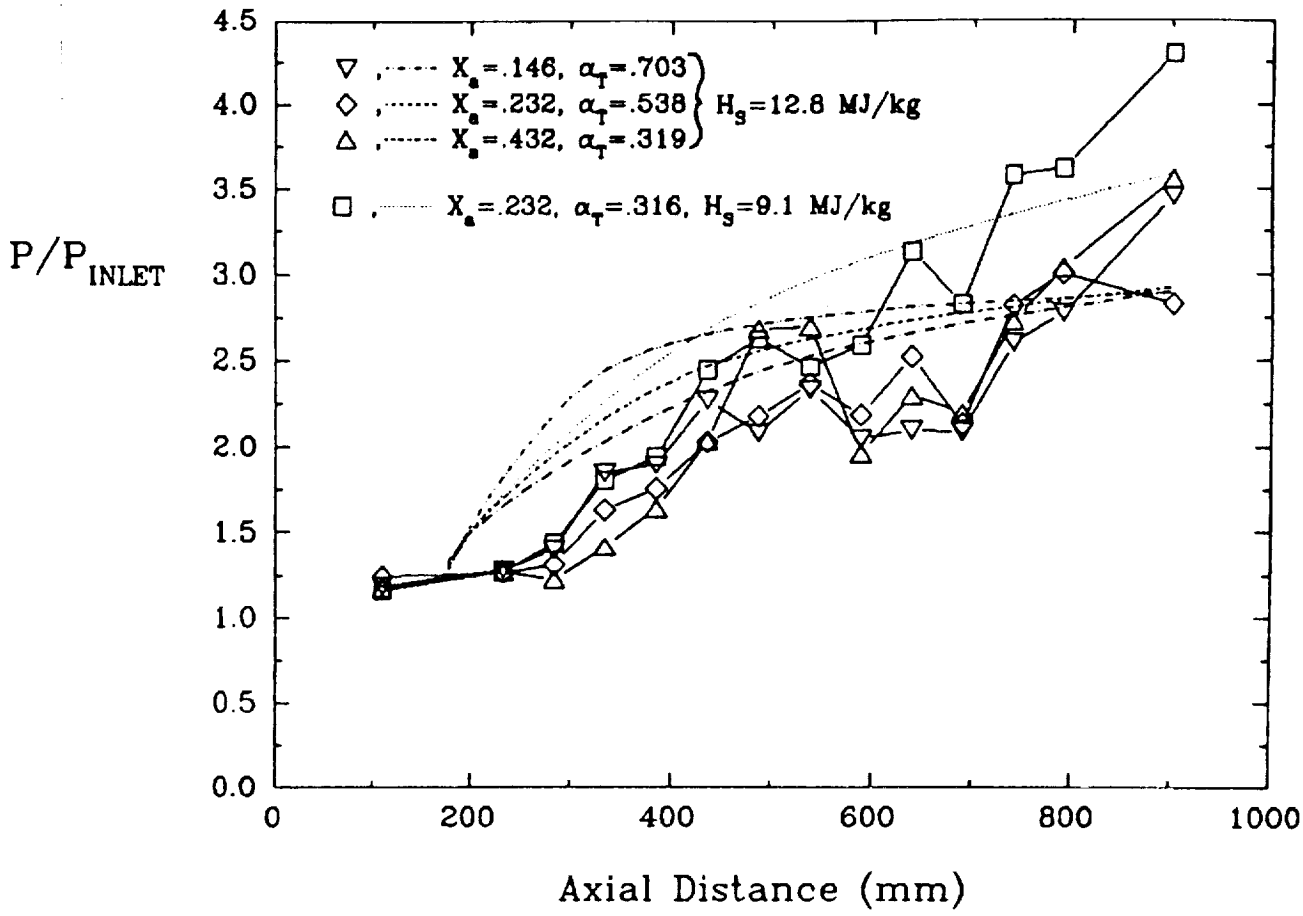


Figure 4. Data and NTRAIN predictions for varying test gas oxygen content and stagnation enthalpy.

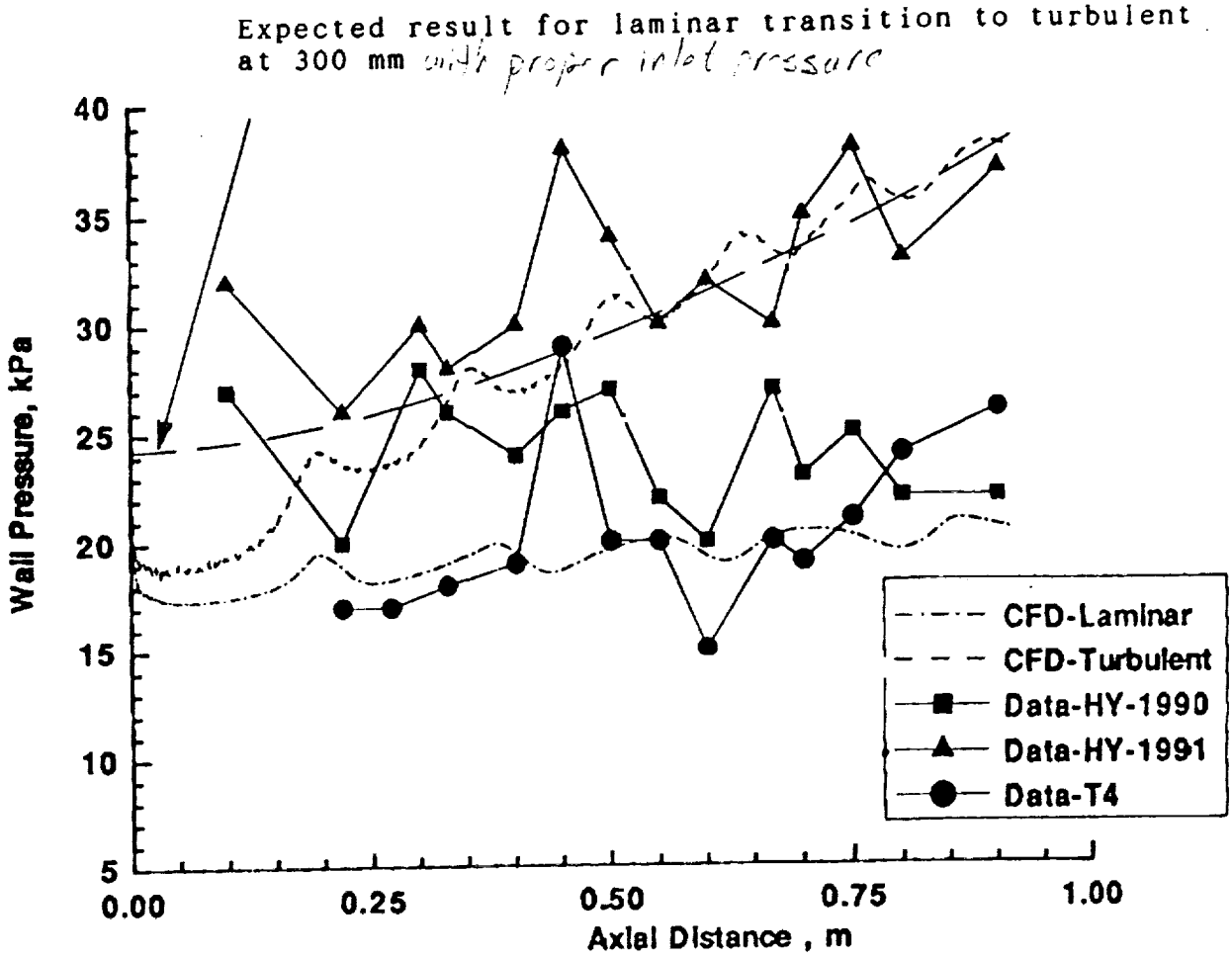


Figure 5. Comparisons of T4 and HYPULSE fuel-off data to PNS computations for fully laminar and turbulent boundary layers.

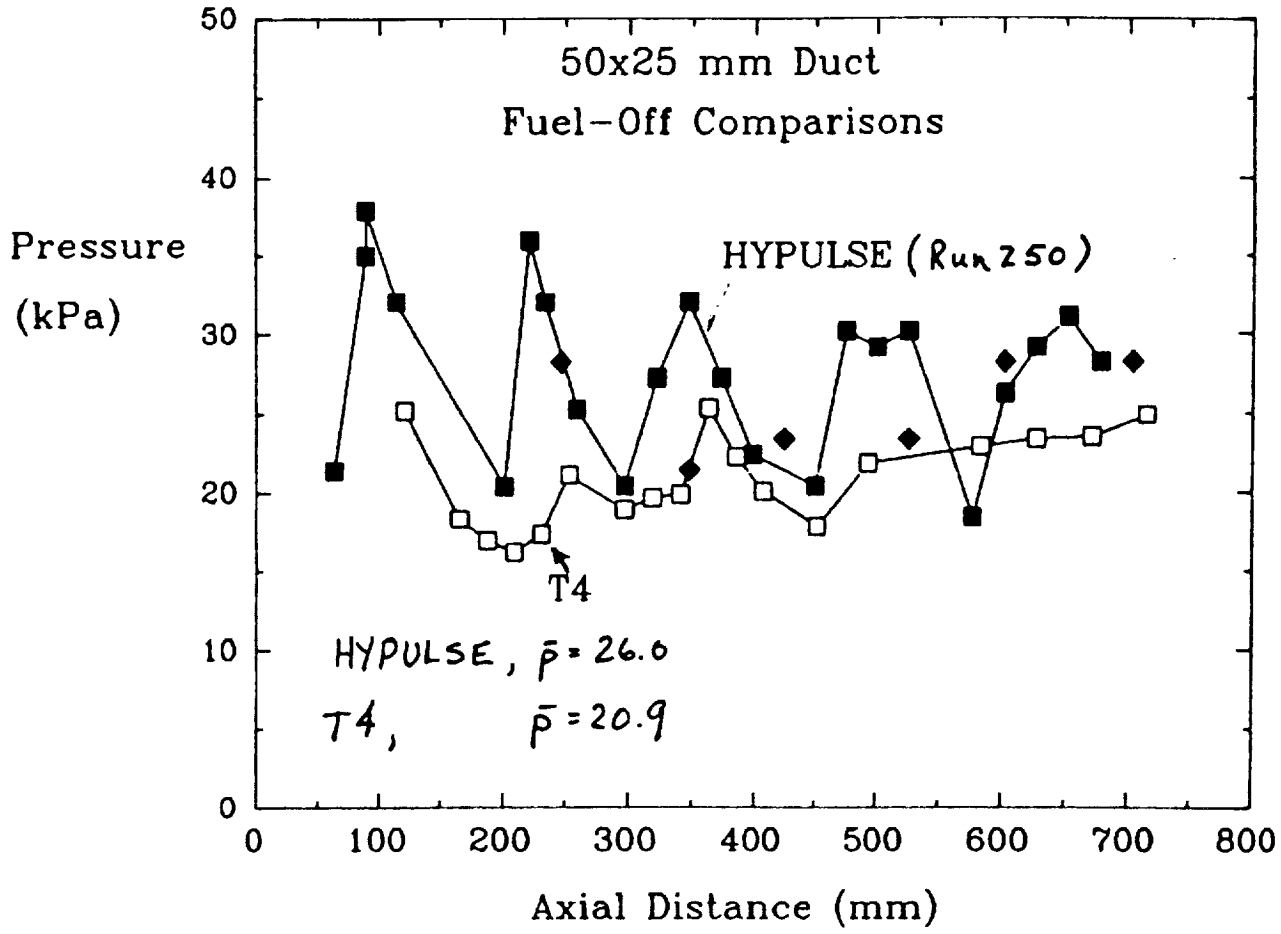


Figure 6. Comparison of T4 and HYPULSE fuel-off data in a 50x25 mm rectangular duct.

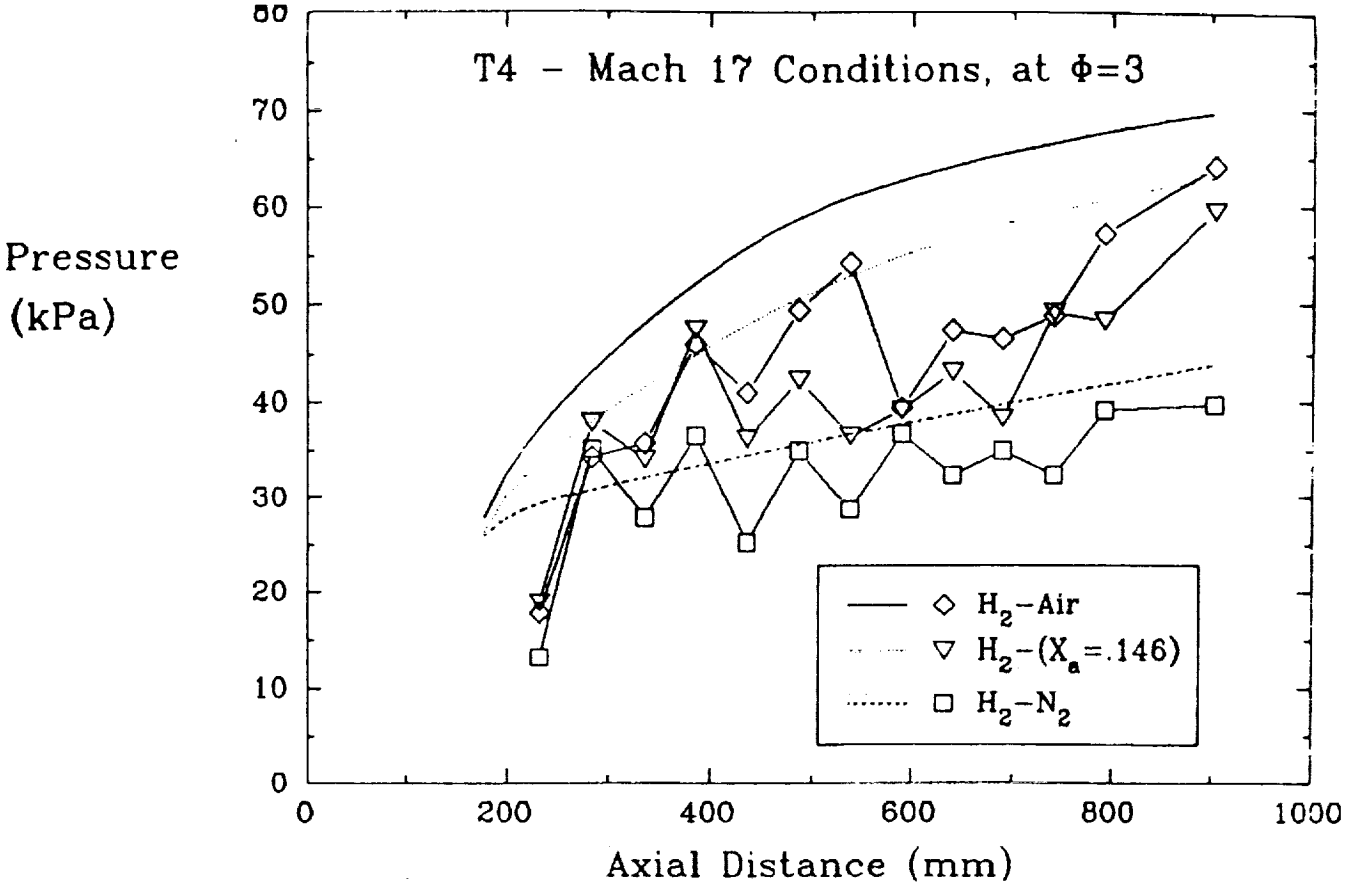


Figure 7. T4 data for fuel into different test gases and NTRAIN predictions.

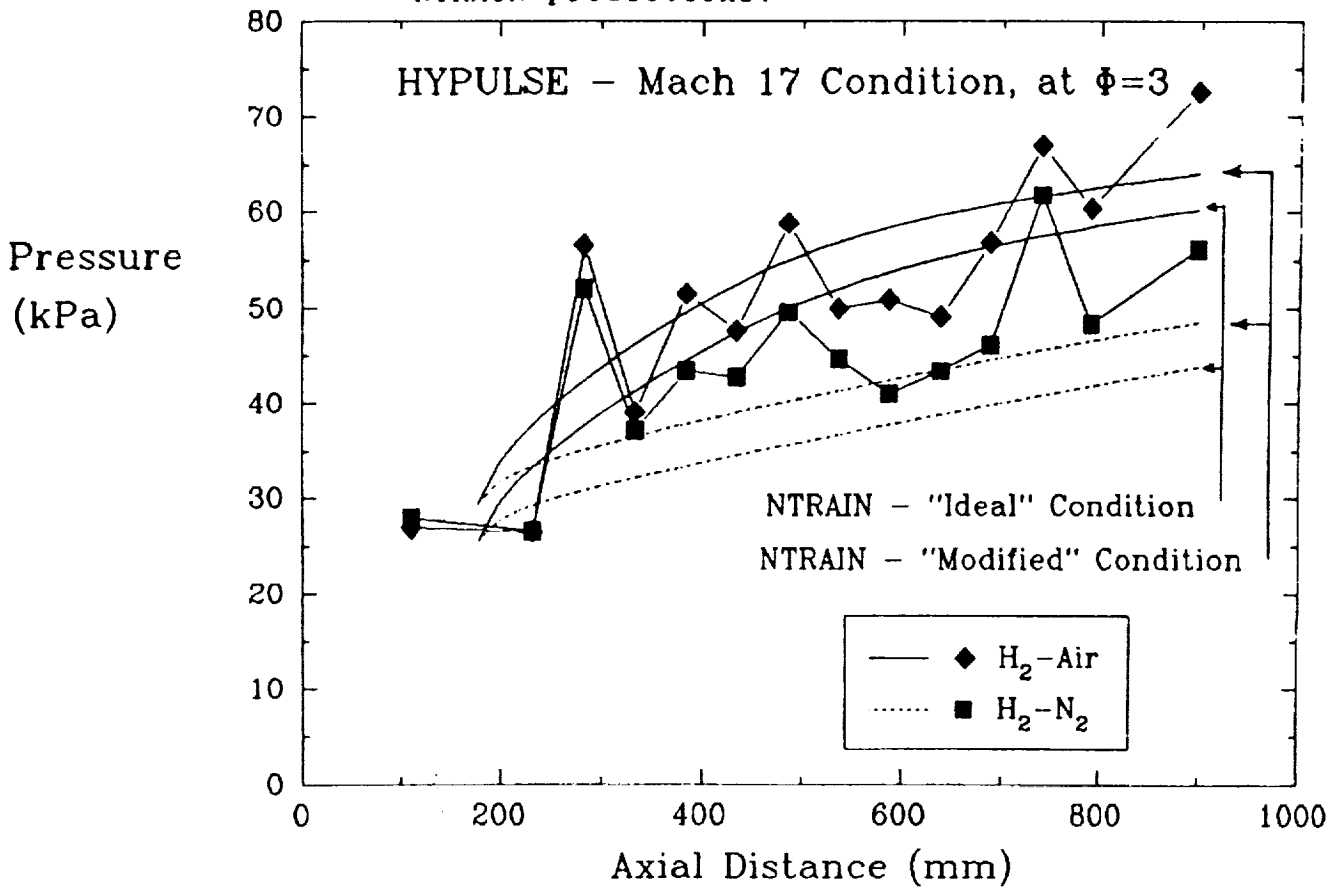


Figure 8. HYPULSE data for fuel into air and nitrogen compared too NTRAIN predictions for different assumed inlet conditions.

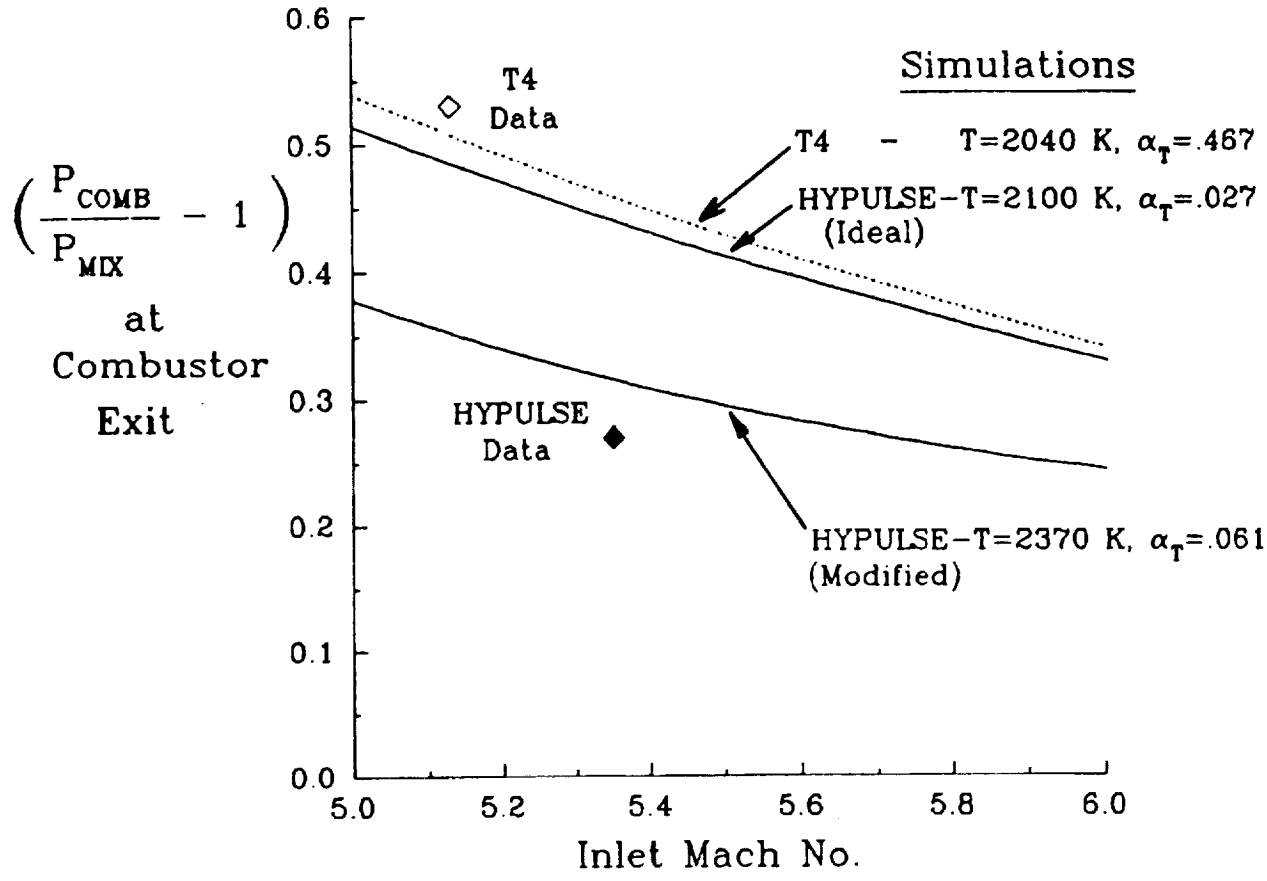


Figure 9. Data and NTRAIN predictions for duct exit combustion to mixing pressure ratio.

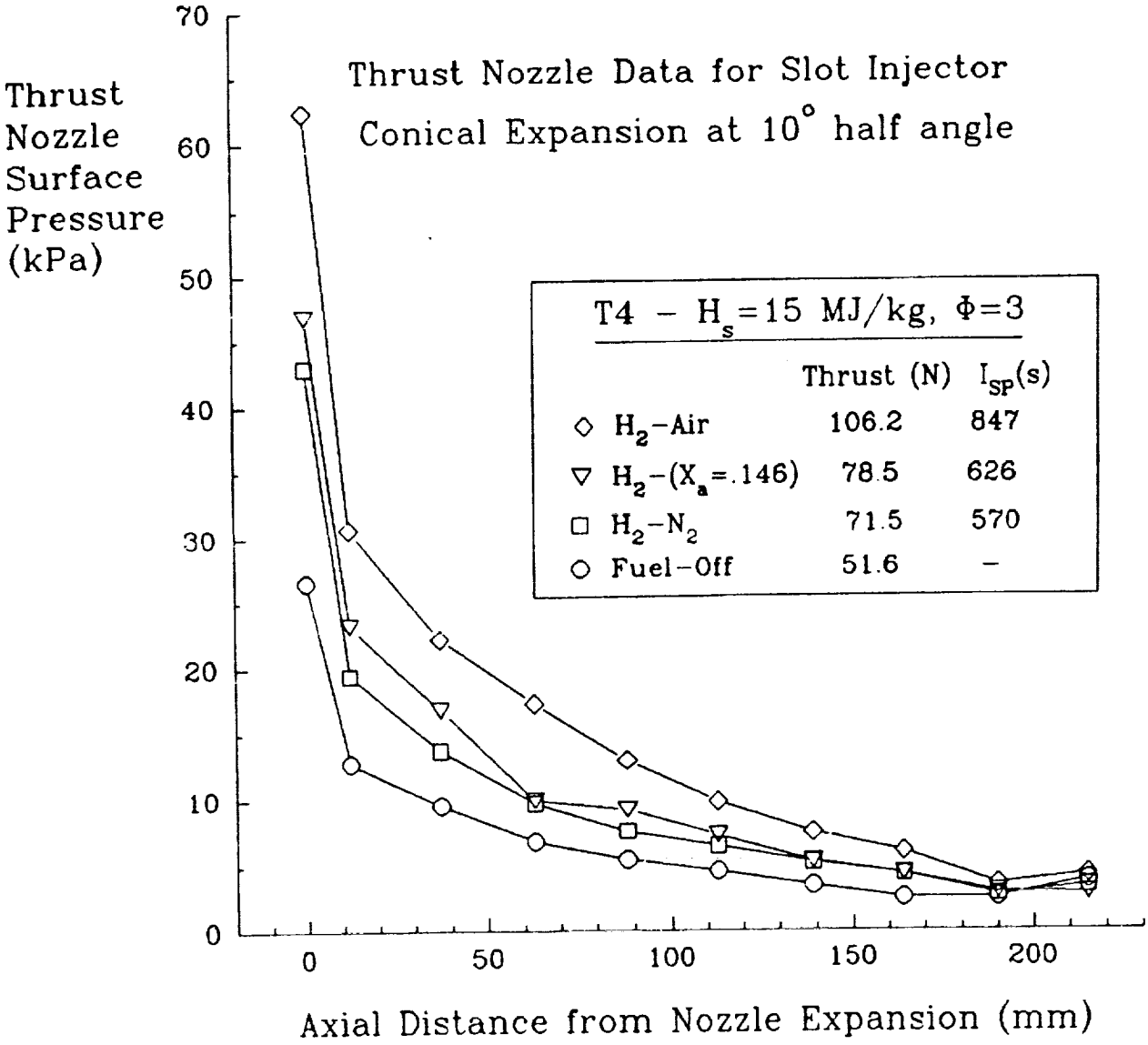


Figure 10. Conical thrust surface pressure measurements and Calculated $I_{sp}$.

## Numerical Simulation of a Scramjet Thrust Balance

S.L. Tuttle

The aim of the thesis is to extend the use of the previously developed drag balance to measuring the net axial thrust (including skin friction) of a scramjet nozzle. The nozzle will initially be a symmetrically diverging, parallel side-walled, rectangular cross-sectioned duct, joined to a 50x25 mm rectangular scramjet combustor.

The force measurement on the cone drag balance (Tuttle, Simmons 1990) was significantly simpler in that only one force measurement component was present : drag in the axial direction. The main initial concern with the thrust measurement is that although the force of interest is the net axial thrust, the nozzle ramp walls diverge at an angle of probably $11^{\circ}$ and so most of the flow pressure is transverse to the direction of the force of interest, and considerably greater in magnitude. Fig. 1 shows the configuration of the proposed thrust balance and the relatively low stiffness of the long stings is at once apparent. Thrust measurement will be via axial strain measurement in the stings. Although strain gauges may be wired to cancel bending effects, minimising the possible large magnitude of flexural stress waves and strains was an overriding criterion during the development of the design. The nozzle loading applies a three dimensional system of forces to the sting, and the transverse components may be large.

A series of experiments was conducted to investigate axial strain measurement in the presence of transverse loading up to two orders of magnitude larger. Some influence on the axial strain measured was observed, but the results were inconclusive.

Analysis of the wave equation for a simple model on a long sting with a step load applied gives the following time constant for this first order system :

$$\tau = \frac{m}{\rho\ c\ A}$$

m is the model mass; $\rho$, c, A, are the sting density, speed of sound and cross-sectional area respectively. If this analysis is repeated with a load applied at some angle $\theta$, the time constant becomes

$$\tau = \frac{m}{\rho\ c\ A\ \sin\theta}$$

i.e. the response of the system is slowed merely by changing the loading orientation. This is due to changing the particle velocity in the material.

The three criteria governing the design of the thrust balance are the time constant (fast response desired), the magnitude of the axial strain (high signal-to-noise ratio) and the ratio of bending to axial strain (to be kept as low as possible). All three of these depend on the cross-sectional area of the sting - this should be small for higher strain measurement, but large for a better transition of the stress waves from the nozzle to the sting and hence a quicker response. Lastly, a shape is required for the sting which provides high bending stiffness but without rendering the axial strain unmeasurable.

For a smooth join to the nozzle walls, some sort of rectangular cross-sectioned sting is required. Four possibilities were evaluated with respect to the above three criteria : a long flat rectangular sting mounted as in Fig. 2 (a) and (b), stings made from angle sections (c), and then (d), a flat rectangular sting with a 90° twist in it, a short distance from the join with the nozzle. The last option, the twisted sting, surpassed the other three options in performance. For the same cross-sectional area (i.e. sane axial strain and same time constant) greater bending stiffness is provided.

The decision was then taken to proceed with thorough finite element modelling of the system. The NASTRAN package has been used for this. The twisted sting is compared with a plain flat one to make sure that the

twist does not introduce new effects.

The first test is a comparison of step responses to a load applied at the free ends of the two stings, with no nozzle attached. Figures 3 (a) and (b) show the step rise in axial stress for the flat and twisted stings respectively. This shows that the twisted sting behaves in a manner suitable for application in the thrust balance.

The next question is where to put the stings? There are four possible configurations (the use of two stings is envisaged mainly for maintenance of symmetry) : two flat stings. mounted either to the ramp walls or the side walls; and two twisted stings, mounted either to the ramp walls or side walls.

Figures 4 and 5 show the axial stress in the sting 200 mm downstream of the nozzle for the cases of flat stings attached to the ramp and side walls respectively. Fig. 6 shows the axial strain 100 mm downstream of the twist (300 mm downstream of the nozzle) for the twisted sting mounted on the ramp surface. Fig. 5 shows clearly that side wall mounting of the stings is unworkable.

The next thing to consider is the variation in axial strain across the width of the sting (this will then give strain variation across the gauge) and the variation of strain through the thickness of the sting (a large difference from one side to the other will give twist or bending).

In order to make the finite element model as realistic as possible, some material damping is applied in the form of a loss factor at a particular frequency. This will remove numerical noise from the solution. Little sensitivity to the frequency at which the loss factor is applied is observed over a range from 100 Hz to 10 kHz. Results shown incorporate a loss factor at 1 kHz, approximately the signal frequency.

Fig. 7 compares the strain on either side of the sting for (a) the flat sting and (b) the twisted sting mounted on the nozzle ramp surface. The reduced difference in case (b) led to the adoption of the twisted sting

- ramp surface (TS-R) configuration for the thrust balance. The shear stress after the twist is zero and the transverse stress is 25% of the transverse stress in the flat sting case. Modal analysis indicates the presence of a small degree of lateral twist and displacement in the direction in which the twist is least stiff.

Improvement to the axial strain signal is now being attempted.

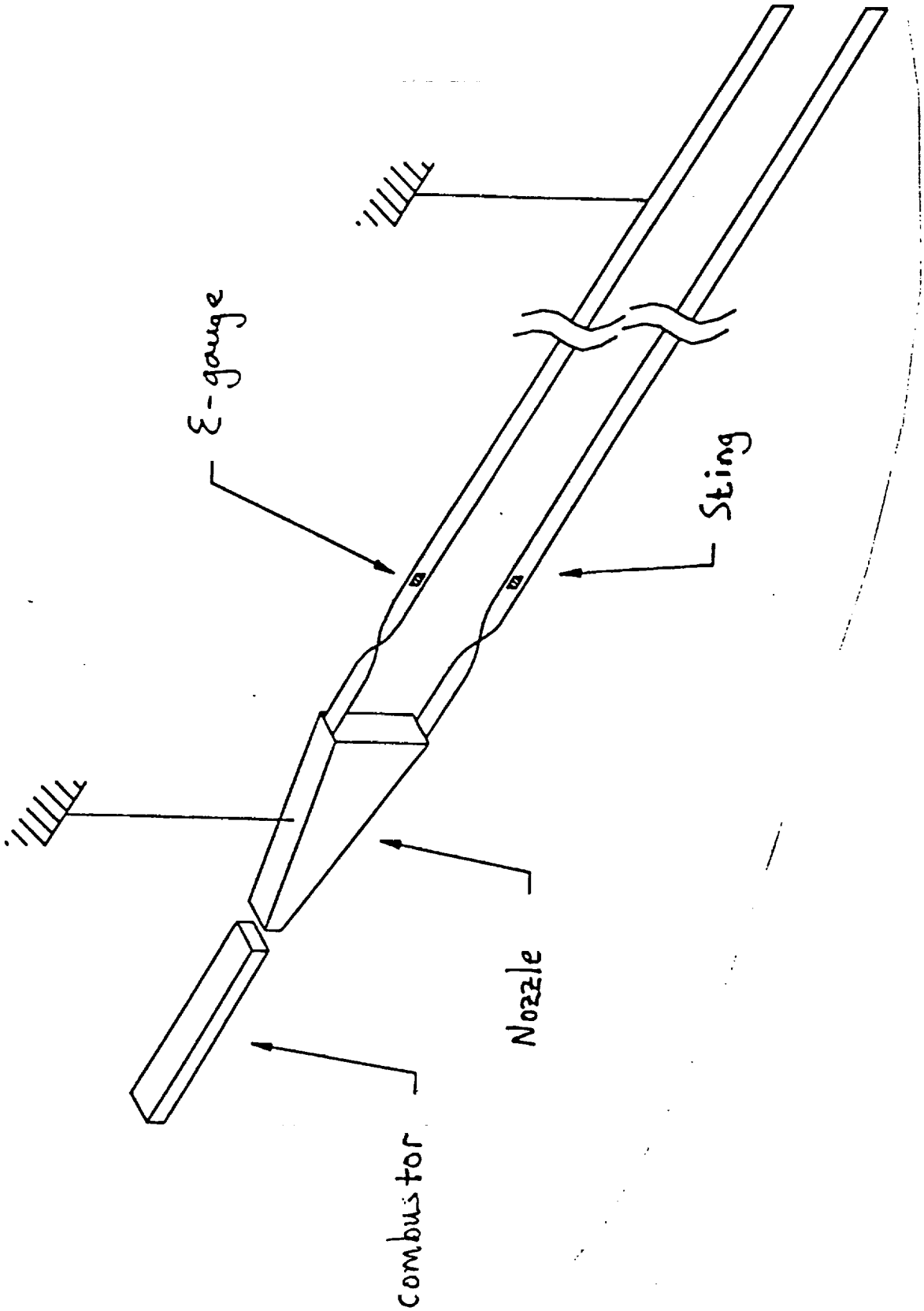




Figure 1. Thrust Balance Configuration.

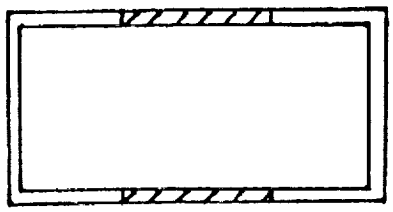

(a)

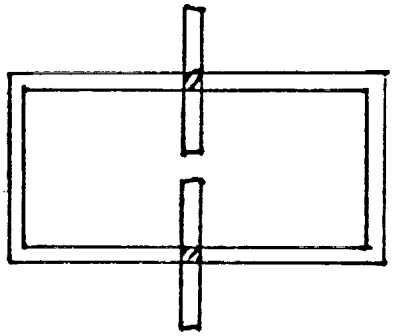

(b)

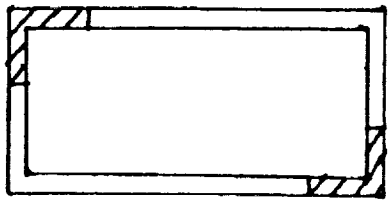

(c)

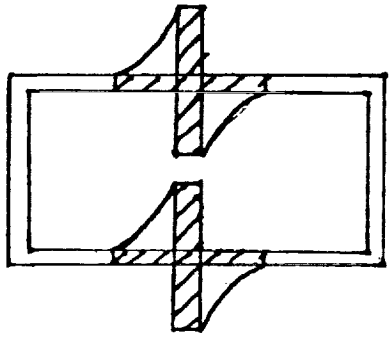

(d)

Figure 2. Possible Sting Geometries

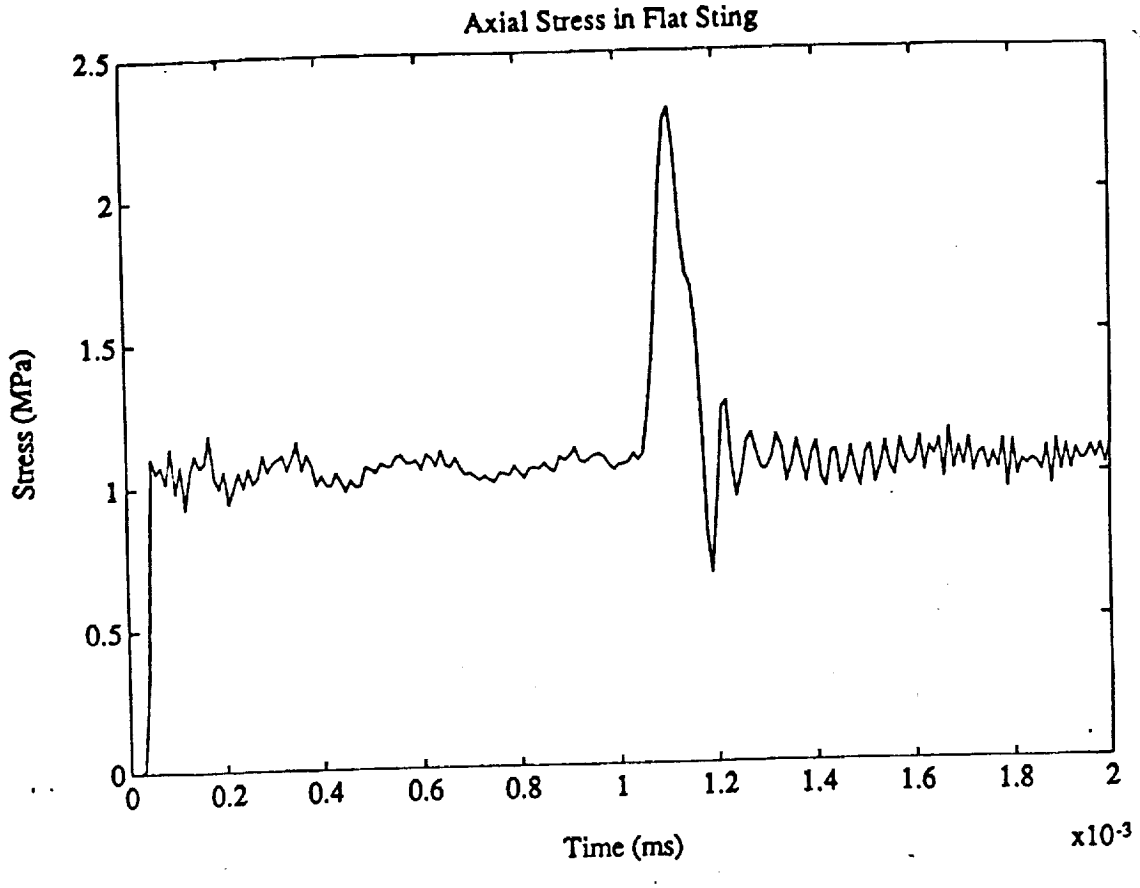


(a)

(b)

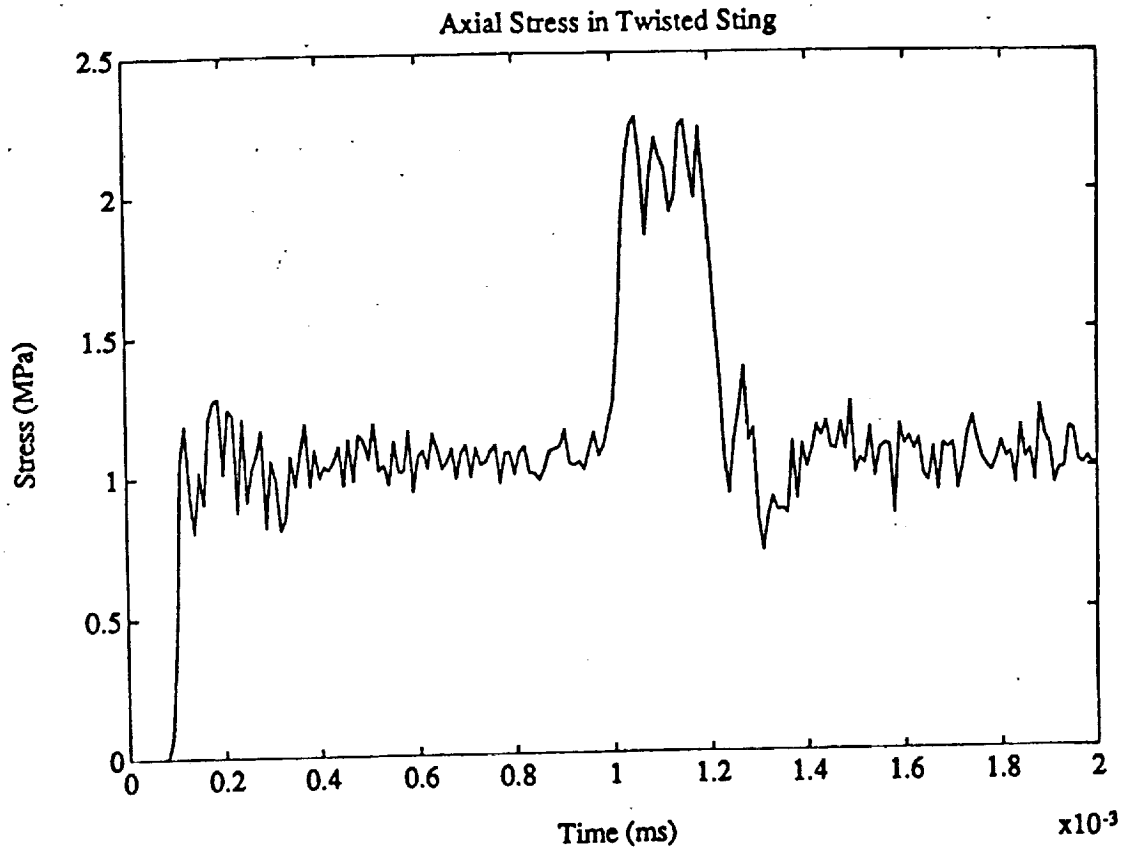


Figure 3. Sting Step Responses

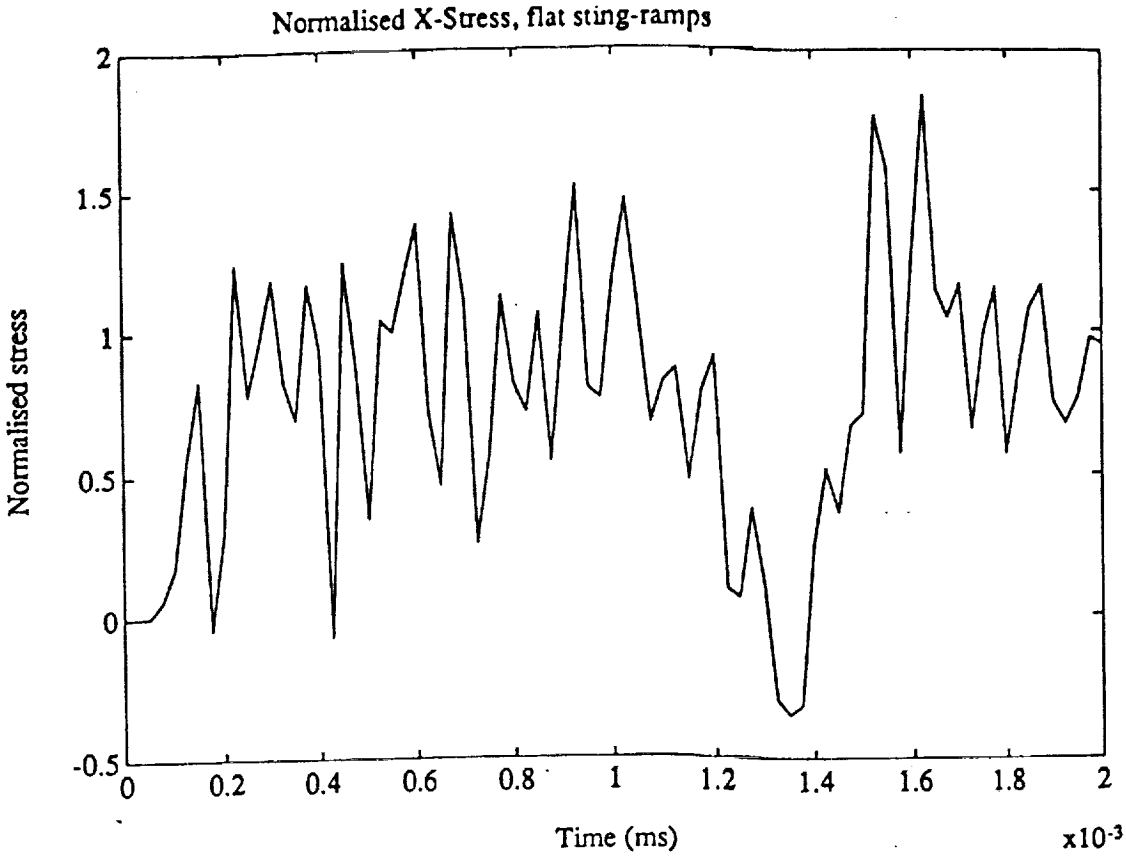


Figure 4.

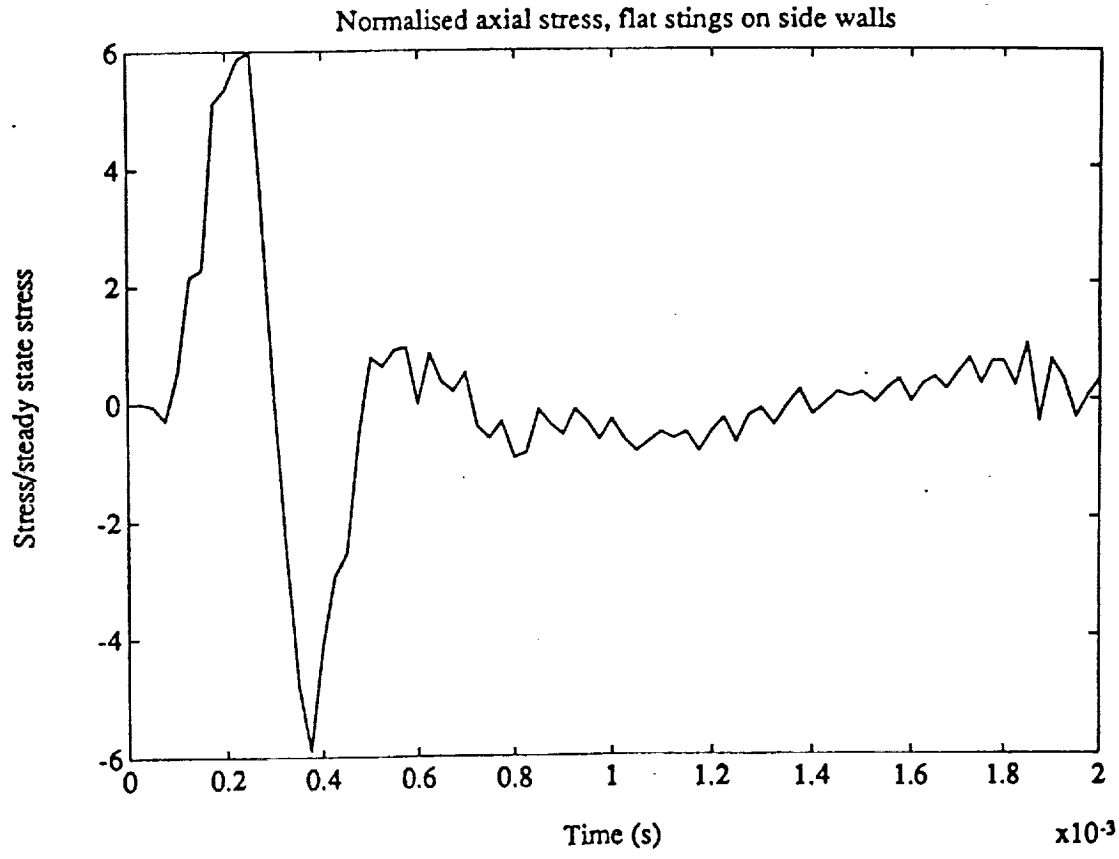


Figure 5.

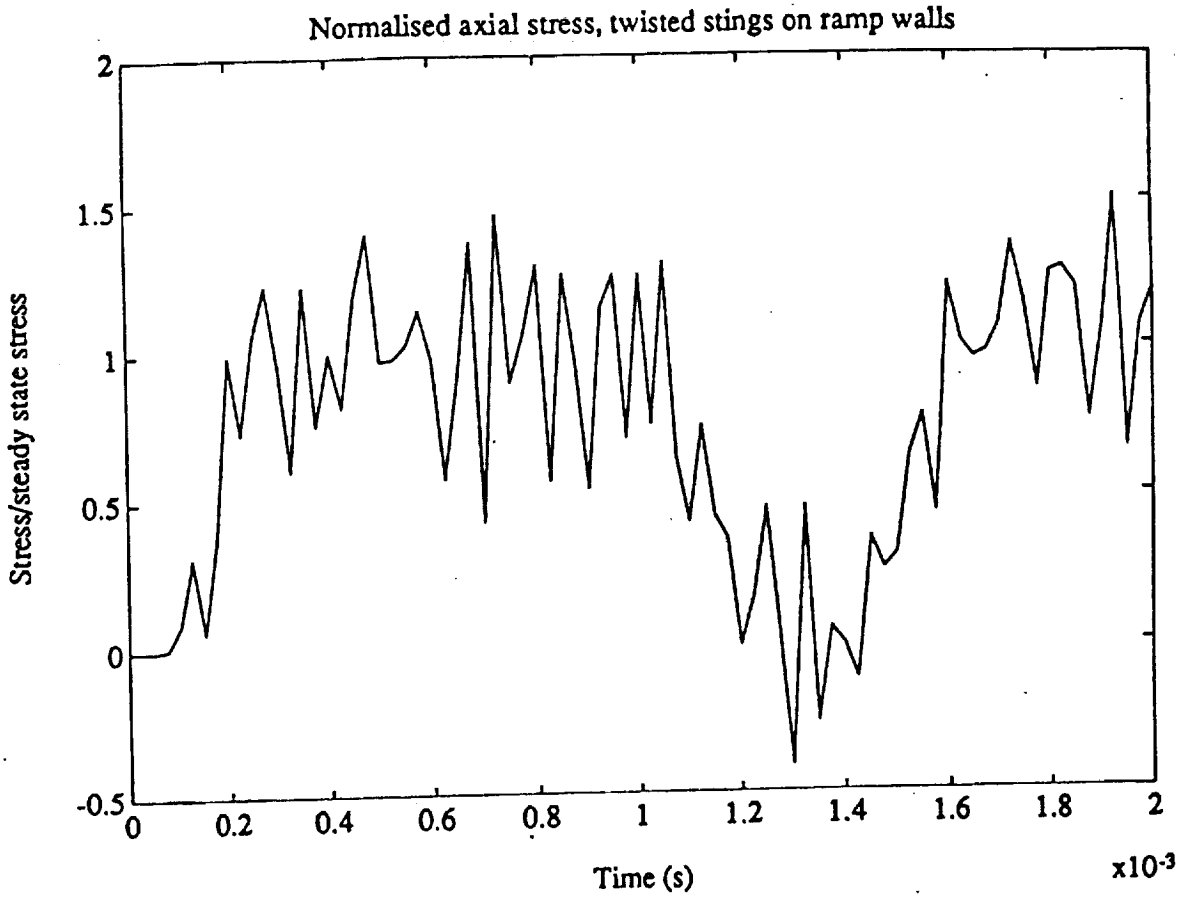
Normalised axial stress, twisted stings on ramp walls
Stress/steady state stress
2
1.5
1
0.5
0
-0.5
0
0.2
0.4
0.6
0.8
1
1.2
1.4
1.6
1.8
2
Time (s)
x10-3

Figure 6.

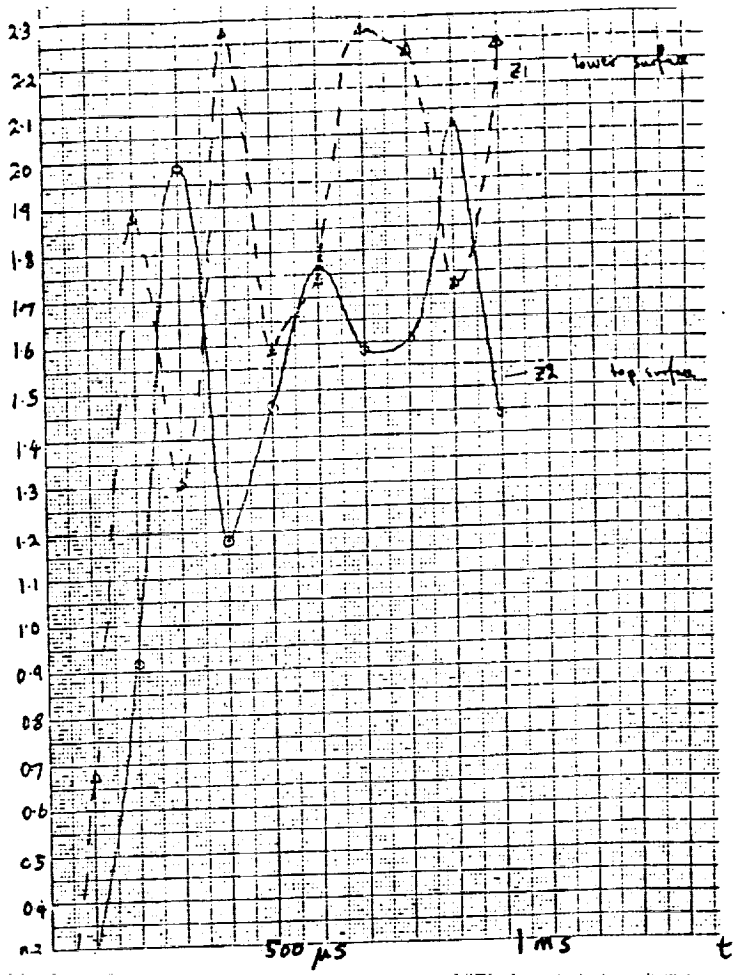
Z1
lower surface
Z2
top surface
500 μs
1ms
time

(a)

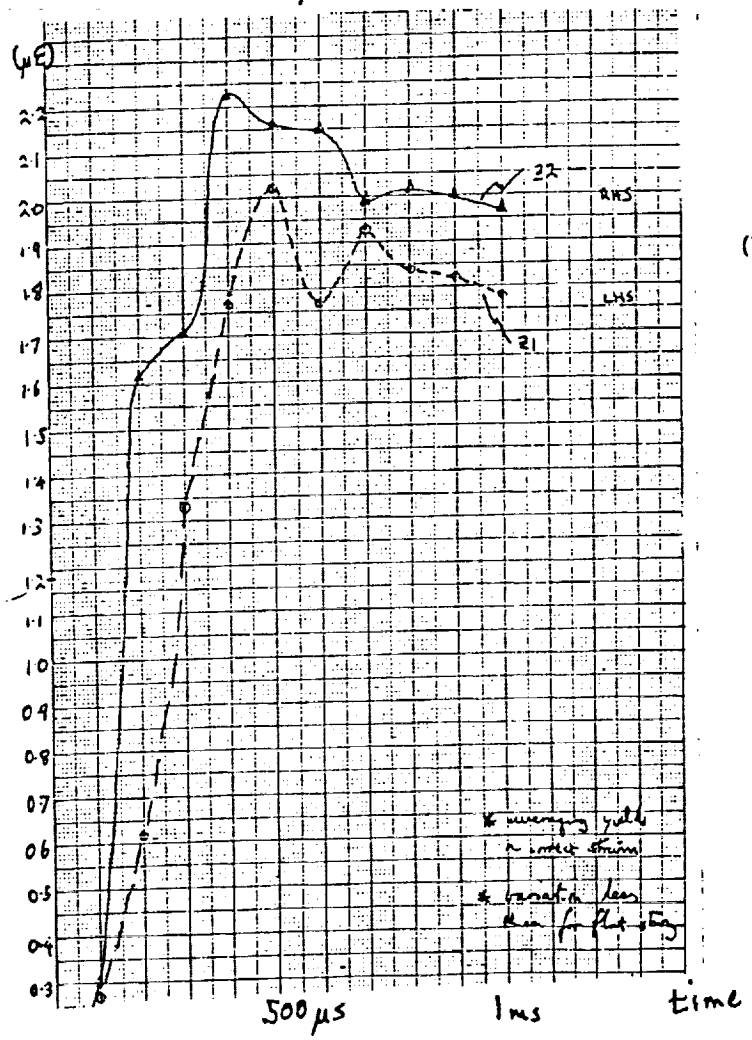
(με)
Z2
RHS
LHS
Z1
500 μs
1ms
time

(b)

Figure 7.

## Further Numerical Studies of the Wall-Injected Scramjet

Craig P. Brescianini

Work over the past year has consisted largely of analyzing the T4 wall-injected scramjet experiments which were performed earlier. This analysis was performed predominantly with a new CFD code developed by the present author, and described in Ref. 1. The code is a two-dimensional, parabolic Navier-Stokes solver, which uses the method of Patankar and Spalding (Ref. 2) to solve the differential equations. The code handles turbulent flow with a compressibility modified k-ε model (Ref. 3), and allows for multi-reaction, finite-rate chemistry. Chemistry is based upon the NASP "Hypersonic Combustion Kinetics" mechanism and rate constants recommended in Ref. 4. An attempt was made to truly "predict" the T4 experimental results without any adjustments of model constants from one flow to the next. Due to the two-dimensional nature of the computations, comparisons of experimental and numerical results had to be limited to flow configurations which did not use "mixers" or transverse (from a single orifice) injection of fuel.

The numerical code proved to be able to predict whether or not significant pressure rises were likely, and also predicted the heat-transfer rates to the scramjet wall within acceptable accuracy. The shape of the pressure distribution along the wall, however, was not well predicted. The reasons for this were difficult to identify without flow visualization. The numerical study indicated that combustion within the scramjet model was mixing limited. At some low-enthalpy conditions, however, finite-rate chemistry was also found to be responsible for reducing the overall combustion levels. A correlation of computed film-cooling lengths (which included simulations of experiments performed in T3, T4, and Calspan) indicated a reasonable correlation with the mass-flux ratio, $(\rho u)_j/(\rho u)_\infty$, indicating that this parameter is important for determining the near-field mixing rates.

Current CFD thus proved itself a valuable engineering tool, capable of assisting experimenters with the analysis of scramjet data. Full details of the experimental data, and the numerical/experimental comparisons, are available in Ref. 1.

1. Brescianini, C.P. (1992), "An Investigation of the Wall-Injected Scramjet," Ph.D. Thesis (submitted), Dept. of Mechanical Eng., University of Queensland.

2. Patankar, S.V., and Spalding, D.B. (1970), *Heat and Mass Transfer in Boundary Layers*, Second ed., Int. Textbook Co. Ltd. (London)

3. Brescianini, C.P. (1992), "A Modified k-ε Model for Compressible Free Shear Flows," accepted for publication in the *AIAA Journal*. (Also appears in this report).

4. Oldenborg, R., Chinitz, W., Friedman, M., Jaffe, R., Jachimowski, C., Rabinowitz, M., and Schott, G. (1990), "Hypersonic Combustion Kinetics," Status Report of the Rate Constant Committee, NASP High-Speed Propulsion Technology Team, NASP TM-1107.

# A Modified k-ε Model for Compressible Free Shear Flows

C. P. Brescianini[1]

University of Queensland, Brisbane, Queensland, Australia

## Introduction

In the landmark conference on turbulent free shear flows, held at the NASA Langley Research Center in 1972 [1], the k-ε model emerged as one of the most capable of the turbulence models available at the time[2]. However, one deficiency of the k-ε model was also brought to light. Namely, the inability to predict the experimentally observed[3] decrease in the spreading rate of turbulent, supersonic, free shear layers as the Mach number was increased. A modification to the k-ε model is proposed here which helps remove this deficiency.

## Theory

Modifications to the k-ε model to account for compressibility effects have been proposed in the past by Dash[4] , and Chuech[5] among others. Sarkar[6] and Zeman[7] have recently proposed dissipation models which account for compressibility effects. The adaptation of these ideas to the k-ε model is also straight forward. An alternative approach is presented here, based upon a recent suggestion by Kim[8].

Kim proposed a simple modification to another turbulence model, the Prandtl mixing length hypothesis (MLH). The MLH involves evaluating the turbulent viscosity by using a "mixing length", $\ell_m$. This mixing length is usually computed by setting it equal to a constant fraction of some characteristic width, $y_G$, such that

$$\ell_m = \lambda\, y_G \tag{1}$$

where $\lambda$ is a constant. For incompressible free shear layers $y_G$ is customarily taken as the width of the shear layer, b , usually defined by

$$y_G = b = | y_{0.9} - y_{0.1} | \tag{2}$$

---

1 graduate student. Department of Mechanical Engineering.

where at $y_{0.1}$ , $u^* = 0.1$, and at $y_{0.9}$, $u^* = 0.9$, where $u^* = (u-u_2)/(u_1-u_2)$. Here u is the velocity, y is the transverse distance, and the subscripts 1 and 2 represent the high and low velocity sides of the shear layer respectively.

Kim, however, proposed a modified formula and a different characteristic width, $y_s$ , defined by

$$y_s = | y_a - y_b | \tag{3}$$

The locations of $y_a$ and $y_b$ were defined by points where sonic flow exists relative to the local point, as shown in Fig. 1. (In Fig. 1 *a* is the local speed of sound). Limitations were placed on $y_a$ and $y_b$ in that these locations could not exceed the edges of the shear layer.

In the "standard" high Reynolds number k-ε model (designated the kεl model in Ref.2), the turbulent viscosity is computed from

$$\mu_t = C_\mu \rho \left( \frac{k^2}{\varepsilon} \right) \tag{4}$$

where $C_\mu$ is a constant, $\rho$ is the density, k is the turbulent kinetic energy, and ε is the turbulent kinetic energy dissipation rate. The values for k and ε are determined by solving a pair of partial differential transport equations. Comparing Eq.(4) with the Prandtl-Kolmogorov formula

$$\mu_t = \rho \sqrt{k}\, \ell \tag{5}$$

where $\ell$ is the length scale, shows that the length scale used in the kεl model is determined from the relationship

$$\ell_\varepsilon = C_\mu \frac{k^{1.5}}{\varepsilon} \tag{6}$$

Now, a new length scale, based upon the characteristic width $y_s$, can also be defined by

$$\ell_s = \lambda_s y_s \tag{7}$$

where $\lambda_s$ is a new model constant. If no relative supersonic flow exists in the layer, $\lambda_s$, is set equal to unity.

It is now proposed that the length scale for use in the modified k-ε model be taken as the smallest length scale determined from Eqs.(6) and (7). Should the local length scale from Eq.(7), be smaller than the usual value

from Eq.(6), then the reduced length scale needs to be introduced into the k-ε model. From Eq.(6), this can be very easily accomplished by either reducing $C_\mu$ or increasing ε. The approach adopted here was to increase ε. Consequently, the dissipation rate in the modified model was computed from

$$\varepsilon = \text{MAX}\left[ \varepsilon_{\substack{\text{from transport} \\ \text{equation}}}, \; C_\mu \frac{k^{1.5}}{\ell_s} \right] \tag{8}$$

It is interesting to note that under conditions where the length scale is effectively determined by Eq.(7), the original two-equation k-ε model is effectively reduced to a one-equation k model (see eg. Ref. 2) where the length scale is now determined algebraically.

## Results

The constant $\lambda_s$ was selected by matching the calculated spreading rate parameter of a Mach 5, single stream, air free shear layer with the experimentally observed value[3] of 37. This resulted in a value for $\lambda_s$ of 0.0445 .

To test the modified k-ε model (here after designated the $k\varepsilon l_{cc}$ model) the spreading rate of various single stream, air mixing layers (including a sample of those compiled for the Langley conference) were computed with the following assumptions

$$p = \text{constant} \; , \; T_{t1} = T_{t2} \; , \; Pr = Pr_t = 0.7 \; , \; T_1 = 300 \text{ K} \; , \; u_2/u_1 = 0$$

where p is the static pressure, $T_t$ and T are the total and static temperatures respectively, and Pr and $Pr_t$ are the laminar and turbulent Prandtl numbers. The computed spreading parameter was determined from the following formula (as required of the "predictors" at the NASA Langley conference)

$$\sigma = 1.855 \frac{1}{db/dx} \tag{9}$$

where b is defined by Eq.(2). The numerical computations were performed using a two-dimensional parabolic Navier-Stokes program described in Ref. 9. The "standard" high Reynolds number k-ε model constants[2] have been used.

Figure 2 shows the computed variation in σ with free stream Mach number, $M_1$. The agreement between the $k\varepsilon l_{cc}$ model and the experimental data compiled for the Langley Conference is excellent. The standard model, in comparison, displays virtually no variation in spreading parameter with Mach number.

Recently, there has been much success at correlating the spreading rates of two stream supersonic shear layers by using the convective Mach number, $M_c$, as proposed by Bogdanoff[10] and Papamoschou and Roshko[11]. Figure 3 shows a selection of experimental normalized growth rates versus $M_c$ as compiled by Samimy and Elliott[12]. The normalized growth rate is obtained by dividing the experimentally observed growth rate of the compressible shear layer (here defined as $\delta = db/dx$) by the so called "incompressible" growth rate, $\delta_1$, which would be observed in a subsonic shear layer with the same velocity and density ratios. The incompressible values are usually estimated by the formula[11]

$$\delta_1 = \left( \frac{db}{dx} \right)_1 = \frac{C_\delta}{2} \frac{\left( 1 - \frac{u_2}{u_1} \right) \left( 1 + \sqrt{\rho_2 / \rho_1} \right)}{1 + \frac{u_2}{u_1} \sqrt{\rho_2 / \rho_1}} \qquad (10)$$

where $C_\delta$ is a constant. To compare the computed results presented here with those obtained experimentally, the computed spreading rates have been similarly divided by the value of $\delta_1$ determined from Eq.(10). The presentation of the results in this way differs from the common practice of dividing the predicted compressible spreading rates by the predicted incompressible ones. It was felt that using Eq.(10) to evaluate $\delta_1$ provided a better comparison with the experimental data, which had been analyzed in a similar fashion. To normalize the computed spreading rates a value of $C_\delta$ = 0.165 was used in Eq.(10), so that $\delta_1$ = 0.165 when $u_2/u_1$ = 0 and $\rho_2/\rho_1$ = 1 in agreement with the recommendations of Rodi[13].

The numerical computations were performed with air in both streams and the following assumptions

$$p = \text{constant} \ , \ T_{t1} = T_{t2} \ , \ Pr = Pr_t = 0.7 \ , \ T_1 = 300 \text{ K} \ , \ u_2/u_1 = 0.25$$
$$Re_{u,1} = 4.4 \times 10^7 \text{ m}^{-1}$$

where $Re_u$ is the unit Reynolds number. The results, also shown in Fig. 3, show that the $k\varepsilon l_{cc}$ model predicts the same trend as the experimental data. The significant improvement over predictions obtained with a standard $k\varepsilon l$ model are immediately obvious.

## Conclusion

A modification to the two-equation $k\varepsilon l$ model was proposed which effectively reduces the model to a one-equation k model in highly

compressible flows. The modification has been shown to improve the prediction ability of the kε1 model when it is applied to supersonic shear layers.


## Acknowledgments

The author gratefully acknowledges the support given by the Australian Research Council and by the NASA Langley Research Center, Hypersonic Propulsion Branch, through NASA Grant NAGW-674.


## References


[1]*Free Turbulent Shear Flows*, NASA SP-321, 1973.

[2]Launder, B.E., Morse, A., Rodi, W., and Spalding, D.B., "Prediction of Free Shear Flows. A Comparison of the Performance of Six Turbulence Models," NASA SP-321, 1973, pp. 361-426.

[3]Birch, S.F. and Eggers, J.M., "A Critical Review of the Experimental Data for Developed Free Turbulent Shear Layers," NASA SP-321, 1973, pp. 11-40.

[4]Dash, S.M., Weilerstein, G., and Vaglio-Laurin, R.," Compressibility Effects in Free Turbulent Shear Flows," AFOSR-TR-75-1436, 1975.

[5]Chuech, S.G., Lai,M.-C., and Faeth, G.M.," Structure of Turbulent Sonic Underexpanded Free Jets," *AIAA Journal*, Vol. 27, 1989, pp. 549-559.

[6]Sarkar, S., Erlebacher, G., Hussaini, M.Y., and Kreiss, H.O., "The Analysis and Modeling of Dilatational Terms in Compressible Turbulence," *Journal of Fluid Mechanics*, Vol. 227, 1991, pp. 473-493.

[7]Zeman, O., "Dilation Dissipation. The Concept and Application in Modeling Compressible Mixing Layers," *Physics of Fluids A*, Vol. 2, 1990, pp. 178-188.

[8]Kim, S.C., "New Mixing-Length Model For Supersonic Shear Layers", *AIAA Journal*, Vol. 28, 1990, pp. 1999-2000.

[9]Brescianini, C.P., Morgan, R.G., and Stalker, R.J., "Numerical Modeling of Sidewall Injected Scramjet Experiments in a High Enthalpy Airflow," Shock Tunnel Studies of Scramjet Phenomena- Supplement 6, Dept. of Mechanical Engineering, University of Queensland Report, 1990.

[10]Bogdanoff, D.W., "Compressibility Effects in Turbulent Shear Layers," *AIAA Journal*, Vol. 21, 1983, pp. 926-927.

[11]Papamoschou, D. and Roshko, A., "The Compressible Shear Layer: an Experimental Study," *Journal of Fluid Mechanics*, Vol. 197, 1988, pp.453-477.

[12]Samimy, M., and Elliott, G.S., "Effects of Compressibility on the

Characteristics of Free Shear Layers," *AIAA Journal*, Vol. 28, 1990, pp. 439-445.

[13]Rodi, W., "A Review of Experimental Data for Uniform Density Free Turbulent Boundary Layers," *Studies in Convection*, Vol. 1, Academic Press, London, 1975, pp. 79-165.

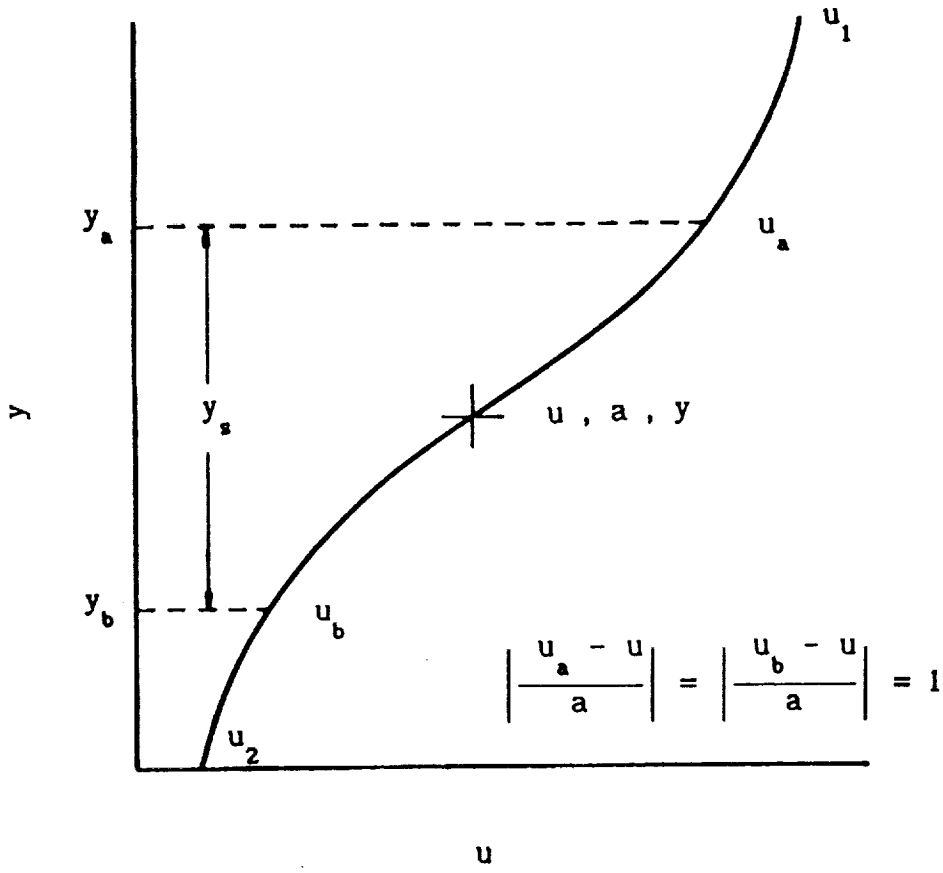


Fig.1 Characteristic Width for Supersonic Shear Layers *(after Kim[8] )*.

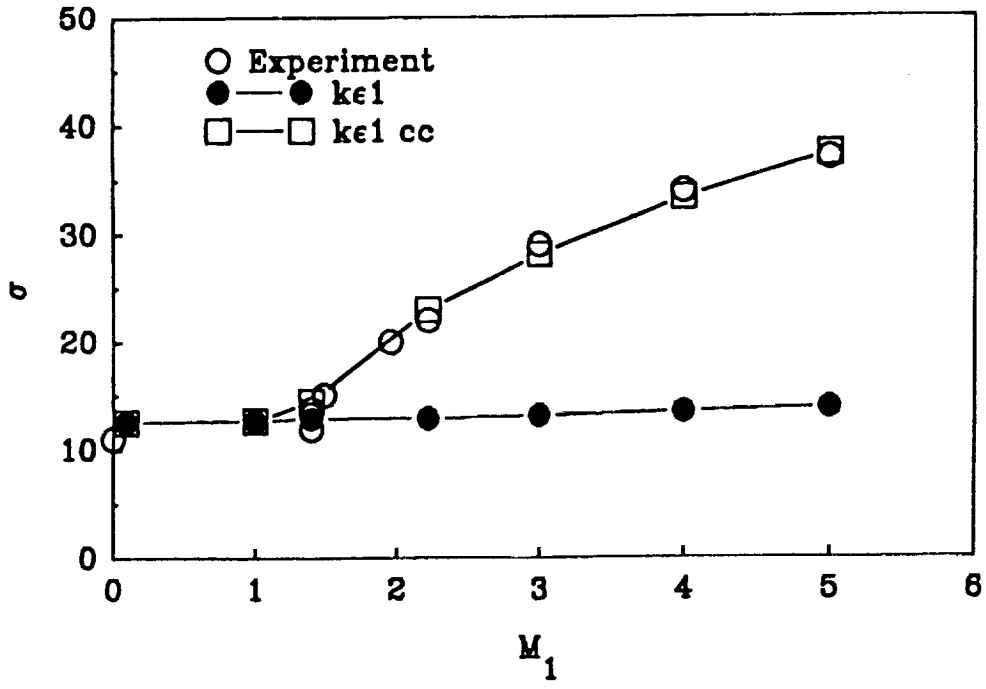


Fig.2 Variation of Spreading Parameter with Mach Number.

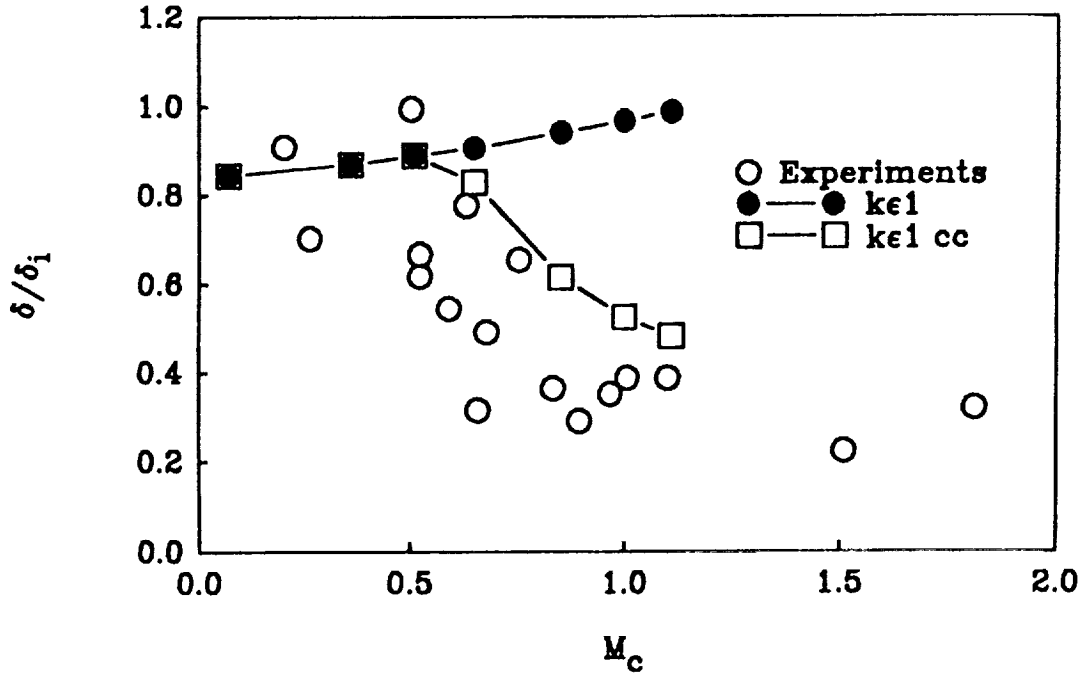


Fig.3 Variation of Normalized Shear Layer Growth Rate with Convective Mach Number.

# Pressure Scaling in a Scramjet Engine

by Maria V. Pulsonetti

At present there is no facility capable of testing a full size scramjet engine. Therefore a way is needed to relate the data we get by testing scaled down models to a full size scramjet engine. Ramjet engine data scaled with a pressure-length scaling factor, meaning that keeping all other properties the same(like Mach number, velocity, species concentrations, etc.) the data would scale the same for twice the pressure and half the length. This was thought to be due to viscous effects. In a scramjet engine, however, there are a number of factors that can affect the scaling, the most important of which are the viscous effects, the ignition time, and the complete reaction time. What is needed to be known is which effect dominates.

Viscous effects, or boundary layer effects, scale with Reynolds number. With Mach number, velocity, entropy, and species concentrations held constant, viscous effects will scale by the pressure-length factor.

$$R_e = \frac{\rho u x}{\mu}$$

$$R_e = (p x) T^{-1.2} M \sqrt{\frac{\gamma}{R}} \frac{T_o^{0.7}}{\mu_o}$$

The ignition reaction is a two body reaction. Thus it may be shown that the fractional change in concentration of one of the reactants is directly proportional to the concentration of the other. One may then integrate to find the relative reaction rate is proportional to the concentration of one of the reactants and thus the pressure. Hence ignition length will scale by the factor pressure-length.

$$A + B \xrightarrow{k_f} C + D$$

$$\frac{dC_A}{C_A} = - k_f C_B \, dt$$

$$\tau_{ig} \propto \frac{1}{C_B}$$

$$\tau_{ig} \propto \frac{1}{P}$$

The final combustion reaction which finally produces $H_2O$ is a three-body reaction. In an analogous analysis to the two-body ignition reaction it may be shown that the relative reaction rate will be proportional to the concentration squared and thus to pressure squared. Thus the reaction length will scale by the factor pressure squared-length.

$$A + B + C \xrightarrow{k_f} D + E$$

$$\frac{dC_A}{C_A} = - k_f C_B \, C_C \, dt$$

$$\tau_{ig} \propto \frac{1}{C_B C_C}$$

$$\tau_{ig} \propto \frac{1}{P^2}$$

Mixing and combustion experiments have been performed in the University of Queensland's reflected shock tunnel (T4) using a 1.32 metre long scramjet model. This model is the largest of the scramjets to be tested in this study. The model was two-dimensional with a duct height of 48mm and a width of 100 mm. It was instrumented with thirty PCB pressure transducers to read static pressure and twelve thin film heat flux gauges manufactured at the University. Figure 1 shows the PRELIMINARY estimates of the eight test conditions used. Stagnation enthalpy was varied from 3-12 MJ/kg causing variations in static temperature and velocity in the model from 740-2200K and 2.5-4.1 km/s, respectively. Stagnation pressure was varied from 15-60 MPa causing variations in static pressure in the model from 7-25 KPa. Please recall, however, that these values are only preliminary since the final data reduction has not been completed yet. Table 1 shows a very rough estimate of a number of properties at the eight test conditions. In all cases ignition was achieved.

Figure 2 shows the variation of ignition times with stagnation enthalpy. Note how the ignition time decreases with increasing stagnation enthalpy except for the lowest stagnation enthalpy. This trend agrees with the empirical relation for ignition time by Harold Pergament[1] which follows.

$$\tau_{ig} = \frac{l_{ig}}{V} = \frac{8 \times 10^{-9}\, e^{(9600/T)}}{P}$$

The values predicted, however, do not match exactly. Table 2 shows the difference between the experimental values of ignition time obtained in the large model and the empirical relation. At condition B to E the empirical relation under predicts the ignition time. It is unclear at present why the ignition time at condition A is so low because the condition A runs have not been reduced as yet. It was also observed that the pressure rise due to combustion decreased with increasing stagnation enthalpy as was expected.

Figure 3 shows the variation of ignition time with stagnation pressure. The predicted trend of decreasing ignition time with increasing stagnation pressure is observed for all four conditions. The results, however, were quite surprising at the lower pressures (conditions F and G) because the empirical relation of ignition time listed above predicted that ignition would not occur in the available model length. Table 3 shows the difference between the experimental values of ignition time obtained in the large model and the empirical relation.

At the lower pressures (conditions F and G) where combustion was observed unexpectedly, one possible explanation is that the flow might not have been steady. For the runs I have examined the flow was steady. Figure 4 shows pitot pressure at the nozzle exit, static pressure at the start of the duct and static pressure at the end of the duct all normalized by stagnation pressure vs. time for a combustion run at condition F. The appropriate time delays were used to ensure that at any time the traces are normalized by the correct stagnation pressure and all traces are in shock fixed coordinates. The time I choose is marked on the graph. Note how the three traces are reasonably steady at that time. Figure 5 shows the corresponding pressure distribution in the duct for the combustion run and a mixing run at condition F. From this figure it is clear to see combustion has occured.

Designs are presently underway for the manufacture of the smallest scramjet in this study. This scramjet will be one fifth the size of the large scramjet with a 2 mm injector. Experiments are scheduled for the end of this year or the beginning of next year.

[1]Pergament, Harold, "A Theoretical Analysis of Non-Equilibrium Hydrogen-Air Reactions in Flow Systems", AIAA, 1963

Table 1 : Preliminary Estimate of Test Conditions in Large Scramjet

| | A | B | C | D | E | F | G | H |
|---|---|---|---|---|---|---|---|---|
| $M_{air}$ | 4.53 | 4.37 | 4.37 | 4.29 | 4.31 | 4.41 | 4.42 | 4.41 |
| $P_{T_{air}}$ (MPa) | 84 | 61 | 52 | 86 | 78 | 18 | 30 | 47 |
| $H_{Tair}$ (MPa) | 3.8 | 5.8 | 7.8 | 9.4 | 12 | 5.8 | 5.6 | 6.0 |
| $P_{air}$ (kPa) | 26 | 23 | 20 | 33 | 29 | 6.8 | 11 | 18 |
| $T_{air}$ (K) | 740 | 1200 | 1500 | 1900 | 2200 | 1100 | 1100 | 1200 |
| $U_{air}$ (km/s) | 2.5 | 3.0 | 3.4 | 3.7 | 4.1 | 2.9 | 2.9 | 3.0 |
| $P_{fuel}$ (kPa) | 8.1 | 5.5 | 4.1 | 6.0 | 4.8 | 1.7 | 2.9 | 4.3 |

$\phi$=1.1

$M_{fuel}$=3.41

$T_{fuel}$=89 K

$U_{fuel}$=2.4 km/s

Table 2. Experimentally and Empirically Obtained Ignition Time for Various Stagnation Enthalpys

| Condition | $H_{stag}$ (MJ/kg) | $\tau_{ig}$ (μs) (experimental) | $\tau_{ig}$ (μs) (empirical relation) |
|---|---|---|---|
| A | 3.8 | 55 | 13000 |
| B | 5.8 | 216 | 105 |
| C | 7.8 | 146 | 24 |
| D | 9.4 | 48 | 4 |
| E | 12 | 24 | 2 |

Table 3. Experimentally and Empirically Obtained Igniton Times for Various Stagnation Pressures

| Condition | $P_{stag}$ (MPa) | $\tau_{ig}$ (μs) (experimental) | $\tau_{ig}$ (μs) (empirical relation) |
|---|---|---|---|
| F | 18 | 304 | 735 |
| G | 30 | 263 | 455 |
| H | 47 | 223 | 134 |
| B | 61 | 216 | 105 |

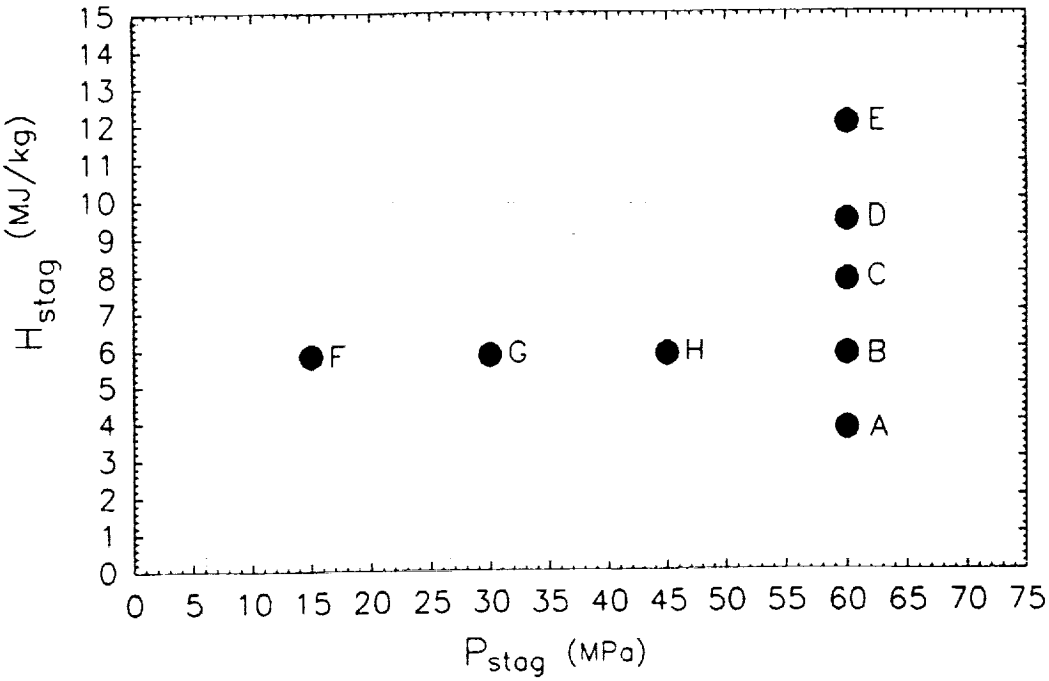


Figure 1. Test conditions in T4 for large scramjet tests

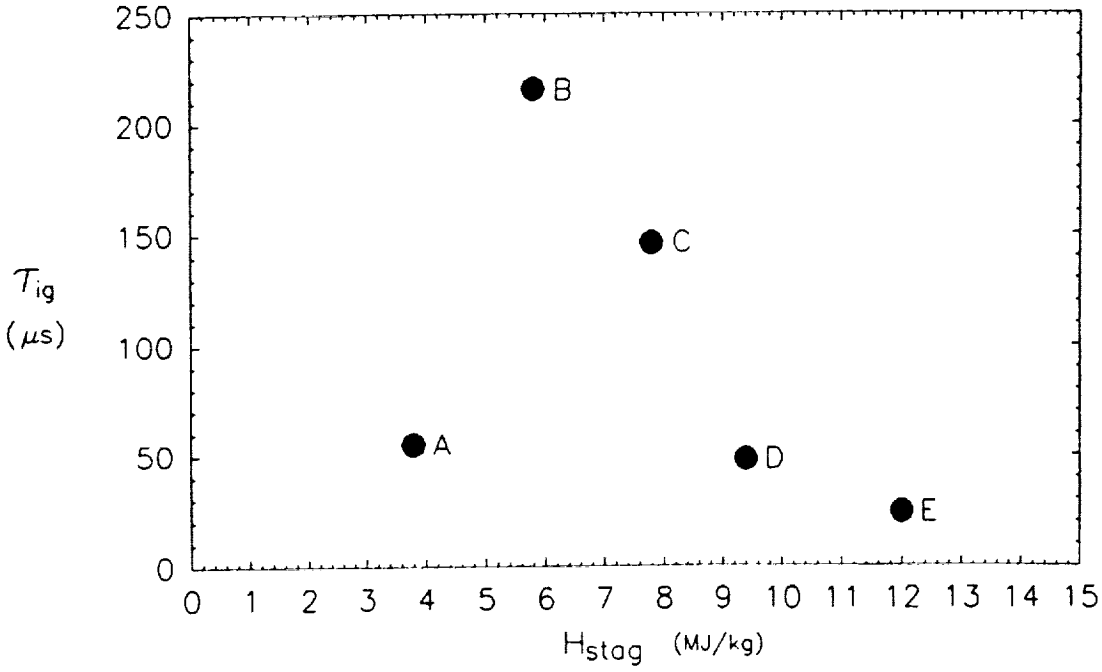


Figure 2. Variation of Ignition Time with Stagnation Enthalpy

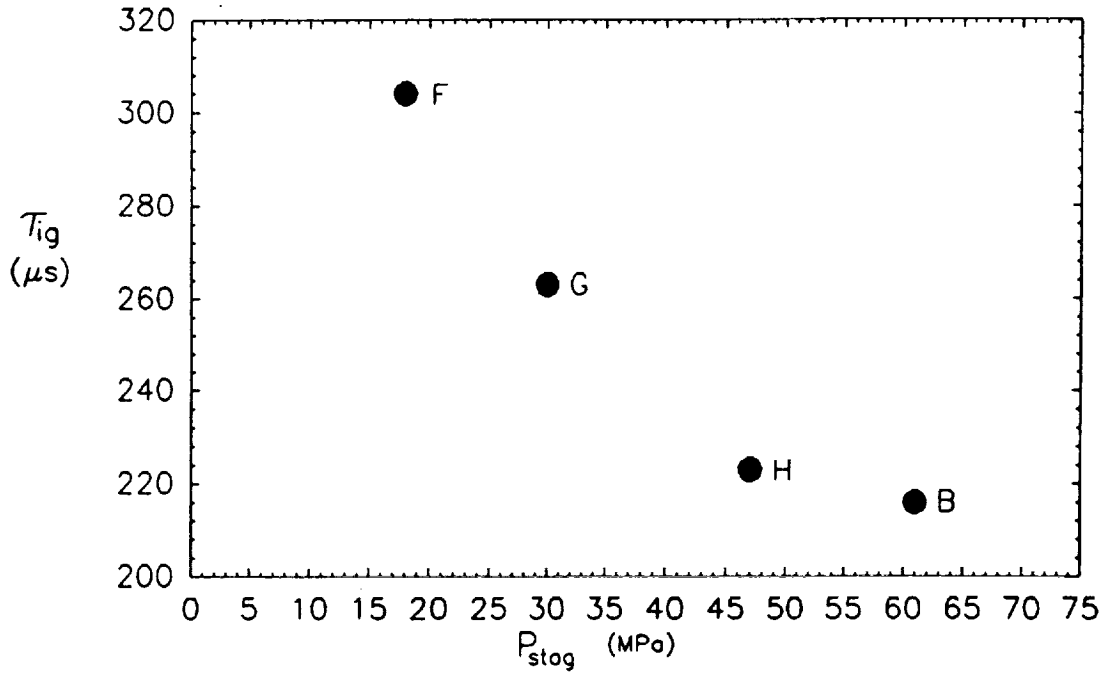


Figure 3. Variation of Ignition Time with Stagnation Pressure

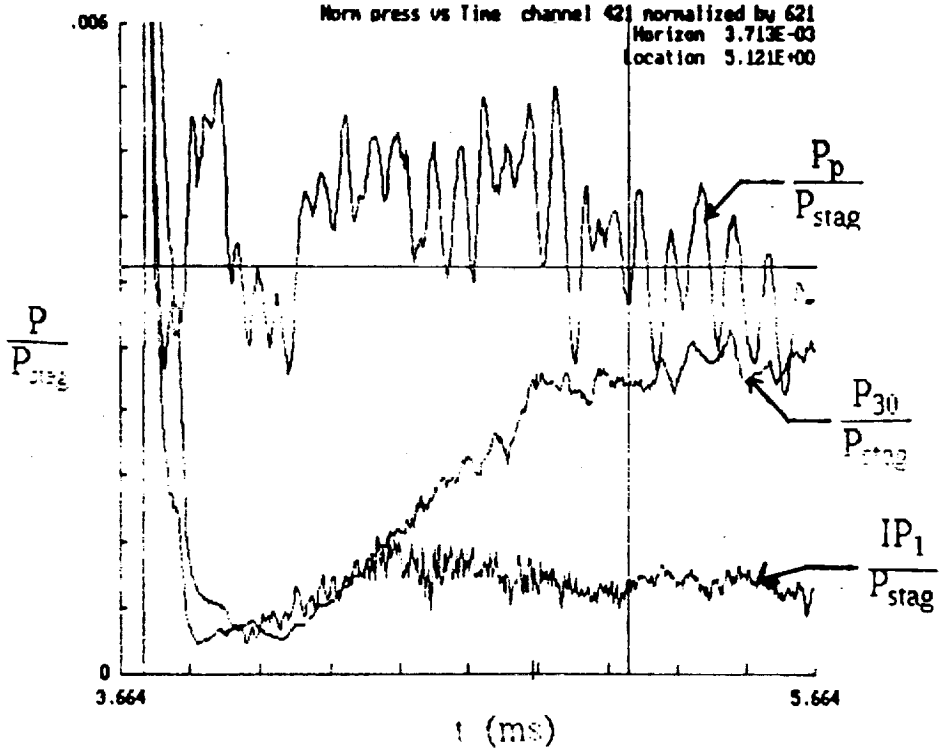


Figure 4. Pitot($P_p$), static pressure at the start of the duct($IP_1$) and static pressure at the end of the duct($P_{30}$) traces normalized by stagnation pressure

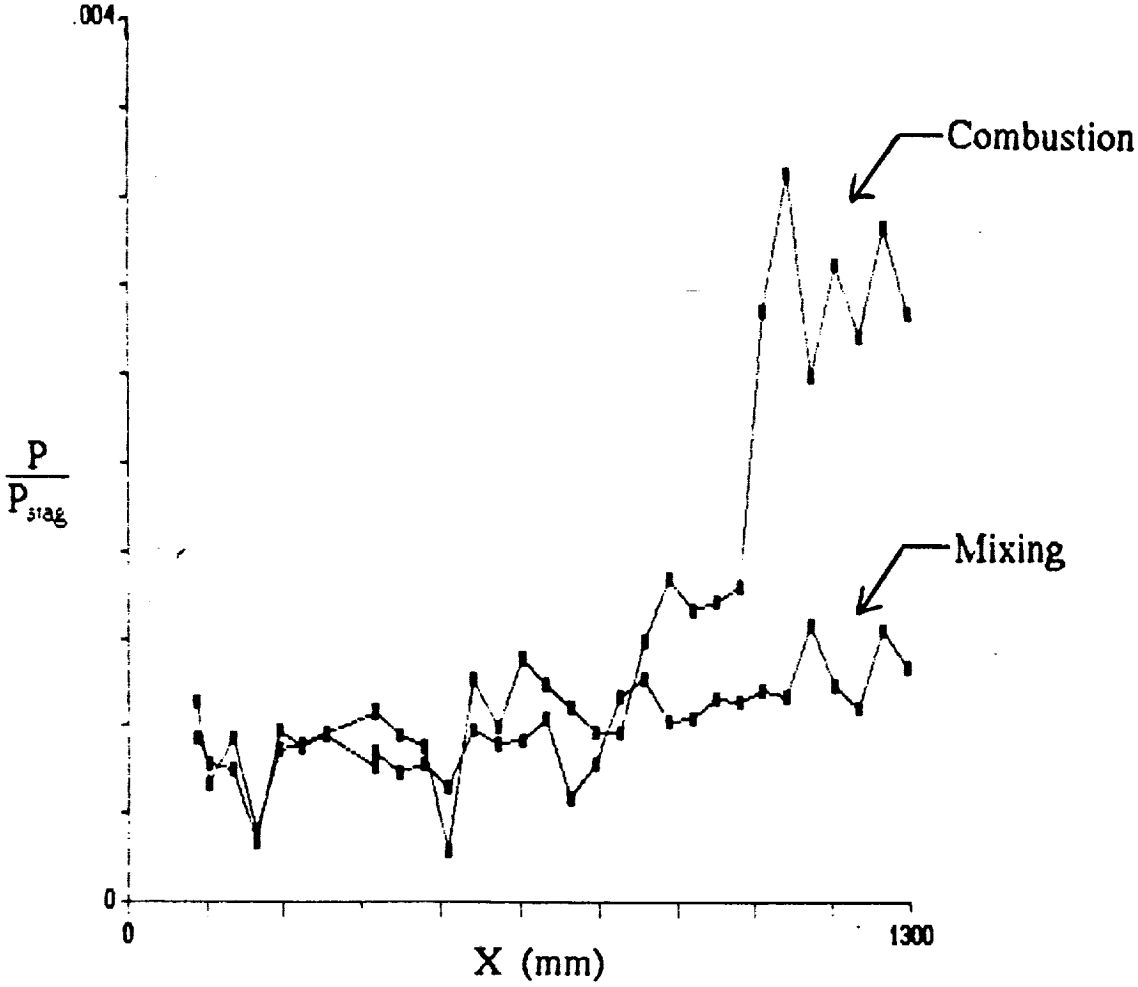


Figure 5. Pressure distributions for a combustion and mixing run at condition F

# SHOCK WAVE IMPINGEMENT ON MIXING REGIONS

DAVID BUTTSWORTH

## INTRODUCTION

The desire to develop a practical scramjet cycle has lead many researchers to focus their attention on the mixing behaviour of supersonic streams. Theoretical and experimental studies have suggested that that the mixing properties of two co-flowing supersonic stream may be controlled by a parameter called the convective Mach number ($M_c$). Results from the recent studies have shown the spreading rate of a compressible mixing layer, relative to its incompressible counterpart, to decrease with increasing $M_c$. Due to the low residence time of the fuel in the scramjet combustor, high mixing and combustion rates will be necessary in order to achieve an effecient system. Various methods have been proposed to enhance the mixing of two supersonic streams. One such method currently receiving attention is shock wave impingement. Computational studies have revealed that a shock wave impinging on a shear layer may favorably alter the turbulence properties and therefore enhance the mixing downstream. Additionally, in a recent experimental study[1], increased turbulent activity was attributed to "...the interaction of the reflected shock wave...and the confined mixing region." However, for the cases reported in ref 2, there appears to have been little sustained improvement in growth rate due to various modes of shock wave impingement.

Instead of attempting to model or investigate the affect that a shock wave has on the turbulence properties in a supersonic mixing region, a mean flow field approach has been taken. The mixing region is modelled simply as a Mach number gradient. The Rankine-Hugoniot shock wave equations demonstrate that the flow downstream of the shock wave can be determined (in terms of upstream properties) provided the upstream Mach number ($M_1$) and the shock wave angle ($\theta$) are known. Assuming the pressure is constant across the mixing region ahead of the shock wave and using the condition that the pressure and flow direction behind the shock wave can only vary in a continuous manner, it is possible to derive the following equation.

$$\begin{aligned}\frac{d\theta}{dM_1} = -\Big\{ & 4 M_1 \sin^2\theta - 2 M_1 (\gamma+1) \tan\theta \tan\omega \\ & + 4 M_1 \sin^2\theta \tan\theta \tan\omega - 8 M_1 A \sin^2\theta \tan\omega \\ & + 8 M_1 \sin^2\theta \tan\theta + 8 M_1^3 A \sin^4\theta \tan\omega \\ & + 4 M_1^3 (\gamma+1) A \sin^2\theta \tan\theta - 8 M_1^3 A \sin^4\theta \tan\theta \Big\} + \\ \Big\{ & 2 \tan\theta - 2 \tan\omega + 4 M_1^2 \sin\theta \cos\theta - 2 M_1^2 \sin^2\theta \tan\theta \\ & - M_1^2 (\gamma+1) \tan\omega + 6 M_1^2 \sin^2\theta \tan\omega + 8 M_1^2 A \sin^2\theta \\ & - 8 M_1^2 A \sin\theta \cos\theta \tan\omega - 8 M_1^4 A \sin^4\theta \\ & + 8 M_1^4 A \sin^3\theta \cos\theta \tan\omega + 4 M_1^4 (\gamma+1) \sin^2\theta \Big\}, \quad \ldots (1)\end{aligned}$$

where

$$A = \frac{\sqrt{M_2^2 - 1}}{M_2^2 \left( 1 - \gamma + 2 \gamma M_1^2 \sin^2\theta \right)} .$$

$M_1$ = pre-shock Mach number
$M_2$ = post-shock Mach number
$\theta$ = shock wave angle
$\omega$ = flow deflection behind shock
$\gamma$ = ratio of specific heats

If a Mach number distribution across the mixing region is known, Eqn 1 may be integrated to yield an approximation for the shape of the shock wave. With the shape of the shock wave determinded, the flow field downstream of the shock wave is also determined.

EXPERIMENTS

In order for the pressure and flow deflection to vary in a continuous manner behind the shock wave, a series of waves must be set up to support the shock wave as it enters a changing Mach number region (Fig 1). Experiments conducted in T4 (with a general arrangement as shown in Fig 2) were aimed at measuring the strength of the waves reflected from the interaction process. In order to compare theoretical predictions (based on Eqn 1) with experimental results, it was necessary to have a Mach number distribution ahead of the shock. This distribution was obtained using a pitot probe and assuming a constant pressure across the flow. A characteristics code was written to calculate the shock shape (with an additional term due to the varying pressure field behind the shock included) and the strength of the waves reaching the shock inducing wedge. A comparison between theoretical and experimental results is given in Figs 3 to 5. The unfortunate distribution of pressure transducers on the shock inducing wedge resulted from an unexpectedly broard Mach number distribution (Fig 6).
Further experiments with transducers spread across a larger area and at different shock tunnel conditions are planned.

REFERENCES

1. Sullins, G.A., Gilreath, H.E., Mattes, L.A., King, P.S., Schetz, J.A., Instabilities in Confined Supersonic Mixing Layers, ISABE 91-7096.

2. Roy, G., Subsonic and Supersonic Mixing and Combustion Enhancemennt, ISABE 91-7093.

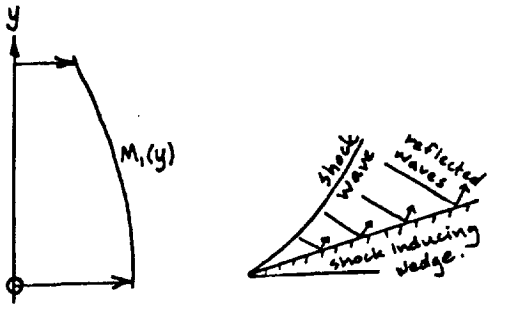


figure 1

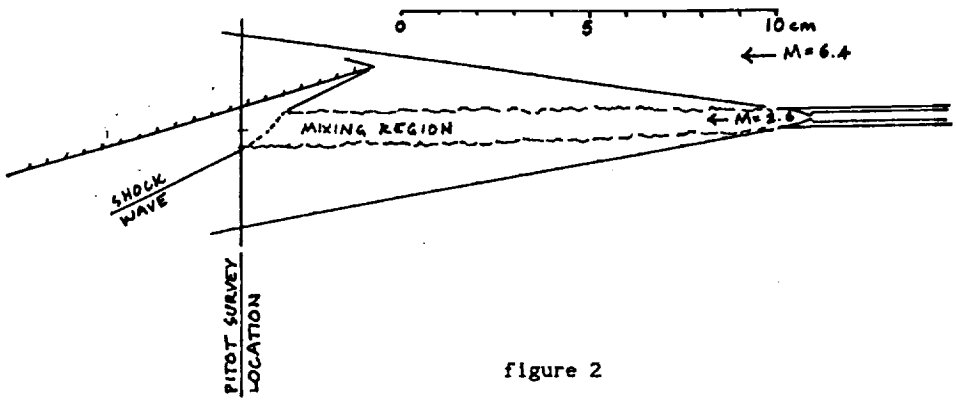


figure 2

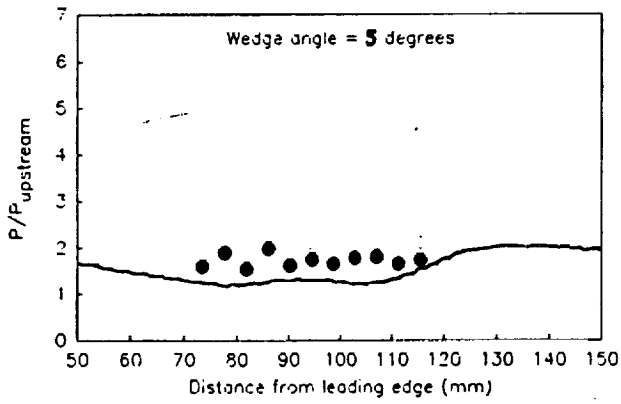


figure 3

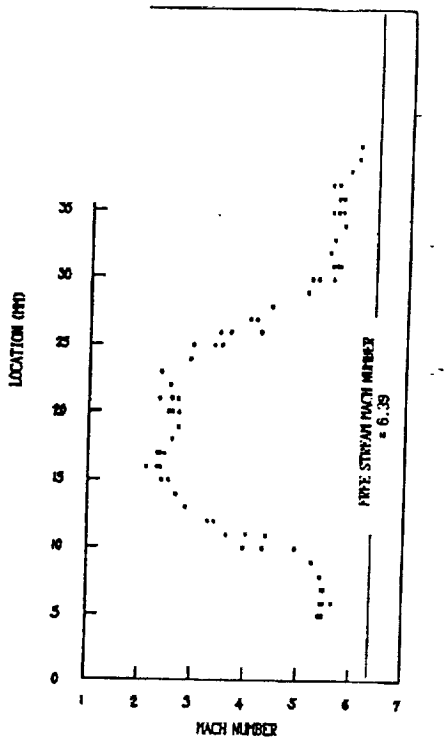


figure 6

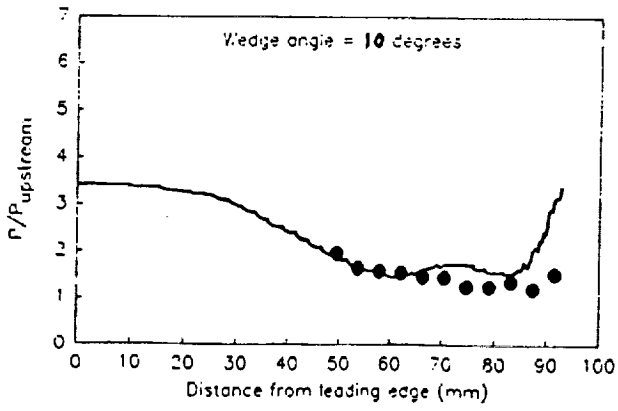


figure 4

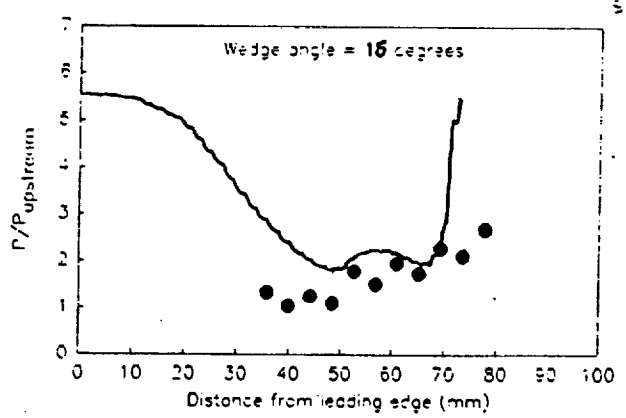


figure 5

# PROGRESS WITH ANALYSIS OF THRUST GENERATION

by

Gary A. Allen, Jr.

In an earlier study a two dimensional wave model describing thrust production in a scramjet was developed. This model was analyzed using the nonhomentropic method of characteristics assuming a two dimensional steady flow for a perfect gas with a ratio of specific heats consistent with partially disassociated air. The scramjet was assumed to be a square rectangular duct with central injection. At the end of the rectangular duct was a flat diverging section which acted as a thrust surface for the scramjet. The flow downstream from the fuel injector but just upstream from the diverging section was described by a guassian Mach number distribution which was symmetrical about the duct's center line with the Mach number lowest in the duct's center. This Mach number distribution came from unpublished experimental data earlier found on the T-3 shock tunnel. No attempt was made to theoretically model this Mach number distribution (modeling this distribution was attempted by University of Queensland Ph.D. student Robert Casey). A computer program was written incorporating the two dimensional method of characteristics with the scramjet's geometry. Using the experimental data it was possible to reproduce the measured pressures found on the scramjet's diverging surface. These results have been published in the AIAA paper 91-0227, "Parametric Study on Thrust Production in the Two Dimensional Scramjet".

The earlier unpublished experimental data used in AIAA paper 91-0227 was measured at only one station in the rectangular duct and was contaminated with shock waves. When writing AIAA paper 91-0227 this experimental data was all that was available for confirming the theoretical model. To provide greater confidence in the validity of the two dimensional model it was necessary to perform additional experiments, this time in the T-4 shock tunnel. A new scramjet model was developed by Allan Paull with the participation of Gary Allen. This model was designed to be particularly "quiet" by providing noise isolation for the pressure transducers and constructing the duct to be as shock wave free as possible. This scramjet model in its current form is simply a straight duct with central fuel injection but initially without a diverging section. Two redundant methods to determine Mach number distributions across the duct were built

into the scramjet. One method was optical and involved placing Schlieren free windows on the side of the duct and test section. This would have permitted Schlieren photography of flow in the duct from which the Mach number distributions could have been determined. We had little confidence in the optical method so a redundant measurement technique was also provided for. This involved placing a pitot rake designed by David Buttsworth into three different stations in the duct measuring the local Mach number directly using the Rayleigh equation. Our low confidence for the optical method proved justified when our laser malfunctioned along with our determination that our CCD camera was providing inadequate resolution. Fortunately our redundant method with the pitot rake provided excellent results for two of the three stations measured in the duct. The one station out of the three which provided unusable results was due to interference from the shock wave generated by the central injector. We were also able to acquire shock luminescent pictures clearly showing the fuel and air layers on the pitot rake. We desired at least three valid Mach number distributions so a quadratic spline field could be derived for the whole duct. Such a spline field would allow for optimal placement of the diverging section onto the straight duct. A bracket for measurement at a fourth station was constructed and will be used when our next time slot on the T-4 shock tunnel becomes available. In this later experiment we hope to add the diverging section to the rectangular duct and determine pressures on the diverging section for comparison with the earlier theoretical model.

# A STUDY OF SHOCK INDUCED HEAT RELEASE

## Report for the period April 1991 to December 1991

by Nicholas Ward

**INTRODUCTION**

In the past the study of the effects of heat release on hypervelocity flow in a SCRAMJET duct has taken the form of injecting hydrogen into the flow within the duct of a shock tunnel model and then measuring the pressure rises, etc, which result from its combustion using wall mounted pressure and heat transfer gauges. This can give a good indication of whether combustion is taking place but very little detailed information about the actual effect on the flow field which is caused by this heat release.

There are three main reasons for this. Firstly although the wall mounted gauges give very good measurements of flow variables as a function of time they are spatially quite discrete. To map the flow pattern, desirable in any detailed study of heat release effects, is virtually impossible, especially away from the walls of the duct. Second, when the hydrogen is injected into the flow within the duct it seems to always burn before it is thoroughly mixed with the air. This incomplete mixing adds an extra variable to make study of the effects of the actual heat release much more difficult. Finally, the injector itself causes massive disruption to the flow field in the duct. The effects of this disturbance tend to camouflage the effects of the heat release on the flow pattern.

The experimental part of this study is an optical study. A double pass differential interferometer is used to obtain interferograms of the flow within the duct during heat release, possible through the use of a SCRAMJET model with an open sided duct. From these interferograms a total spatial picture of the flow pattern is obtained, and measurements of changes in flow variables or detection of unexpected features within the flow pattern is possible. This overcomes the first problem described above.

The flow produced by the T4 shock tunnel at the University of Queensland has a quite high dissociation fraction, even when the test gas is nitrogen. This is a consequence of the extremely high temperatures which the gas is subjected to in the stagnation zone just before acceleration through the converging-diverging nozzle. The flow emerging from the nozzle is frozen, but after passing through the intake shocks of a SCRAMJET model this is no longer the case. Recombination takes place and heat is released. This is entirely analogous to combustion. It was decided rather than using the combustion of hydrogen to study heat release to use the recombination of nitrogen. The dissociated nitrogen atoms are perfectly 'mixed' through the nitrogen test gas, solving the second problem above, and there is no injector at all, solving the third problem.

Thus the effects of heat release on hypervelocity flow in a SCRAMJET duct can be studied relatively unencumbered by extra variables or disturbances, and with good spatial detail. This study of what is in effect a premixed flow takes on even more significance now that international favour has started shifting to SCRAMJET designs in which the hydrogen fuel is released into the flow far upstream of the duct intake rather than using an injector within the duct. By the time the flow reaches the duct intake shocks the fuel is well mixed and injector disturbance is minimal. In this premixed SCRAMJET configuration 'perfect mixing' is achieved as is the case in the recombining nitrogen situation studied here. No longer is this just an investigation into the effects of heat release on SCRAMJET duct flow but a potentially complete simulation of the flow pattern generated in the duct of the premixed SCRAMJET aerospace plane.

**BACKGROUND**

Previous to March 1991 two sets of shock tunnel experiments using the differential interferometer to examine the flow with recombining nitrogen in the model SCRAMJET duct had been completed. The differential interferometer optics system had been found to be in need of modification, including the upgrading of some components, in order to obtain satisfactory quality interferograms. A computer program had been written to predict the dissociation fraction $\alpha$ throughout the SCRAMJET duct under different experimental conditions.

**REPORT**

Although some experimental interferograms had now been obtained, the optics system still required substantial improvement.

The possibility of using a spatial filter to clean up the laser beam before it passed through the bulk of the optics was investigated and found to greatly improve evenness of illumination and virtually eliminate background fringes in the final image. A spatial filter was purchased and installed.

The beamsplitter cube which had been in the system was apparently the source of some nuisance reflections showing up in the image. This was replaced with a pellicle beamsplitter and the reflections disappeared.

The differential interferometer is shown in Figure 1.

In preparation for another set of T4 experiments some runs with the $\alpha$-predicting computer program were undertaken over a variety of T4 conditions. As a result a range of conditions was selected to provide a wide choice of $\alpha$ values for the incoming flow and a range of flow pressures and temperatures.

A third set of experiments were completed with the modified differential interferometer. The picture quality was found to be greatly improved over the previous set of experiments. It was discovered however that viscous shocks were forming from the sharp edges at the entrance to the parallel walled duct. It was attempted to counter these shocks

by creating a slight expansion by angling the walls of the duct, but to no avail. Another problem discovered was an apparent 'shrinking' of the width of the parallel section of duct in the interferograms. It is thought this was caused by the flow in the duct spreading out from the open sides of the duct and effectively behaving as a convex lens. This would then optically converge the light as it passed through the duct.

Following these experiments some modifications were made to the model. New wedges were constructed to increase the overall model scale by a factor of 2.5, producing a new width of 2.5cm for the parallel section of duct. This was to allow more detail to be seen in the flow within the duct, as wall effects tended to disturb the fringe pattern. Also, the surfaces of the duct were lined with hardened gauge plate steel. This was to make it possible to obtain sharper edges at the front of the wedges and at the leading edges of the parallel section of duct, thus keeping viscous shock effects at these edges to a minimum.

The SCRAMJET model is shown in Figure 2.

In order to eliminate the optical shrinkage of the width of the parallel duct it was decided to refine the focussing of the differential interferometer so that the plane of the test section was brought into focus while maintaining an appropriate beam width for the model silhouette to be well scaled in the image. In this way any convex-lens-like effects of the flow in the duct could be eliminated in the same way as focussing on the central axis of a normal lens eliminates its effect. This focussing was first attempted using a combination of two lenses, but this could not be achieved without unacceptable distortion. Eventually it was achieved with excellent effect by remounting the camera lens to allow it to be moved closer to the CCD, which captures the image. This allowed the test section to be focussed directly onto this image plane.

Another set of experimental conditions were then selected and a fourth round of experiments undertaken. During these experiments there were some problems when the gauge plate on the duct walls broke loose and some damage was done by flying diaphragm fragments but overall they were highly successful. The focussing of the test section worked in eliminating the distortion caused by flow in the duct acting like a convex lens, and although the viscous shocks coming from the lead edges of the duct were still present their effect was minimal. The increased scale of the model made it possible to see fringes in the duct more clearly, although the detail was insufficient to be able to learn much in the densely packed area around the shocks.

At this stage it was decided to analyse experimental results by comparing interferograms to the flow patterns predicted theoretically by the $\alpha$-predicting computer program. It was decided to expand the computer program to take into account the Prandtl-Meyer compression inflicted on the expanding flow by the duct walls as it recombines. An algorithm was devised to include this Prandtl-Meyer compression as well as the chemical effects of the

recombination, and a new computer program was written. This program outputs all of the flow variables in addition to the dissociation fraction $\alpha$.

**FUTURE**

The program is intended to be expanded in the future to calculate the refractive index, its gradient and a predicted differential interferometer fringe pattern throughout the duct. This will then be able to produce theoretical predictions of flow pattern for shock induced heat release which can be compared to experimental interferograms of nitrogen recombination in the SCRAMJET duct model.

**FIGURE 1.** Double Pass Differential Interferometer

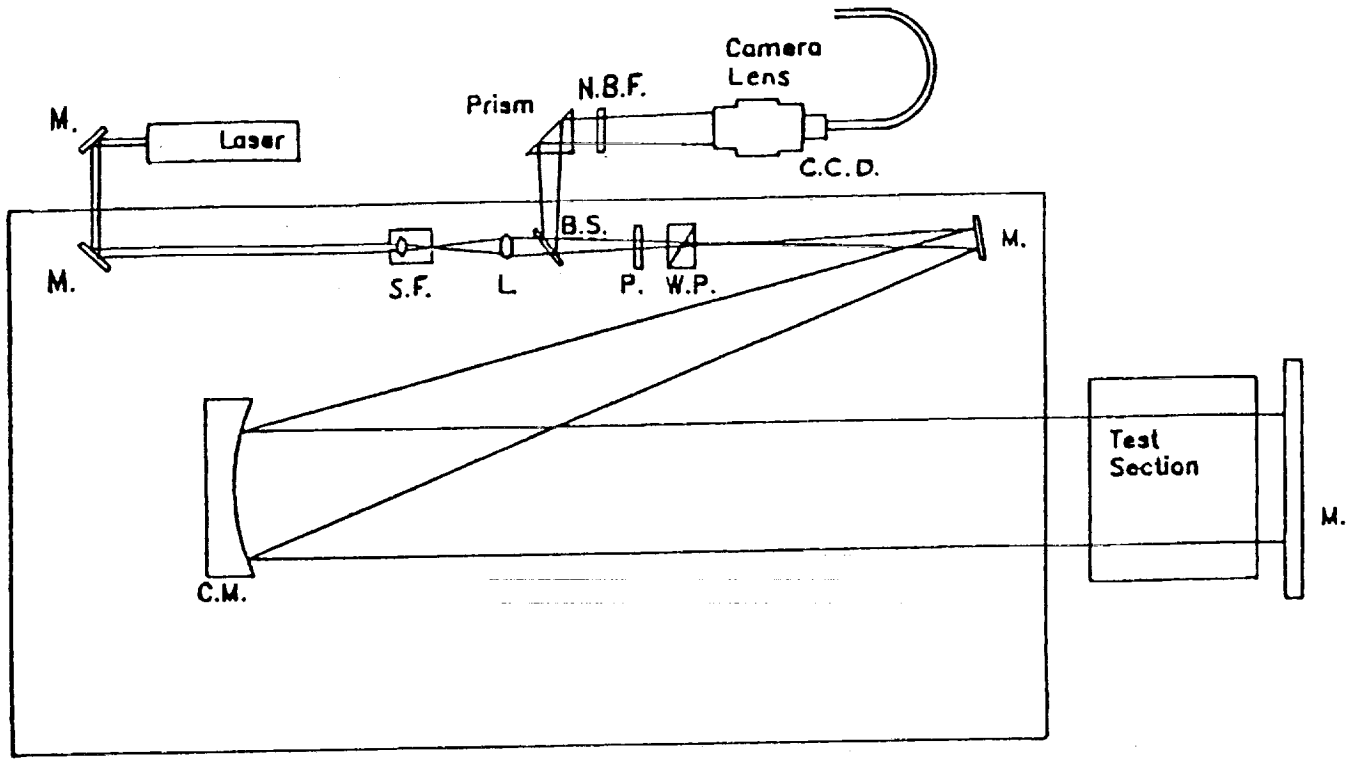


ABBREVIATIONS

| | |
|---|---|
| L. | Lens |
| M. | Plane Mirror |
| C.M. | Concave Mirror |
| B.S. | Beam Splitter |
| P. | Polaroid |
| W.P. | Wollaston Prism |
| S.F. | Spatial Filter |
| N.B.F. | Narrow Band Filter |
| C.C.D | CCD Camera |

**FIGURE 2.** SCRAMJET model

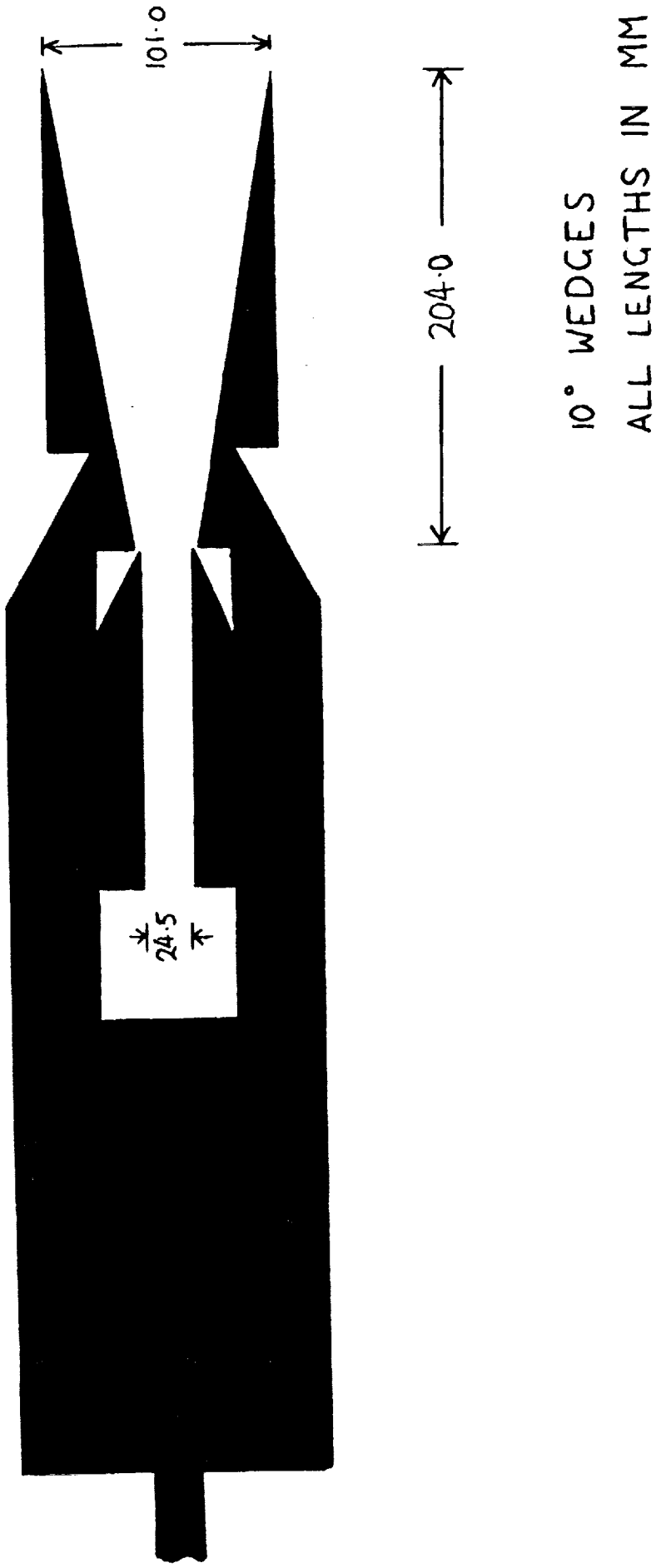

## Mass Spectrometry in Shock Tunnels

K.A. Skinner

During 1991 the Mass Spectrometer was tested in T4 and failed to produce an ion signal at the particle detector. Two problems were later found, either of which could have accounted for this failure.

Firstly, the vacuum inside the inner cavity of the Mass Spectrometer was not low enough to allow the ions unimpeded travel to the particle detector along the drift tube. Although the Penning vacuum gauge indicated that sufficient vacuum had been obtained, the gauge was later found to be dirty. This was presumably from backstreaming diffusion pump oil as the gauge was located on the downstream pumping end of the drift tube, next to the electron multiplier. When the gauge was finally cleaned and recalibrated, it was relocated to the back end of the afterbody dump volume, away from diffusion pump oil vapours, (see Figure 1.).

It was then discovered that the vacuum in the drift tube was only $6x10^{-5}$ torr where the vacuum required for a clear mean free path was $2x10^{-5}$ torr. The reason for the increase in pressure over what had previously been attainable in a closed system, was that the leak rate through the skimmer from the outer vacuum cavity to the inner vacuum cavity was higher than allowed for in the design calculations. This in turn occured because the vacuum in the outer vacuum cavity was not maintained at its design level of $10^{-2}$ torr by the rotary vane pump attached to it. To overcome this problem a second diffusion pump was installed, connected to the outer vacuum cavity. This pump could hold the outer vacuum cavity at $10^{-2}$ torr to $10^{-3}$ torr (the lower end of a pirani vacuum gauge reading), and therefore the inner cavity could quickly be pumped down to the $10^{-5}$ torr required for the ion beam.

The second flaw in the Mass Spectrometer was in the electron gun. The gun being used was a commercial type as used in black and white CRT's. This gun had as its cathode a barium and strontium-coated nickel surface heated by a tungsten filament to approximately 1000 K. The beam current from this gun however was only of the order of 50 microamps, instead of the milliamps required. This limitation was inherent in the choice of cathode as the cathode would not provide more than 100 microamps current to the first anode of the gun. Of even greater concern, however was the extremely short lifespan of the cathode. The design of the Spectrometer is such that exposure to atmospheric air is a regular occurence. With each exposure to air the cathode required re-activation as the barium/strontium coating oxidised. The oxides needed to be evaporated away again after each venting of the Mass Spectrometer. This evaporation/reactivation process required approximately one hour. Each cathode lasted only three to four reactivations before losing all ability to produce current at greater than 1 microamp. For these reasons this type of electron gun source was abandoned.

A new electron source has been designed. It operates off a tungsten filament which is much more robust with regard to oxide poisoning. Because the focussing of an electron beam is heavily dependent on the geometric accuracy of the electrodes, the electron source is located as close as possible to the path of the molecular beam without interfering with its free motion. The electron beam is therefore not well collimated, but with only 10 mm of travel to the ion beam, the spread is not greater than the spread in the molecular

beam. The emmiter consists only of a filament, a gate electrode, and an acceleration anode. (Figure 2). This allows the beam to be pulsed on/off quickly and the anode doubles as a potential cage to accelerate the ions to the detector. The behavior of the electron source and the ion acceleration fields have been analysed using the charged particle trajectory package SIMION. (Figure 3).

This new design for the electron beam source has been constructed and tested outside T4. It has given satisfactory performance although as yet the pulse width applied to the gate electrode is not as narrow as will be required. Nevertheless, mass separation has been recorded consistently with a test rig which allows short bursts of gas into the mass spectrometer. With an electron beam pulse duration of 3 microseconds and an ion acceleration energy of 200 eV, distinct peaks of Helium, Water vapour and Oxygen/Nitrogen have been observed. (Figure 4). The pulse width is too large to separate Oxygen and Nitrogen, whose arrival times at the detector are only separated by 2 microseconds.

The problem of the electron beam pulse duration is expected to be overcome in the near future and the Mass Spectrometer will then be re- installed in T4.

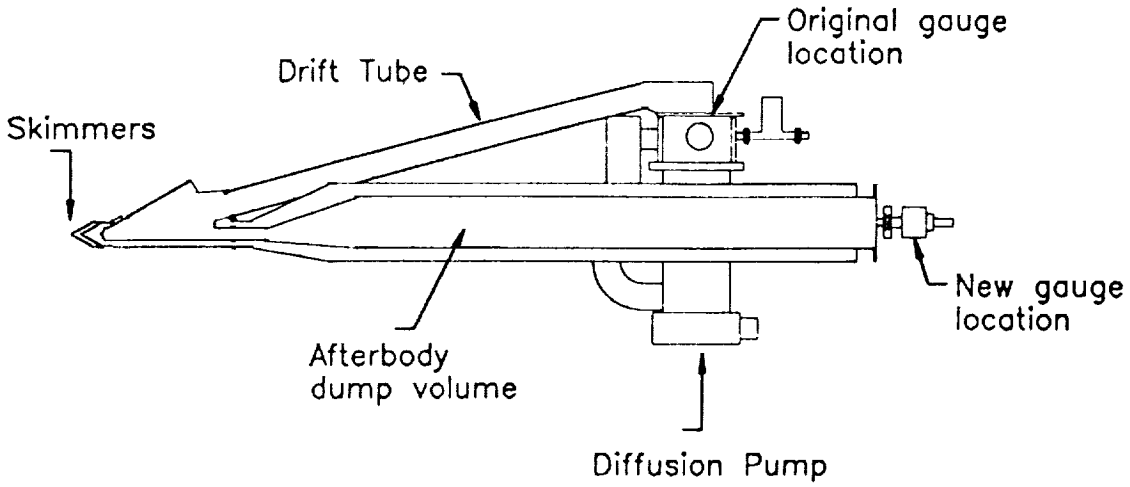


Figure 1. Location of Penning Vacuum Gauge

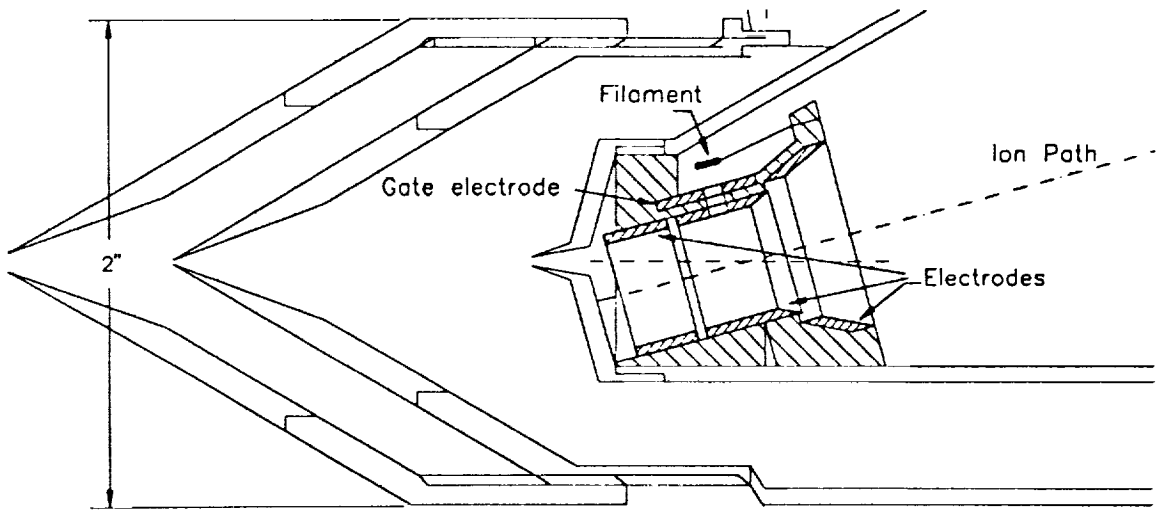


Figure 2. Schematic of Electron Beam source

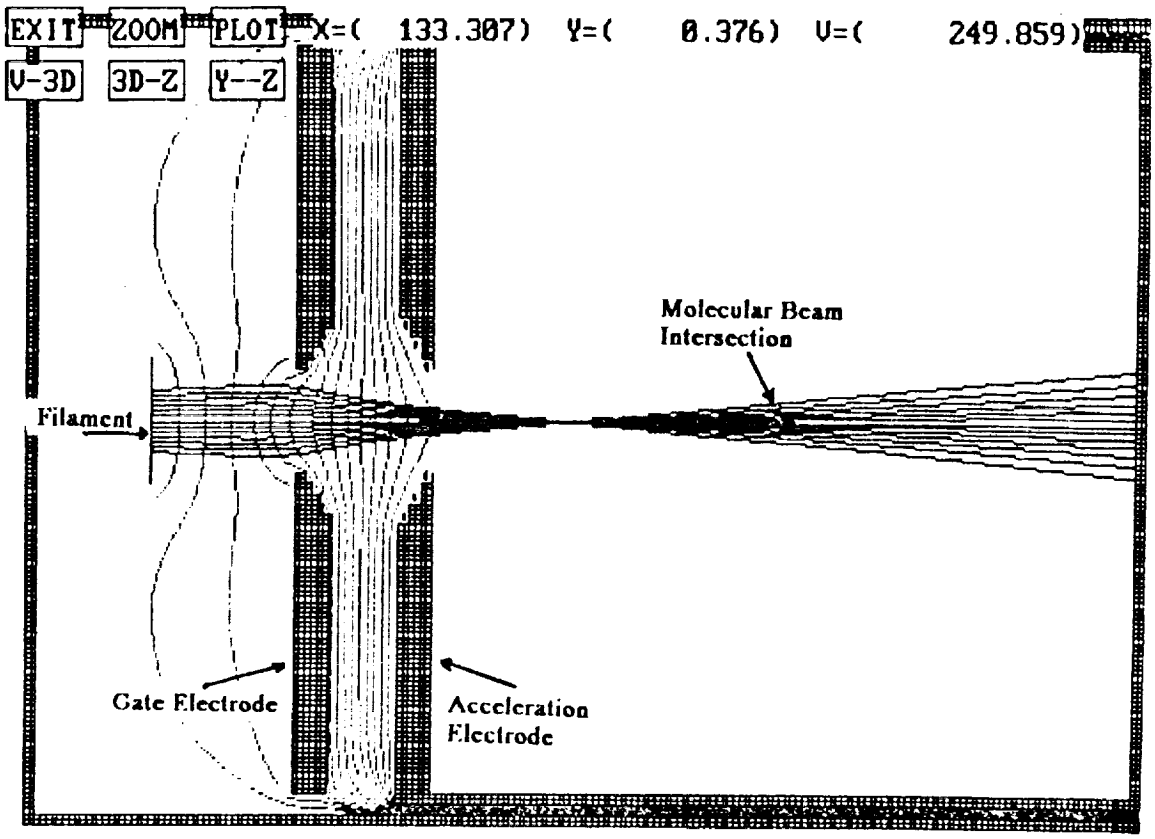


**Figure 3.** Axisymmetric model of Electron Beam source showing electron trajectories and equipotential contours

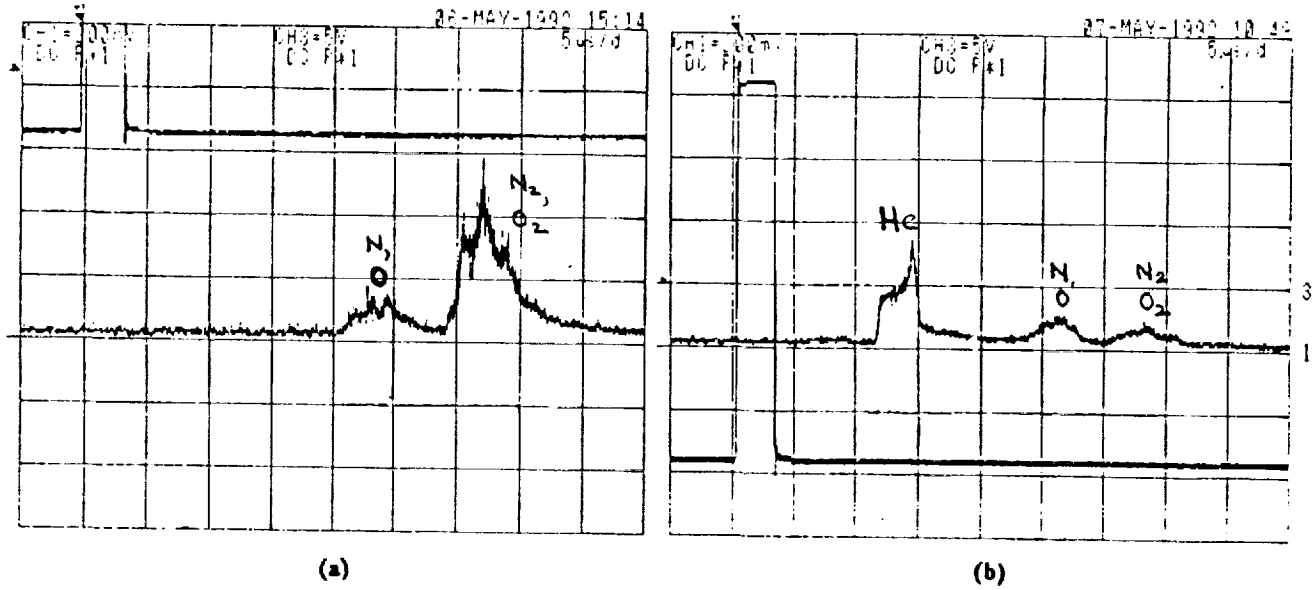


**Figure 4.** Mass Separation in the Mass Spectrometer with an electron beam pulse duration of 3 microseconds and an Ion energy of 200eV.
(a) Air (b) Helium and Air

# COMPARATIVE FEATURES OF FREE PISTON SHOCK TUNNEL AND EXPANSION TUBE FACILITIES

R.J. Stalker, A. Paull, A.J. Neely

The University of Queensland
Department of Mechanical Engineering
Queensland, 4072.
Australia.

Tenth National Aero-Space Plane Technology Symposium
April 22-26, 1991.

Paper number 241

ACKNOWLEDGEMENT

This work was conducted under NASA grant NAGW-674, together with grants from the Australian Research Council.

# Comparative Features of Free Piston Shock Tunnel and Expansion Tube Facilities


## Outline

Free piston shock tunnels offer a means of conducting ground facility experiments for aerodynamics and propulsion purposes at speeds up to Earth orbital velocity. However, as speeds exceed 4 $km.s^{-1}$, they experience free stream "freezing" of atomic components of air, and this may be a particular disadvantage for propulsion studies. Theoretically, free piston expansion tubes offer reduced free stream freezing effects, but in past experiments with expansion tubes it has proven very difficult to establish a test flow of acceptable quality. The results of analysis and experiments directed towards this problem are reviewed here, taking the following approach:

(i) Typical performance characteristics of reflected and nonreflected shock tunnels are reviewed.

(ii) The basis of an analysis which explains the flow degradation in expansion tubes is outlined and compared with experiments.

(iii) Typical performance characteristics of expansion tubes operating within the bounds defined by the analysis are calculated.

(iv) A "spin-off" is identified, as a projected ability to operate expansion tubes at stagnation enthalpies well in excess of those corresponding to Earth orbital velocity.


## 1. INTRODUCTION

Airbreathing propulsion at high flight velocities demands efficient management of wave phenomena, boundary layer behaviour, fuel-air mixing and combustion effects in hypersonic flows. Facilities for experiments and testing in this area therefore must include ones in which flight stagnation enthalpies are produced in hypersonic flows at densities which are high enough to provide a reasonable representation of the viscous and chemical effects which are expected to take place.

Only impulse facilities can fill this need at flight speeds substantially in excess of 2.5 $km.s^{-1}$, and the most successful of these has been the reflected shock tunnel. This was conceived in the 1950's [1] and has been effectively employed by a number of laboratories, and particularly by the group at Calspan, for more than 30 years. Another theoretically promising development has been the expansion tube. Although, as noted below, early experiments with this type of facility were disappointing, later work at NASA Langley Research Centre held out some hope that ways could be found of realizing their promise.

The development of the free piston shock tunnel in the 1960's made it possible to increase the stagnation enthalpies which could be achieved in shock tunnels[3] and, amongst other things, opened up the possibility of conducting experiments on supersonic combustion over the range of flight speeds likely to be of interest for an Earth orbital launch vehicle. This

possibility focused attention on the effects of chemical "freezing" in the steady expansion nozzle of a high enthalpy shock tunnel and it was noted that, for comparable flow stagnation enthalpies, the expansion tube produced a lower level of free stream freezing than the shock tunnel. As a result, the Langley expansion tube was transferred to General Applied Science Laboratories, and brought into operation as the "Hypulse" facility, whilst a study of the application of the free piston driver to an expansion tube was initiated at The University of Queenland.

This paper summarizes the results of that study. However, in order to put the application of these results to expansion tube operation into a comparative framework, the characteristics of free piston shock tunnels are reviewed first.

## 2. PRINCIPLES OF OPERATION

Both the shock tunnel and the expansion tube are derived from the shock tube. The way in which they differ is shown in Fig. 1. As is evident in the figure, there are two types of shock tunnel, reflected and non-reflected. In the reflected shock tunnel, the shock heated flow following the primary shock wave in the shock tube is brought to rest by shock reflection at the downstream end of the shock tube, from where the stagnant hot gas is allowed to expand and accelerate through a steady flow hypersonic nozzle. This is shown by the wave diagram at the top left of the figure. In the non-reflected shock tunnel, shown on the bottom left of the figure, a steady flow nozzle is again used, but the flow following the primary shock passes directly into the nozzle without shock reflection. The expansion tube is shown at the top right of the figure, and does not use an expansion nozzle. Instead, a very light diaphragm is placed at the end of the shock tube, followed by an acceleration tube, which initially is at a much lower pressure than the shock tube. The primary shock ruptures the diaphragm, and an unsteady expansion is set up in the flow which follows the primary shock, to yield an expanded, hypersonic flow of test gas in the test region.

Some free piston shock tunnels and expansion tubes are shown in Fig. 2. All of these are either in operation, or have substantial parts of their necessary hardware in existence. The largest is the "Rhyfl" facility; which is shown in its original design mode of a reflected shock tunnel, as is "T5" which now is in operation at Caltech. "Hypulse" is in operation as an expansion tube at General Applied Science Laboratories, but does not yet have a free piston driver. "T4" is in operation at The University of Queensland as a reflected shock tunnel, and "T3", in Canberra, is in operation both as a reflected and a nonreflected shock tunnel.

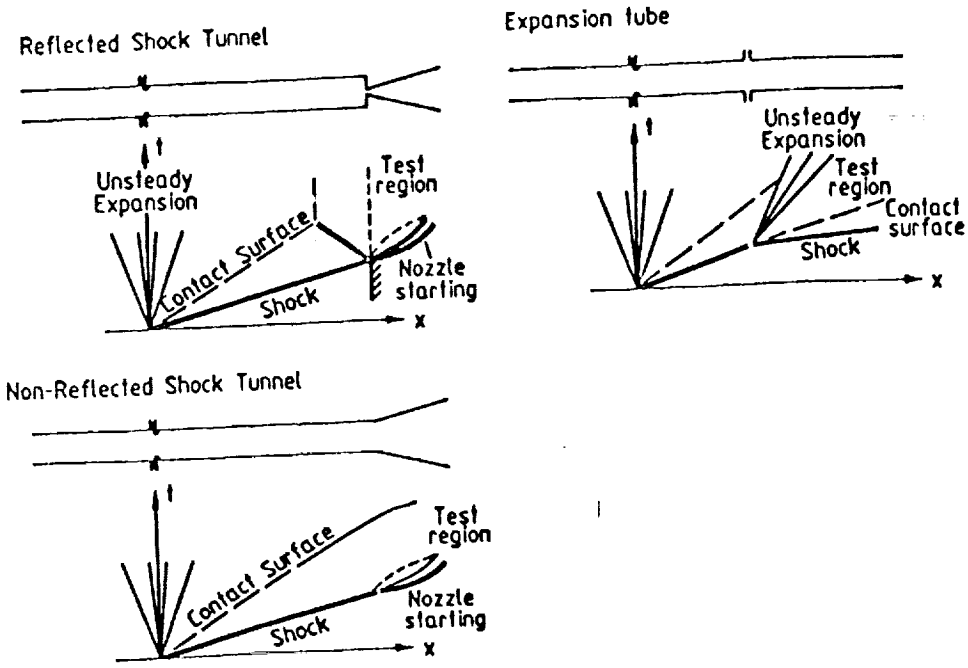


Fig. 1 Aerodynamic Facilities Derived from Shock Tube.

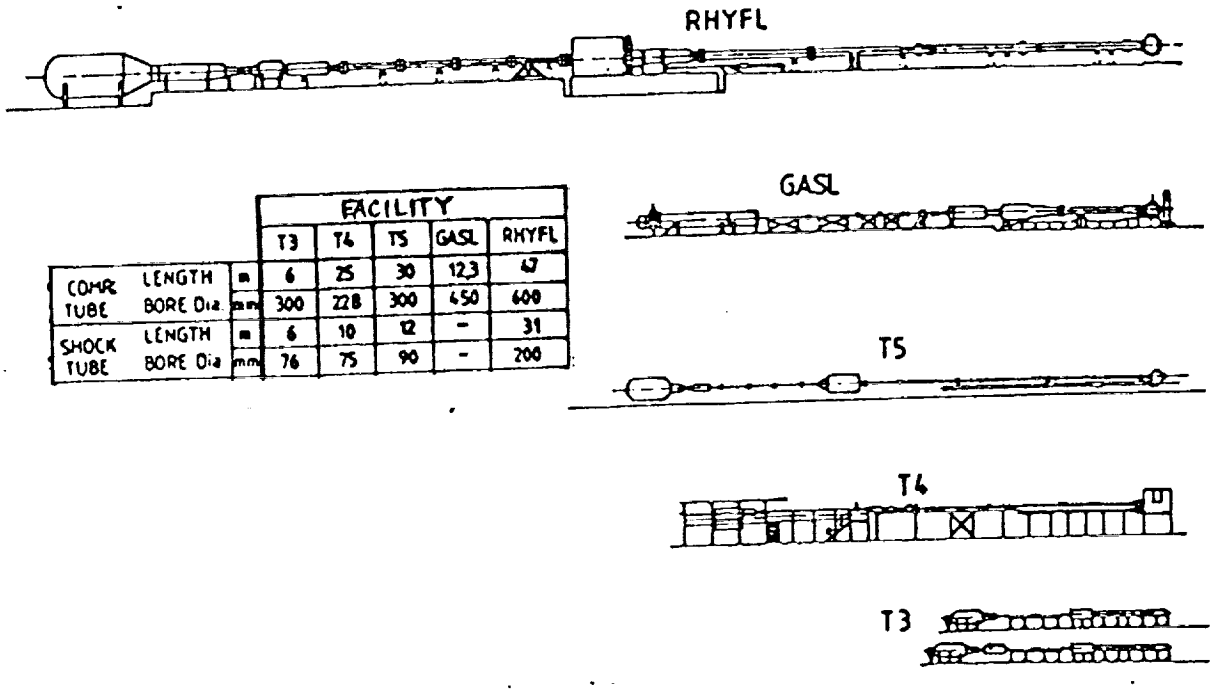


| | | | FACILITY | | | | |
|---|---|---|---|---|---|---|---|
| | | | T3 | T4 | T5 | GASL | RHYFL |
| COMP TUBE | LENGTH | m | 6 | 25 | 30 | 123 | 47 |
| | BORE Dia | mm | 300 | 228 | 300 | 450 | 600 |
| SHOCK TUBE | LENGTH | m | 6 | 10 | 12 | - | 31 |
| | BORE Dia | mm | 76 | 75 | 90 | - | 200 |

Fig. 2 Free Piston Impulse Facilities

## 3. THE REFLECTED SHOCK TUNNEL.

At first glance, it would appear that the stagnation enthalpies achieved in a reflected shock tunnel are limited only by the shock speeds achieved in the shock tube. In fact, the limit on stagnation enthalpy at the test section flow is determined by driver gas contamination[5]. This is due to the shock-boundary layer interaction that occurs as the shock wave reflects from the downstream end of the shock tube, which causes "jetting" of the driver gas along the walls of the shock tube, and premature arrival of driver gas at the entrance to the hypersonic nozzle. With a given sound speed in the driver gas, attempting to increase the test section stagnation enthalpy by increasing the shock speed causes the test time to reduce, until it becomes too short to be useful.

The definition of "useful" depends, of course, on the experiment to be performed but, noting that a steady boundary layer flow is established on a model if the test time is sufficient for an element of the gas to travel three model lengths, it follows that the length of the test gas pulse produced by the shock tunnel becomes a performance parameter of primary importance.

This parameter has been calculated[6] for four driver gas conditions in the "Rhyfl" facility, and the results are displayed in Fig. 3. The three driver gas conditions at a volumetric compression ratio of 40 have been chosen with scramjet combustion testing in mind, and therefore they are considered in conjunction with a nozzle area ratio of 100. For these flows, assuming a perfect gas expansion with a ratio of specific heats of 1.3 provides a reasonable approximation for the relation between static pressure and nozzle cross sectional area, and this yields a test section static pressure of 0.8 atm. Consideration of the time for drainage of gas, from the shock reflection region, through the nozzle throat then leads to a permissible test section diameter of 0.8 m. If the test section diameter is taken as a measure of a typical model dimension, then the product of pressure and test section diameter serves as a measure of the chemical binary scaling parameter. In the present case, this has a value of 0.64 atm.m which, at appropriate temperatures, is sufficient to ensure ready ignition of hydrogen-air mixtures.

The driver gas condition at a volumetric compression ratio of 100 is included as an example of conditions which could be used for testing of external aerodynamics. With the restraint on test section pressure levels thus removed, lower nozzle reservoir pressures can be tolerated, together with a larger test section. For example, a test section diameter of 2 m could be used, with a nozzle area ratio of 1000. This would allow aerodynamic testing of models 3 m long at stagnation enthalpies corresponding to flight speeds up to 7 $km.s^{-1}$.

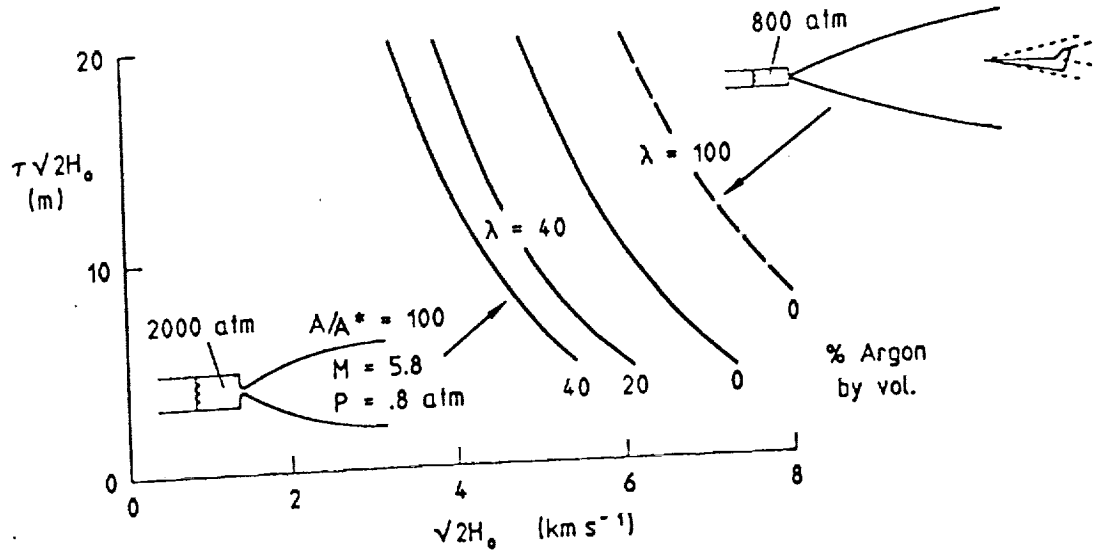


Fig. 3 Free Piston Reflected Shock Tunnel Performance. Shock tube dia. = 200 mm, Driver gas: He/Argon, $\lambda$ = volumetric compression ratio, $H_0$ = stagnation enthalpy, $\tau$ = test time.

## 4. THE NON REFLECTED SHOCK TUNNEL

Because it makes direct use of the flow following the shock wave, the test time available in a non-reflected shock tunnel is relatively short. This is its major disadvantage and, to minimize its effect, special measures must be taken to ensure rapid initiation of steady flow in the nozzle, and to reduce test flow disturbances arising from mismatch between driver and test gas conditions at the contact surface. The latter can usually be accomplished by approximately matching driver and test gas Mach numbers at the contact surface.

When the shock tube pulse of test gas is sufficiently long, the former can be accomplished by the usual practice of locating a lightweight diaphragm at the entrance to the hypersonic nozzle, and thoroughly evacuating the nozzle before the test. When the test gas pulse is too short to allow the diaphragm fragments to be removed early in the flow time, a prior steady flow technique[7,8] can be used to ensure rapid flow initiation.

Fig. 4 displays the variation of test gas pulse length with equivalent flight speed for a nonreflected shock tunnel involving the "Rhyfl" driver, and a shock tube extended by 9 m to a total length of 40 m. The test flow pulse length is taken as the shock wave-contact surface separation in the shock tube, and is calculated according to the theory of Mirels[9], (which may lead to overestimation of the test time at the lower equivalent flight speeds on the figure). These pulse lengths will be reduced by the delay in establishing steady flow in the nozzle. As a rough rule of thumb, a reduction of half the test section diameter should be allowed.

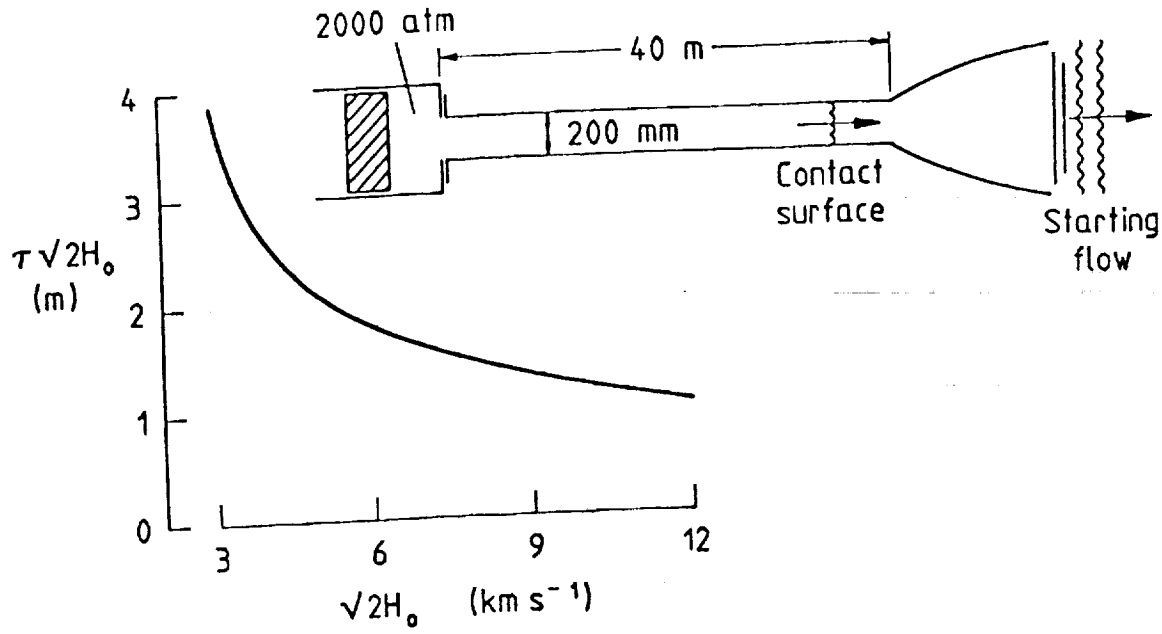


Fig. 4 Free Piston Nonreflected Shock Tunnel Performance. Shock tube dia. = 200 mm, Driver gas: He/Argon, $H_0$ - stagnation enthalpy, $\tau$ = test time.

Thus, an equivalent flight speed of 4.7 km.s$^{-1}$, a nozzle area ratio of 16, leading to a test section diameter of 0.8 m, yields a reduced test flow pulse length of 1.8 m. Therefore model lengths typically are limited to 0.6 m. However, the associated static pressure in the test section is 1.9 atm, yielding a value of 1.5 atm.m. for the product of test section pressure and diameter. Although the useful model lengths are too short for most supersonic combustion studies, the large value of the chemical binary scaling parameter makes this type of flow suitable for experiments on flow details which involve real gas effects, such as shock wave - leading edge interactions.

It should also be noted that the nonreflected shock tunnel allows operation at much higher equivalent flight speeds than the reflected shock tunnel, albeit that this can only be achieved with smaller nozzle diameters and test section model lengths than in the case noted in the preceding paragraph.

## 5. THE EXPANSION TUBE

The wave diagram of Fig. 5 displays the operation of an expansion tube in more detail than in Fig. 1. It can be seen that the test flow in region 5 takes place between the passage of the contact surface in the acceleration tube flow and trailing edge of the accelerating expansion. It can also be terminated by the reflected expansion which arises from the interaction of the upstream head of the expansion with the shock tube contact surface. Although the test pulse length is shorter in an expansion tube than in a reflected shock tunnel, the flow produced has the theoretical advantages that there is substantial gain in both stagnation enthalpy and effective flow

stagnation pressure in passing through the unsteady expansion and, as mentioned above, chemical "freezing" of the test gas is reduced.

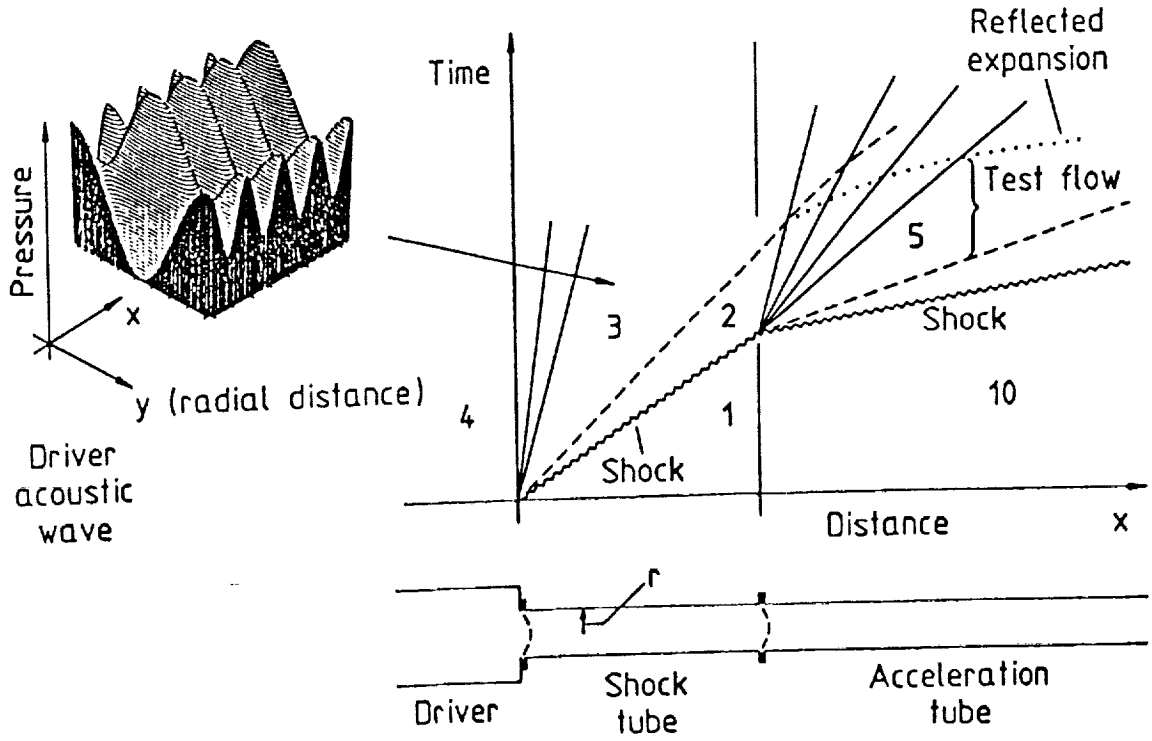


Fig. 5 Expansion Tube Flow

The advantages of expansion tubes have been realized for nearly three decades[10] and, when they were first explored in some detail by Trimpi, led to an active program of experimental evaluation in a number of laboratories [11,12,13,14]. It was found that the test flow was not steady, even for the relatively short test times which were predicted from the theory. The unsteadiness took the form of high frequency fluctuations in the test flow pressures and densities, which were particularly evident in pitot records taken on the tube centreline.

Notwithstanding these disappointing results, a persistent research effort was maintained at the NASA Langley Research Centre, and was rewarded by the discovery of a narrow band of acceptable test conditions, at flow stagnation enthalpies near 17 MJ $kg^{-1}$[2]. A pitot pressure record corresponding to this test condition is shown in the middle of Fig. 6(a), together with records for unacceptable conditions at the top and the bottom of the figure. It can be seen that these records exhibit the same features as those displayed in Fig. 6(b), which were obtained with a small free piston driven expansion tube at The University of Queensland, with a diameter only one quarter of that of the Langley tube[15].

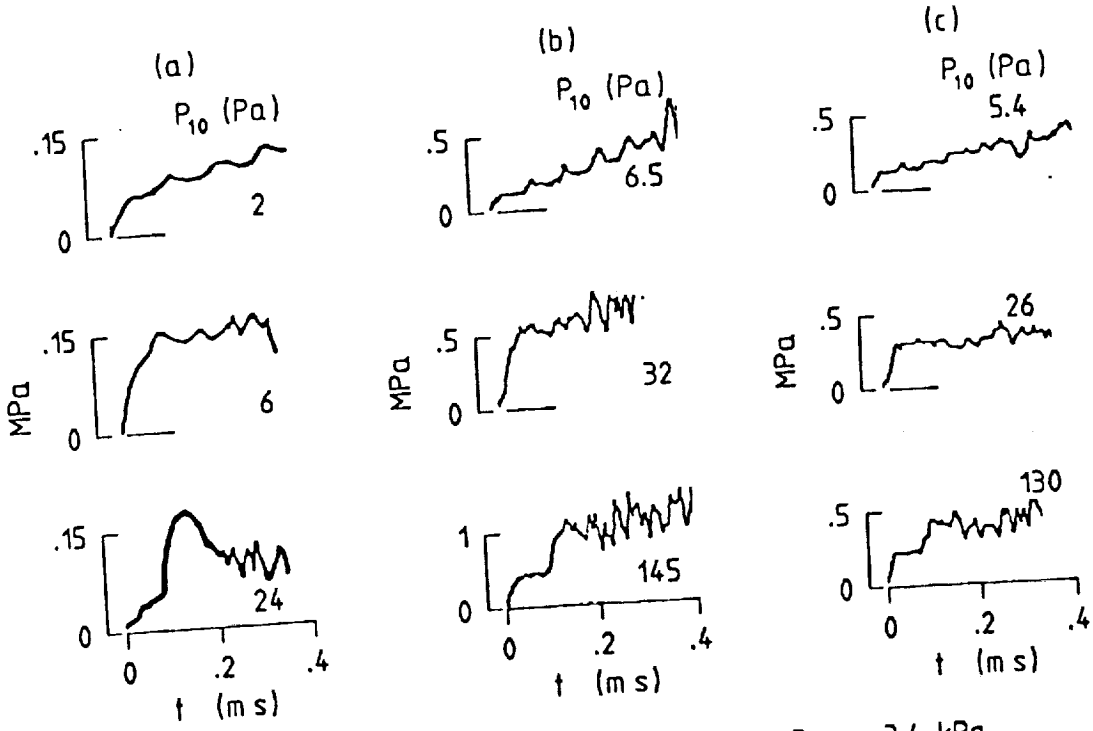


(a) Tube diam = 150 mm , He driver , $P_1$ = 3.4 kPa
(b) " " = 37 mm , Ar driver , $P_1$ = 13.7 kPa
(c) " " = 37 mm , Ar driver , $P_1$ = 3.5 kPa

Fig. 6 Expansion Tube Test Flows - Centreline Pitot Records

Considering the records of Fig. 6(b), the test condition in the middle of the figure is characterised by a period during which the mean pitot pressure remains steady. However, the high frequency fluctuations noted above are superimposed on the record, and it is only acceptable as a test condition because, over a period of some 80 μsec, these fluctuations are small enough not to influence measurements in many practical flows.

When the pressure ratio across the expansion is reduced, as shown at the bottom of the figure, the amplitude of the fluctuations rises to an unacceptable level at an earlier time, and there is no useful test period. When the pressure ratio is increased, as shown at the top of the figure, the fluctuations take on a nearly uniform frequency. The mean pitot pressure also increases with time, due to the earlier arrival of the downstream edge of the expansion fan in the test gas, implying that there is no useful test time in this case as well.

Acoustic Theory

Paull[15] investigated these fluctuations by treating them as acoustic waves originating in the driver gas. Whilst bursting of the main diaphragm is an obvious source of such waves, it was not necessary to assume this in

the analysis. Based on analysis of pitot measurements in the driver gas flow in the shock tube, it was assumed that a dominant transverse acoustic mode existed, as represented at any instant by the pressure plot shown in Fig. 5. As is evident from the figure, the transverse wavelength is approximately one tube diameter and, if the transverse frequency is $\omega$, then the wavelength in the axial direction is $2\pi a\ (\omega\beta)^{-1}$, where a is the local speed of sound, and

$$\beta = \sqrt{1 - \{3.83a/(\omega r)\}^2} \quad , \tag{1}$$

where r is the shock tube radius. In order for the wave to exist the expression under the square root must be positive, indicating that these waves exhibit a minimum frequency given by $\omega = 3.83\ a/r$. There is no upper limit on the frequency, except that higher frequencies imply higher energies and, as with any wave system, most energy tends to reside in the lowest allowable levels.

If the speed of sound in the test gas in the shock tube is higher than in the driver gas then, when a wave crosses the boundary represented by the contact surface between the two, the increase in the speed of sound implies that $\beta$ can become imaginary, and the wave then cannot exist in the test gas. Thus waves with the lower of the allowable frequencies in the driver gas will not be transmitted into the test gas and, noting that these waves are expected to be the most energetic, it follows that the intensity of the waves is reduced in the test gas. On the other hand, if the speed of sound reduces in passing across the contact surface, then all the waves which exist in the driver can be transmitted into the test gas.

Noting that the gas velocity is constant across the contact surface, it is clear that the contact surface will act as a filter if the Mach number in the driver gas is higher than in the test gas, and the greater the relative difference, the greater the effect. If the waves thereby are eliminated in the test gas in the shock tube, they will not be evident in the expanded flow in the test section of the expansion tube. This is apparent in comparing Fig. 6(b) and Fig. 6(c), where calculations for Fig. 6(b) yield values of the driver gas and test gas Mach number of 4 and 1.8 respectively, whilst for Fig. 6(c), they are 5.5 and 2.0. It can be seen that the relative amplitude of the pressure fluctuations is much less in Fig. 6(c) than in Fig. 6(b).

Some experiments using helium driver gas were also conducted. Although the shock speeds in the shock tube were much higher than with argon driver gas, allowing real gas effects to increase the test gas Mach number from 1.8 to 2.9, while the driver gas Mach number remained at 4, the fluctuations of pitot pressure during the test time remained at the same relative amplitude as those in the middle record of Fig. 6(b). Thus a smaller contact surface Mach number difference is required with helium than with argon, an effect which possibly could be associated with the higher fundamental frequency of the waves in helium.

Another interesting aspect of the transverse waves is their behaviour as they pass through the unsteady expansion in the acceleration tube[16]. This can be analysed by considering the unsteady expansion as a series of pressure pulses which propagate upstream at the local speed of sound in the gas. Each pressure pulse is treated as a boundary, across which the gas velocity

increases and the speed of sound decreases. An observer in the frame of reference in such a boundary sees a wave with a frequency made up of the fundamental frequency, $\omega$, plus a component associated with the motion of the boundary with respect to the gas (i.e. a doppler shift) leading to an effective transverse frequency at the boundary of $\omega(1 + M\beta)$, where M is the Mach number seen by the observer. Because this effective frequency must be the same on both sides of the boundary, two competing effects occur. The first is that the doppler effect associated with the increase in gas velocity in crossing the boundary causes the observer to see a reduction in the axial wavelength of waves downstream of the boundary, implying that a wave must have a longer fundamental wavelength if it is to match a given upstream one at the boundary. That is, $\beta$ tends to decrease across the boundary. The second is that the reduction in the speed of sound implies that the matching wavelength must be shorter downstream of the boundary. That is, $\beta$ tends to increase across the boundary.

For values of $\beta$ which are greater than $(\gamma - 1)/2$, where $\gamma$ is the ratio of specific heats in the gas, the first effect dominates, and $\beta$ decreases, whilst for values less than $(\gamma - 1)/2$ the second effect dominates, and $\beta$ increases. Thus, as the expansion proceeds, all the transverse waves present converge to the one value of $\beta$ and, by equation (1), to the same frequency. This is seen at the top of Fig. 6(a) and Fig. 6(b). For these two figures, the theory predicts the period of the observed waves to be 104 $\mu$sec and 29 $\mu$sec respectively, which compares satisfactorily with the measured values of approximately 100 $\mu$sec and 39 $\mu$sec.

Producing the Test Flow

It follows from the acoustic theory that a primary criterion for producing satisfactory expansion tube flows is that the shock tube flow should be such that the penetration of acoustic waves into the test gas is limited to an acceptable level. Of course, this involves a somewhat subjective judgement in determining a tolerable intensity of flow fluctuations in the test section. However, if the test flow in Fig. 6(b) is taken to be acceptable, then the criterion for air test gas and a monotonic driver gas is that the driver gas Mach number at the contact surface should be approximately 4.

It must also be noted that transmission of the high frequency fluctuations will be enhanced by the reduction in sound speed associated with interaction of the upstream head of the accelerating expansion with the shock tube contact surface. The resulting reflected expansion can prematurely transmit fluctuations from the contact surface to the test flow. In fact, the relatively large amplitude high frequency disturbances which are seen to develop with time in the pitot records of Fig. 6 can be attributed to this cause. This effect, together with the need to delay arrival of the downstream edge of the accelerating expansion at the test region, combines with the driver gas Mach number criterion to determine the range of conditions over which an expansion tube may be expected to operate successfully.

The conditions under which useful test flows have been obtained are generally consistent with these criteria. For example, the pitot record at

the middle of Fig. 6(c) represents a test condition which meets the criteria, as does the associated condition where the same filling pressures are used throughout the expansion tube and its driver, but helium replaces argon as the driver gas. In both cases, the utility of the test flows produced (at least, for heat transfer studies) has been explored by using thin film gauges to measure the heat transfer to a flat plate mounted in the test section. A typical heat transfer record is shown in Fig. 7, for a case where helium driver gas was used. The absence of high frequency fluctuations and the steady level of heat transfer during the test time are indicative of suitable flow quality. The levels of heat transfer with argon and helium driver gas are shown at the bottom and the top of the figure respectively. The latter indicate that the expansion tube has an interesting capability as a very high enthalpy facility.

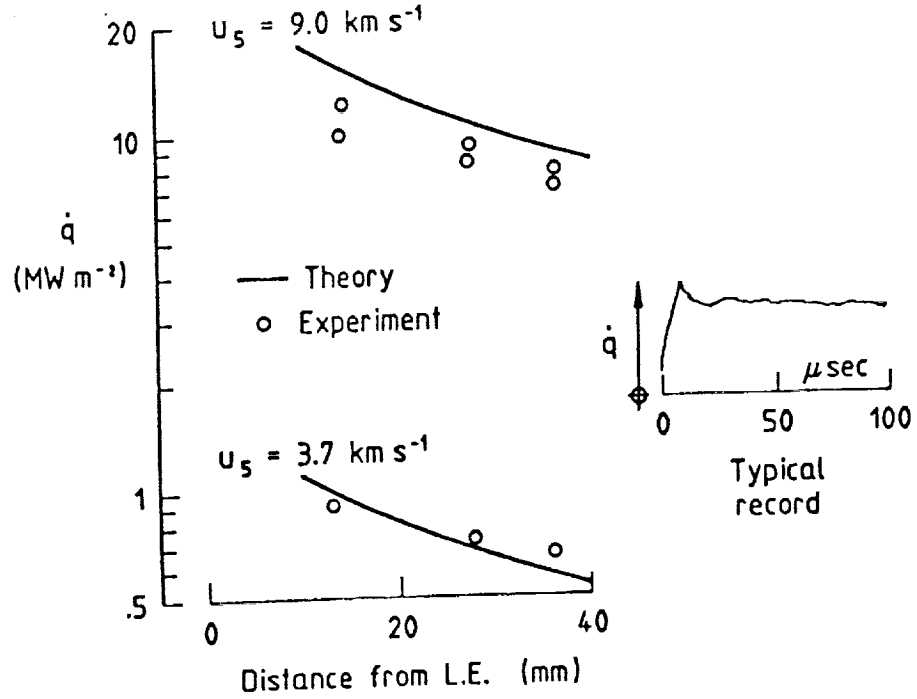


Fig. 7 Flat Plate Laminar Heat Transfer in Expansion Tube Test Section.

The above criteria can be applied to calculate the performance of larger expansion tubes with free piston drivers, and this leads to the curves shown in Fig. 8. These were obtained for a contact surface driver gas Mach number of 4, and a velocity ratio of 2 across the expansion. The pressure change across the expansion was calculated by assuming a perfect gas with $\gamma = 1.3$. For driver sound speeds up to 3050 m.s.$^{-1}$, the driver gas was an argon/helium mixture, at a volumetric compression ratio of 30, and for higher sound speeds, it was helium at higher volumetric compression ratios. The two facilities indicated as "a" and "b" in the figure are, respectively, the "Rhyfl" driver and shock tube with an acceleration tube added, and the "Hypulse" facility, at GASL, with a free piston driver added.

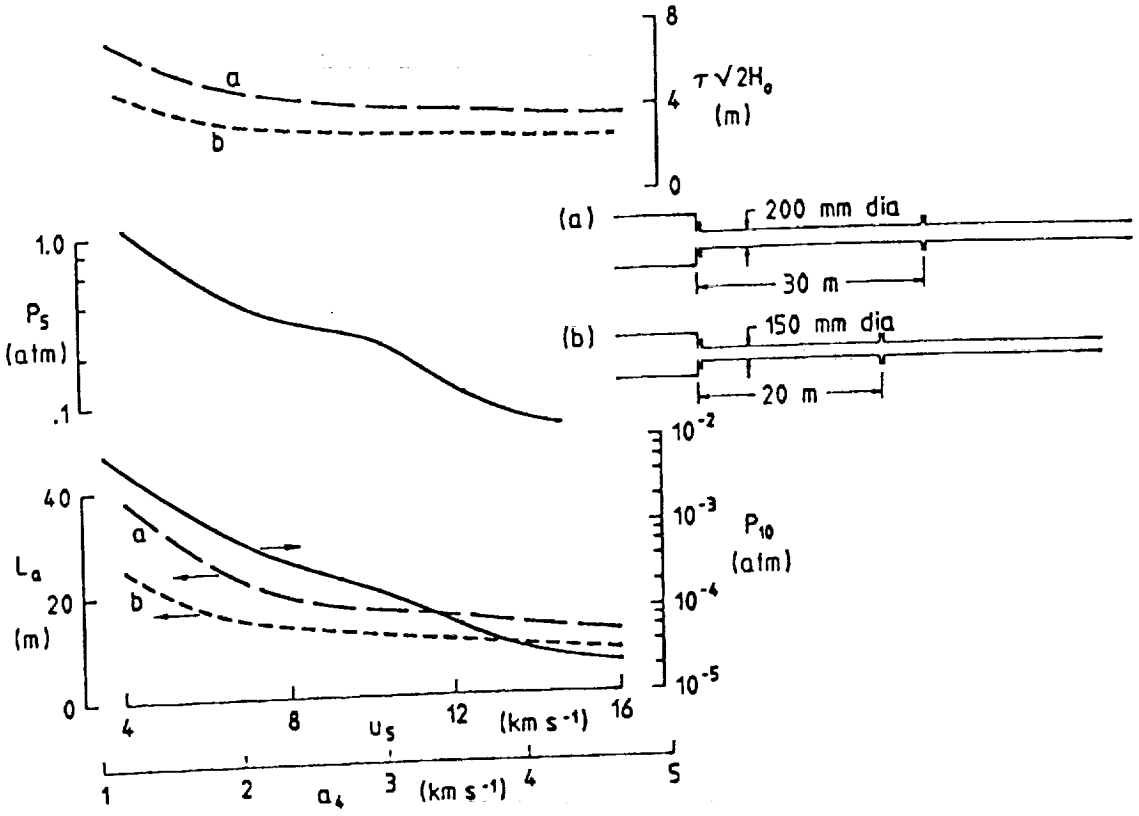


Fig. 8 Expansion Tube Performance with Free Piston Driver
$P_4$ = 2000 atm, $U_5/U_2$ = 2, ($L_a$ = length of acceleration tube, $\tau$ = test time, $H_0$ = stagnation enthalpy).

For both facilities, test section pressure, $P_5$, exceeds 0.5 atm for test section velocities, $U_5$, between 4 and 6 km.s$^{-1}$, and these pressures could be increased by reducing the test gas expansion ratio. This is important for hypersonic combustion studies. The test times are maximized by choosing the acceleration tube length, $L_a$, to ensure the simultaneous arrival at the test section of the reflected expansion and the downstream edge of the unsteady expansion. For a longer acceleration tube, the former reduces the test time and, for a shorter tube, it is reduced by the latter. It is interesting to note that this optimization requires acceleration tube lengths which are only half the shock tube length at the highest test section velocities, but that the resulting test pulse lengths remain sufficient for many experimental purposes.

In comparing "a" and "b", it should be noted that "a" does not represent the ultimate performance capability of the "Rhyfl" facility, but only that which may be obtained with very limited modification. If the diaphragm section were changed to allow a larger diameter shock tube and acceleration tube, test gas pulse lengths theoretically could be increased by a factor of two or three.

## 6. CONCLUSION

Relatively minor modifications allow a shock tube to operate as a hypersonic, aerodynamic, facility in any one of three alternative modes. Of the two shock tunnel modes, the reflected shock tunnel offers the longest test pulse length, combined with adequate test section pressure levels. The test pulse lengths are much shorter for a nonreflected shock tunnel, but somewhat higher pressure levels can be obtained. The use of a free piston driver allows the reflected shock tunnel to operate at speeds approaching Earth orbital velocity, while the nonreflected shock tunnel will operate up to speeds which are another 50% higher.

Analysis indicates that the high frequency flow fluctuations in the test section, which have limited the utility of expansion tubes in the past, can be explained as transverse mode acoustic waves which originate in the driver gas. These tend to be filtered by the contact surface in the shock tube when the driver gas Mach number exceeds that of the test gas. With air as test gas, and a monatomic driver gas, experimental results indicate that the filtering effect is sufficient to allow reasonable test flow quality when the driver gas Mach number reaches 4.

By employing this criterion, and choosing the acceleration tube length to maximize the test time allowed by arrival at the test section of the reflected expansion and/or the downstream edge of the accelerating expansion, it was shown that with a free piston driver, typical test conditions would yield test pulse lengths which were shorter than those in a reflected shock tunnel but longer than those in a nonreflected shock tunnel. The test section pressure levels at sub-orbital flight speeds were comparable with those of a reflected shock tunnel, and the calculations indicated that a test flow could be produced at equivalent flight speeds up to twice orbital velocity.

The primary aim of the expansion tube study reported here was to define conditions under which an expansion tube may be operated for testing supersonic and hypersonic combustion concepts. This aim has been achieved but, in addition it has become clear that, by exploiting the understanding gained in the study, the expansion tube may be expected to realize its original theoretical potential as a very high stagnation enthalpy impulse hypersonic facility.

## REFERENCES.


1. Hertzberg, A., Wittliff, C.E. and Hall, J.G., "Development of the shock tunnel and its application to hypersonic flight". "Hypersonic Flow Research", ed. F.R. Riddell (Academic Press, N.Y.) p. 701, 1962.

2. Miller, G.G., "Operational experience in the Langley expansion tube with various test gases", NASA TM 78637, 1977.

3. Stalker, R.J., "Development of a hypervelocity wind tunnel", Aero. Journ. of Roy. Aero. Soc. V76. pp374-384, 1972.

4. Stalker, R.J., Morgan, R.G., Paull, A. and Brescianini, C.P., "Scramjet experiments in free piston shock tunnels", NASP CR-1100, August 1990.

5. Stalker, R.J., "Hypervelocity aerodynamics with chemical non equilibrium", Ann. Rev. Fluid Mech. V21, pp37-60, 1989.

6. Crane, K.C. and Stalker, R.J. "Driver gas contamination in a high enthalpy reflected shock tunnel" AIAA Journ, V16, pp 277-278, 1978.

7. Mudford, N.R. and Stalker, R.J., "The production of pulsed nozzle flows in a shock tunnel", AIAA paper no. 76-357, 1976.

8. Stalker, R.J. and Mudford, N.R., "Starting process in the nozzle of a nonreflected shock tunnel" AIAA Journ., V11, pp. 265-266, 1973.

9. Mirels, H., "Shock tube test time limitation due to turbulent-wall boundary layer", AIAA Journ. V2. pp84-93, 1964.

10. Trimpi, R.L., "A Preliminary Theoretical Study of the Expansion Tube. New Device for Producing High-Enthalpy Short-Duration Hypersonic Gas Flows", NASA Tech. Report R-133, 1962.

11. Jones, J.J., "Some Performance Characteristics of the LRC $3\frac{3}{4}$" Pitot Tube using an Unheated Hydrogen Driver", Fourth Hypervelocity Techniques Symposium, A.E.D.C. Tullahoma, Tennessee pp7-26, Nov. 1965.

12. Givens, J.J., Page, W.A. and Reynolds, R.M., "Evaluation of Flow Properties in a Combustion Tube Operating at 7.5 km/sec." Fourth Hypervelocity Techniques Symposium, A.E.D.C., Tullahoma, Tennessee, pp.27-48. Nov, 1965.

13. Spurk, J.H., "Design, Operation, and Preliminary Results of the BRL Expansion Tube". Fourth Hypervelocity Techniques Symposium, A.E.D.C. Tullahoma, Tennessee, pp.112-144. Nov, 1965.

14. Norfleet, G.D., Lacey, J.J., Whitfield, J.D., "Results of an Experimental Investigation of the Performance of an Expansion Tube". Fourth Hypervelocity Techniques Symposium, A.E.D.C., Tullahoma, Tennessee, pp49-110. Nov. 1965.

15. Paull, A. and Stalker, R.J., "Disturbances in the Driver Gas of a Shock Tube", Report on NASA grant NAGW-674, Supplement 5, 1989.

16. Paull, A. and Stalker, R.J., "The Effect on an Acoustic Wave as it traverses an Unsteady Expansion", to be published in Physics of Fluids.

# EXPERIMENTS on SPACE SHUTTLE ORBITER MODELS in a FREE PISTON SHOCK TUNNEL

by

R. M. KREK* & R. J. STALKER**

Department of Mechanical Engineering

The University of Queensland, Brisbane.

## ABSTRACT

Heat transfer and pressure measurements, were made on a model of the United States Space Shuttle Orbiter in the The University of Queensland's T4 shock tunnel at three angles of attack, with stagnation enthalpies which varied by a factor of 11, from 2.1 MJ/kg to 23 MJ/kg and normal shock Reynolds numbers which varied by a factor of 38, from $2.1\times10^4$ to $8.1\times10^5$. Leeward pressure results were obtained for comparison with flight data and equilibrium calculations, but the majority of the experiments were conducted to investigate the heat transfer distributions around the shuttle model. Both the windward and leeward heat transfer results exhibit the onset of transition to turbulent flow. The leeward results are compared with flight data as well as with conventional wind tunnel data, and are used to establish trends associated with variation in the major flow and geometry parameters. It was found that, although high enthalpy effects could be important, Reynolds number effects played a dominant role in determining the flow.

## NOMENCLATURE

| | |
|---|---|
| A | constant |
| $c_p$ | specific heat at constant pressure, J/kg K |
| E | voltage across the heat transfer gauge |
| h | enthalpy, MJ/kg |

* PhD Student

** Professor in Space Engineering

| | |
|---|---|
| $H_o$ | stagnation entahlpy, MJ/kg |
| k | thermal conductivity, W/m K |
| k | characteristic dimension of roughness element (3μm) |
| K | constant |
| L | model length |
| M | Mach number |
| n | data sample index |
| p | pressure, kPa |
| $P_p$ | Pitot pressure, kPa |
| q | Velocity, m/s |
| q | heat transfer rate, MW/m² |
| $q_s$ | stagnation point heat transfer rate of a sphere, MW/m² |
| R | radius of sphere |
| Re | Reynolds number |
| s | distance along a streamline, m |
| St | Stanton number |
| t | sample point time |
| T | temperature, K |
| U | velocity, m/s |
| x | chordwise distance from model nose |
| α | angle of incidence |
| $\alpha_R$ | temperature coefficient of resistance, $K^{-1}$ |
| β | oblique shock wave angle |
| γ | ratio of specific heats |
| χ | Shock mapping variable |
| ε | inverse density ratio |
| η | length scale for the attachment line boundary layer |
| Λ | leading edge sweep angle |
| μ | viscosity, kgm/s |

| | |
|---|---|
| $\rho$ | density, $kg/m^3$ |

*Subscripts*

| | |
|---|---|
| e | equilibrium conditions |
| f | frozen conditions |
| ns | post normal shock conditions |
| o | stagnation conditions |
| s | shock layer conditions |
| s | conditions along a streamline |
| w | wall conditions |
| x | axial position from nose of model |
| $\infty$ | freestream conditions |
| $\beta$ | post oblique shock conditions |

# 1. INTRODUCTION

The free piston shock tunnel[1] offers a means of improving the test simulation of sub-orbital hypervelocity flight. It raises hypersonic test flow stagnation enthalpy limits from values corresponding to approximately half Earth orbital velocity, where air is just beginning to experience thermal dissociation[2], to values somewhat exceeding orbital velocity, where high dissociation levels can be experienced. In principle, this capability provides an opportunity for exploring the influence of such high enthalpy effects on flight vehicle aerodynamics but, although these effects have been studied on simple models as part of the fundamental research which has been carried out in such tunnels[2,3,4], no systematic study of the validity of tests conducted on a flight configuration has been reported. This is the purpose of the present investigation.

The experiments involved 0.0054 scale models of the U.S. Space Shuttle Orbiter. This configuration was chosen not only because of the availability of published flight data, but also because it represents the type of re-entry glider which is likely to be of interest in the near future.

One particular feature of these gliders is that re-entry is accomplished at a relatively large angle of incidence, leading to an extensive region of separated flow on the leeward side of the vehicle. Since separated regions respond relatively slowly to changes in freestream conditions, and shock tunnels have short test durations, the simulation of steady flow flight data in such regions presents an interesting challenge for a shock tunnel.

The transition from laminar to turbulent boundary layer flow on the model is another point of interest. It is well known that hypersonic wind tunnel transition Reynolds numbers tend to fall well below flight values and, for model testing purposes, it is useful to know how free piston shock tunnels compare with other facilities in this regard.

The experimental measurements were confined to the streamwise midplane of the model, on both the leeward and windward surfaces. Unfortunately, this meant that many interesting flow regions, such as the leeward wing or the fuselage side were neglected. On the other hand, by retaining a fixed pattern of instrumentation it was possible to exploit the operational flexibility of the shock tunnel to cover a wide range of basic flow variables, with stagnation enthalpies varying by a factor of 11, and Reynolds numbers by a factor of 38.

The paper begins with a short description of the facility, model and instrumentation, followed by a discussion of simulation variables. Because shock tunnels accelerate the test gas through a steady nozzle expansion, "frozen" atomic species begin to appear in the freestream as stagnation enthalpies are increased above values corresponding to half orbital velocity. The influence of this on model flows is included in the discussion. The evidence for the existence of quasi-steady flow over the model is next presented, together with the leeward pressure distributions. Heat transfer on the windward surface is then considered, followed by that on the leeward surface, before proceeding to the conclusions which may be drawn from experiments.

# 2. FACILITY, MODEL AND INSTRUMENTATION

## 2.1. Facility

The experiments were carried out in The University of Queensland T4 free piston shock tunnel[5]. This shock tunnel is capable of producing test gas samples with stagnation enthalpies to simulate reentry flight conditions. A sketch of the facility is shown in Figure 1.

The operation of the T4 shock tunnel is as follows. The piston is released and is driven along the compression tube while accelerating and acquiring energy from the expanding air in the reservoir. The piston adiabatically compresses the driver gas (either Helium or Argon) in front of it to a high pressure and temperature. Once the driver gas has reached a sufficient pressure to rupture the main diaphragm separating the compression tube from the shock tube, a high speed shock is produced that passes through the test gas initially residing in the shock tube. The test gas is processed by this shock as it moves along the shock tube. The shock is reflected off the end of the shock tube causing additional compression and heating of the test gas. After the mylar diaphragm (separating the shock tube from the nozzle and test section) bursts the test gas is expanded in an axisymmetric, contoured, hypersonic nozzle to the required flow conditions in the test section.

## 2.2. Model

The first model used was a 0.0054 scale alloy steel model of the Space Shuttle Orbiter supplied by British Aerospace PLC. Moulds of the model were made and a further two models was cast from the moulds. The casting material was an Aluminium filled epoxy resin (CIBA-GEIGY, Araldite CC264-1, Hardener HY956). One model was instrumented with thin film gauges and thermocouples, while the other cast model was used for flow visualisation. Figure 2(a) shows a typical time integrated luminosity photograph of the flow about the shuttle orbiter model. Three series of experiments were performed on the instrumented models. The first series of experiments were performed on the original model which was returned to British Aerospace. The second and third series of experiments were performed on the cast

model. A sketch showing a streamwise section of the midplane of the model is shown in Figure 2(b). The sketch shows the position of the heat transfer gauges and pressure transducers used during the experiments.

## 2.3. Instrumentation

The pressure gauges used were Kulite semiconductor strain gauge type transducers (XCQ-080 SERIES). These gauges were sensitive to model vibration, but it was found that, under given flow conditions, their vibration sensitivity was reproduced from shot to shot. Therefore, in measuring pressure, the vibration component could be subtracted from the recorded signal in order to obtain the pressure. A pitot probe was also used, and was placed adjacent to the model, such that the flows from the model and the probe did not interfere with each other. A PCB 112A pressure transducer was used for the pitot probe.

Thin film heat transfer gauges were used on the leeward surface of the model. They were vacuum deposited on a substrate of quartz of approximately 2mm in diameter and 3mm long. The thin film was made of platinum with a 1000 Å $SiO_2$ overlay, and was approximately 0.5 mm wide.

Two types of thermocouples were used during the course of the experiments. On the original model, Chromel-Alumel thermocouple gauges were used, while on the cast model, Chromel-Constantan thermocouple gauges were used. The thermocouples were used on the windward surface of the models, since their robust nature and high thermal conductivity ensured that they were capable of withstanding the high heat transfer rates, and the relatively harsh post test flow environment encountered on the windward surface.

# 3. TEST CONDITIONS, STEADY FLOW AND DATA REDUCTION

## 3.1. Test Conditions

The free stream conditions within the test section of the tunnel were obtained, by first calculating the stagnation conditions for the nozzle, by measuring the speed of the shock travelling down the shock tube, and the pressure experienced in the stagnation region. The shock speed was determined by 3 PCBs in series equally spaced down the shock tube and the stagnation pressure was measured by 2 PCB 118 pressure transducers.

The stagnation conditions are calculated by a computer program known as ESTC[6] (Equilibrium Shock Tube Calculation). Input to the program are the initial fill pressure of the shock tube, shock speed, stagnation pressure and the composition of the test gas. From these ESTC calculates the conditions behind the primary shock and the reflected shock for a gas in chemical equilibrium.

To calculate the exit conditions of the nozzle a further program known as NENZF[7] (Non-Equilibrium Nozzle Flow) is used. This program uses the output from ESTC for its calculation of nozzle flow assuming one dimensional non equilibrium expansion. For conditions with a stagnation enthalpy of 3 MJ/kg and less, an inhouse program, SHOCK, was used to calculate the freestream conditions. This program calculates the nozzle flow, by assuming one dimensional, perfect gas (with variable ratio of specific heats) expansion. The freestream conditions for the experiments are presented in Table 1.

### 3.1.1. Choice of Reynolds Number

In hypersonic flight, a body such as the Shuttle Orbiter forms a strong bow shock wave. The Mach Number Independence Principle[8] ensures that, at sufficiently high Mach numbers, the flow downstream of this bow shock is independent of the upstream static temperature. Since the temperature is uniquely related to the viscosity, this implies that it is also independent of

upstream viscosity. Therefore the Reynolds number which governs the viscous effects in such flows should be based on post-shock flow parameters.

With this in mind, it is noted that Throckmorton and Zoby[9] follow Bertin and Goodrich[10] in using a post normal shock Reynolds number. The same approach is used here, defining the Reynolds number as

$$Re_{ns} = \rho_\infty U_\infty L / \mu_{ns} \quad (1)$$

where $\rho_\infty U_\infty$ is the product of density and velocity after a normal shock (which is equal to the upstream value, due to continuity), L is the length of the model, and $\mu_{ns}$ is the post shock value of viscosity for equilibrium air, calculated by the Sutherland formula. The test values of $Re_{ns}$ are presented in Table 1.

For the windward surface, it was possible to define the effective Reynolds number more closely as

$$Re_{x\beta} = \rho_s U_s x / \mu_s \quad (2)$$

where x is the distance downstream of the nose, and $\rho_s$, $U_s$ and $\mu_s$ are the density, velocity and coefficient of viscosity respectively after the oblique shock at the windward surface. The viscosity is calculated using the Sutherland formula. As indicated below, the shock layer variables are calculated for equilibrium thermodynamic conditions.

### 3.1.2. Chemical Relaxation and Freestream Freezing

The molecular vibration and dissociation phenomena which occur in hypervelocity flows may generally be classified as chemical effects. These are initiated as the air crosses the bow shock about a vehicle or a model but, because they proceed at a finite rate, they usually have not reached equilibrium in the time that the air passes through the inviscid flow field. This is particularly true for re-entry gliders[2].

Chemical effects therefore scale as binary reactions[2]. This means that the shock mapping variable,

$$\chi = \int_0^s p/q \, ds, \qquad (3)$$

will determine the progress of chemical reactions with distance along a streamline downstream of the shock. This is expressed in figure 3(a), which shows the numerically calculated[7] variation of density, due to reactions along a constant pressure streamline for given streamline enthalpies. The pressure chosen is typical of those prevailing in the experiments, and the density is normalised with respect to the equilibrium density obtained at the quoted pressure and streamline enthalpy. Three full curves are shown, corresponding to zero freestream enthalpy, together with two broken curves, corresponding to freestream enthalpies equal to half the streamline enthalpy. This represents typical conditions after an oblique shock in the experiments. The freestream enthalpies include both the sensible enthalpy and that invested in "frozen" vibration and dissociation. No broken curve is shown for $h_s$ = 5 MJ/kg, because the conditions under which this might be achieved in the experiments are such that $h_\infty$ is much less than one half of $h_s$.

It can be seen that the broken curves differ from their corresponding zero freestream enthalpy curves by no more than 5% for values of $\chi$ exceeding 0.1 $Nm^{-2}s$. In the experiments, for shocks which made an angle greater than 30° with the upstream direction, a value of $\chi$ = 0.1 $Nm^{-2}s$ was reached within a normal distance no greater than 2 mm from the shock. For practical purposes, this may be regarded as within the shock transition, indicating that the effective post shock conditions depend only on the pressure and the static enthalpy, regardless of the degree of freestream freezing.

Now, the windward surface of the Shuttle Orbiter is nearly flat, implying that a good approximation to a constant pressure flow is experienced after crossing the shock. Therefore the zero freestream enthalpy curves of figure 3(a) provide a good representation of the density variation along a streamline. In the tests, the value of $\chi$ at the midchord point, in the midplane, varied from 0.35 to 18 $Nm^{-2}s$, in a way such that the density there was always greater than 90% of the equilibrium density. Because the pressure is constant, and relative

changes in dissociation fraction tend to be small with respect to changes in temperature, this implies that the temperature is within 90% of its equilibrium value or, since the viscosity varies approximately as the square root of the temperature, that the viscosity and Reynolds number differ from their equilibrium values by some 5% and 15% respectively. Thus, for the purposes of data analysis, equilibrium conditions were assumed to prevail in the windward shock layer.

It might be noted that similar values of $\chi$ are obtained in flight, and a similar approximation could be made for the shock layer. In this case the approximation would be somewhat less accurate, since the pressures experienced in flight are lower than the value used for figure 3(a), and values of $\chi$ required to reached equilibrium would be increased by an order of magnitude.

In order to calculate equilibrium conditions within the shock layer, it is necessary to know the freestream enthalpy. This depends upon the expansion of the test gas through the hypersonic nozzle[7], and is shown in figure 3(b) for the nozzle used in all but one of the present tests. The figure is drawn for a nozzle reservoir pressure of 30 MPa, but $h_\infty$ is not very sensitive to $P_o$; for example $h_\infty$ typically changes by only 10% as $P_o$ is reduced by a factor of 10.

For interest, the part of the enthalpy, $h_i$ which is contained in "frozen" dissociation and vibrational energy is also shown, the difference between $h_\infty$ and $h_i$ being sensible enthalpy. Because of the relatively low hypersonic Mach numbers used, the latter represents a substantial part of the freestream enthalpy.

Taking account of $h_\infty$, and neglecting terms of $O(\rho_\infty/\rho_s)^2$, the enthalpy in the shock layer is given as

$$h_s = h_\infty + 0.5\, U_\infty^2 \sin^2\beta \qquad (4)$$

This is normalised with respect to $h_s'$, the shock layer enthalpy for $h_\infty = 0$, a condition which approximates flight, and is plotted in figure 3(c) for two stagnation enthalpies. It can be seen

that the shock layer enthalpy exceeds $h_s'$ by a margin which is very considerable at the lower shock angles. The effect on the inverse density ratio, $\varepsilon$, also is shown, by comparing it with $\varepsilon'$, the value which would be obtained with $h_\infty = 0$. It can be seen that the density ratio can be changed by more than a factor of two at the lower shock angles. These effects obviously influence the shock layer Reynolds number, and this was taken into account in the data analysis by using $h_s$, together with the Newtonian pressure in the shock layer and the assumption of chemical equilibrium, to calculate the density and the temperature. The Sutherland formula then yielded the coefficient of viscosity.

The increased shock layer enthalpy implies a correspondence with flow at a higher stagnation enthalpy. A shock layer flow similitude arising out of this correspondence is outlined in reference 2 but, because it would have involved scaling the model span as $\varepsilon^{1/2}$, it was not used here. Thus the inviscid flow patterns in the shock layer strictly do not relate to specific flight cases. However, because the shock layer remains thin enough to ensure that crossflow velocities are small, the heat transfer will not be affected significantly by any differences. Also, because the spanwise flow velocity on a delta wing[11] varies approximately as $\varepsilon^{1/2}$, the time taken for a gas particle to pass from the shock to the wing leading edge is expected to be no less than half of that for the $h_\infty = 0$ case, and this difference is not great enough to significantly influence the state of the gas as it leaves the windward surface to pass to the leeside of the fuselage.

Thus, the heat transfer to the windward surface will be governed by the nozzle stagnation enthalpy, in combination with a shock layer density and viscosity obtained at conditions corresponding to a higher stagnation enthalpy flow with $h_\infty = 0$. The same condition will also govern the state of the flow in passing from the windward to the leeward surface.

Most of the leeward surface flow involves flow from the windward surface. This is illustrated by flow streamlines, such as those presented in reference 10, which show flow from near the nose reaching the leeward surface upstream of x/L = 0.3. At higher incidence, it may be

expected to reach it even closer to the nose. Reference 12 indicates that a complicated vortex flow exists in the leeward region, suggesting mixing there which is likely to involve both gas which has passed through the windward shock layer and gas which has passed through the leeward bow shock. This makes it difficult to estimate the effect that freestream freezing may have on the leeward flow, and it will be necessary to rely on experimental results for information on this aspect.

## 3.2. Steady Flow

Typical stagnation pressure signals for a range of stagnation enthalpies are shown in Figure 4. Figures 4(a) to 4(c) are characteristic of undertailored operation, and were obtained with a helium driver gas, while figure 4(d) was obtained with an argon driver, being characteristic of slightly overtailored shots. The number of model lengths, N, which the flow travels over the model during the test time is also shown, together with the test period during which results were obtained. The test period is the time between T and T'. The time at which the test flow becomes contaminated by driver gas also is shown, as calculated by the method of reference 13, which tends to be conservative. Contamination therefore occurs after the test period in all four cases.

It can be seen that the nozzle stagnation pressure decays significantly during the test period for the undertailored conditions. However, the decay never exceeds 7% over the time interval required for the flow to pass one model length and, having regard to the accuracy of the measurements, this is not expected to significantly influence the results.

The main aim of these experiments was to investigate the leeward surface flow, and this required a quasi-steady flow over the upper surface of the model. To check this, the distributions of surface pressure and heat transfer were plotted at the beginning, middle, and end of the test period, as shown in Figure 5. In order to allow for the variation of freestream conditions over the test time, the pressure was normalised with respect to the pitot pressure,

and the heat transfer to the stagnation point heat transfer rate on a reference sphere (see equation 8 below). Results of three test conditions are shown, two at high enthalpy and one at low enthalpy.

It can be seen that no measurable variation in the pressure distribution occurred over the test time, a result which is typical of all tests. There is also no systematic variation in the heat transfer rate indicating that, to within the accuracy of the measurements, the flow is steady.

This is not a suprising result. Helms[12] has pointed out that the leeward flow of the shuttle can be thought of as a swept cylinder flowfield. The reattaching vortices in such a flowfield are generically similar to those which can occur in swept shock boundary layer interaction, and in numerical studies, Knight[14] has shown that these become steady within three to four times the time required for a fluid element in the inviscid flow to pass along the streamwise length of the flow region. In the present case, the flow is maintained for 10 to 15 times the time required for the flow to pass over the length of the model, so a steady leeward flow would be expected.

## 3.3. Data Reduction

As stated above the pressure signals from the model were normalised by the pitot pressure to account for the change in the flow properties during the course of the test time. Pressure results were only obtained for the first series of experiments which were performed on the original model.

The heat transfer rates are calculated by integrating the temperature signals using the semi-infinite one dimensional heat transfer model and neglecting gauge and insulation thickness. These assumptions lead to the expression given in equation 5[15].

$$\dot{q}(n) = \frac{2\sqrt{\rho ck}}{\alpha_R E_o \sqrt{\pi}} \sum_{i=1}^{n} \frac{E(t_i) - E(t_{i-1})}{\sqrt{t_n - t_i} + \sqrt{t_n - t_{i-1}}} \qquad (5)$$

The values for $\alpha_R$ were found by calibration and the thermal product $\sqrt{\rho ck} = 1530 Ws^{1/2}m^{-2}$ for the thin film gauges.

The integrated signal is then normalised by pitot pressure, again to take account of the changing freestream, then this value is multiplied by a nominal value of pitot pressure to bring the units back to those of heat transfer rate. This procedure was justified by an analysis of the effect of decaying stagnation enthalpy with falling stagnation pressure, for a constant area ratio nozzle. The analysis assumed laminar heat transfer, dependent on the normal shock Reynolds number, a pitot pressure proportional to the stagnation pressure, and a value of 1.3 for the ratio of specific heats in the stagnation region. The heat transfer then varies as (pitot pressure)$^{0.73}$, and, having regard to the assumptions made in the analysis, it was reasonable to approximate this by normalising the heat transfer by the pitot pressure.

## 4. Flow Visualisation

The methods of flow visualisation used during the course of these tests included, time integrated luminosity photography, and HYCAM camera photography, capable of taking approximately 9000 frames/sec.

Figure 2(a) shows a time integrated luminosity photograph taken at an angle of incidence of 40°, with test conditions corresponding to Condition 2. This luminosity photograph shows the major flow features that are visible in the HYCAM photos, which were taken during the test time. These flow features are the strong shock waves coming off the wing roots, a weak

inflection in the windward shock wave, and the weakening of the bow shock as it progresses to the leeward flow field.

The shock waves emanating from the wing roots may have some effect on the upper surface flow just upstream of the fin. The inflection in the windward shock wave that occurs at about 25% of the chord length from the nose, is thought to be due to the interaction between real gas dynamics and the expansion due to the transition from the blunt nose to the after body[16].

# 5. PRESSURE DATA

## 5.1. Windward Pressure Data

The range of incidence was such that Newtonian flow was assumed. This was checked by pressure measurements at one station, indicating values which, typically, were approximately 75% of the expected ones at $\alpha = 50^{\circ}$. Whilst the source of this discrepancy has not been identified, it is not large enough to significantly influence the interpretation of the experiments, and so it is ignored.

## 5.2. Leeward Pressure Data

Figure 6(a) displays the effect of changing incidence on the leeward pressure distribution. As shown in Figure 2, the upstream pressure orifice is forward of the cockpit canopy and measures an increase in surface pressure as the incidence is reduced. This is consistent with the expected reduction in the strength of the expansion following the bow shock. The measurements downstream of the canopy show a weak effect as the incidence is varied. It can be seen that as the incidence decreases, the pressure gradient at the downstream station decreases. Noting that this station is less than one body radius upstream of the fin and the orbital manoeuvering unit pods, it could be influenced by a separation zone engendered by these obstacles.

There is no detectable effect of stagnation enthalpy or Reynolds number on the pressure distribution. This is evident in comparing the results at different stagnation enthalpies for $\alpha$ = 50° and $\alpha$ = 40° in Figure 6(a), and in comparing these results at $\alpha$ = 50° with the pressure distributions in Figure 5. The stagnation enthalpy varied by a factor of 8 in these particular tests and, although the Reynolds number varied only by a factor of 5.5, it will be seen below that this was sufficient to encompass transition from laminar to turbulent flow on the leeward surface. Thus, the changes in both parameters were sufficient to provide a strong indication of the insensitivity of leeward pressures to these effects.

In figure 6(b), tunnel pressure distributions are compared with those obtained in flight and by numerical calculation at a stagnation enthalpy of 24 MJ/kg[17]. It can be seen that the low surface pressures immediately aft of the canopy are evident in both the tunnel and the flight data, as well as the calculations. Forward of the canopy, the tunnel measurements appear to be in excess of the flight value. However, the tunnel measurements were taken at x/L = 0.09, and the flight measurements at x/L = 0.12. If the steep pressure gradient evident near the nose in the calculations were to occur somewhat downstream of its calculated location, then the tunnel and flight measurements would be consistent.

# 6. HEAT TRANSFER DATA

## 6.1. Windward Heat Transfer Data

The heat transfer to the windward surface is most conveniently non-dimensionalised as a Stanton number, $St_\beta$, given by

$$St_\beta = \dot{q}/(\rho_s u_s H_o) \qquad (6)$$

Because a nearly constant pressure flow prevails on the windward surface, the quantity $St_\beta \sqrt{Re_{x\beta}}$ may be expected to be invariant with $Re_{x\beta}$ in regions where the boundary layer is laminar[18]. Figure 7 shows plots of the variation of this parameter for the three incidences tested at each station on the windward centreline.

The error bars indicated in the figure represent data reading accuracies. The absolute value of heat transfer is uncertain, since an accurate absolute calibration of the thermocouple heat transfer gauges could not be obtained. This is because they were manufactured as coaxial thermocouples, with the junction made by drawing emery cloth over the gap between the two thermoelectric materials. This meant that the microscopic configuration of the junction was not controlled and therefore, although the gauge calibration factor remained constant over a series of tests, its value was uncertain. It also meant that the heat transfer distribution along the surface in any one test could not be obtained with an assured accuracy, and led to the mode of presentation used in figure 7, where the effect of changing flow conditions on the heat transfer is shown independently for each station.

6.1.1. Effect of Reynolds Number - Transition

As outlined by Poll[19], transition of the attachment line boundary layer will determine the point of transition on a body at incidence. In the case of the shuttle, the attachment line is located on the windward centreline for the incidences and Mach numbers studied in the present tests. A Reynolds number as given by Poll for an attachment line on the windward centreline, is defined as

$$Re \approx \left[\frac{x}{k}\frac{1}{A\tan\alpha\tan\Lambda}\right]\frac{k}{\eta} \qquad (7)$$

where Re is the Reynolds number calculated at the reference temperature,

x is the distance along the attachment line,

k is the characteristic dimension of the surface roughness ($\approx 3\mu m$),

$\alpha$ is the angle of incidence,

$\Lambda$ is the leading edge swept angle,

and $\eta$ is the length scale for the attachment line boundary layer.

Using this relation, the model roughness here is found to be small enough that transition of the attachment line boundary layer is determined by freestream disturbances. Transition can be seen most clearly in the results presented in figure 7(b), where the rise in heat transfer

with $Re_{x\beta}$, which signals the onset of transition, occurs at a Reynolds number of approximately $7\times10^5$ for $H_o < 8$ MJ/kg. In other experiments with a zero incidence flat plate in the same tunnel[20], a transition Reynolds number of $1.3\times10^6$ was obtained at approximately the same stagnation enthalpy and unit Reynolds number. Allowing for the lower Mach number in the model shock layer[21], these results are consistent with the presence of a smooth model surface.

Miller[22] reports shock layer transition Reynolds numbers, on a similar model, of approximately $2.3\times10^6$ in a conventional hypersonic wind tunnel. Whilst the difference between this and the present results can be accounted for in terms of differing unit Reynolds numbers and wall to recovery temperature ratios in the two sets of tests[21], it serves as a reminder of the caution needed in comparing results in different facilities.

### 6.1.2. Effect of Incidence

As $\alpha$ is increased the shock layer velocity is reduced, and the temperature increases. Therefore the Reynolds number decreases. Thus the flow will need to proceed further along the model in order to obtain the Reynolds number needed for transition. The results for $\alpha$ = 40° and 30° indicate that this Reynolds number remains approximately constant as the incidence is increased. The transition Reynolds number is not well defined for $\alpha$ = 50°, but it appears that it may be somewhat higher than the other two incidences.

### 6.1.3. Effect of Enthalpy

Examining Figure 7, the flow is predominantly Reynolds number dependent. However, there is a consistent tendency for the results at $H_o$ = 20-24 MJ/kg to display an increase in heat transfer at a Reynolds number which may be as little as one half the lower enthalpy results. This suggests the possibility that real gas effects involving air chemistry may be having some influence on transition.

## 6.2. Leeward Heat Transfer Data

### 6.2.1. Effect of Reynolds Number - Transition

Flight data[9] indicates that transition from laminar to turbulent flow in the boundary layer on the leeward surface takes place at a normal shock Reynolds number of approximately $4\times10^5$. This was made apparent in the flight data by plotting the leeward heat transfer data, normalised with respect to the stagnation point heat transfer for a 0.305 m radius sphere. As the Reynolds number passed through the transition region, the normalised heat transfer increased by a factor of 2 or more.

The same effect is evident in the data presented here. Figure 8 shows heat transfer measurements, normalised with respect to the stagnation point heat transfer for a sphere with a radius 0.0093 of the model length. According to Sutton and Graves[23] the equilibrium heat transfer rate to a sphere is given as

$$q_s = K\sqrt{\frac{P_{ns}}{R}}\ (h_o - h_w) \qquad (8)$$

where $q_s$ is the heat transfer at the sphere

K is a proportionality constant (= 0.1113 kg/s $m^{3/2}atm^{1/2}$ for air)

$P_{ns}$ is the pressure behind the bow shock in atmospheres

R is the radius of the sphere

$h_o$ is the enthalpy behind the bow shock and

$h_w$ is the enthalpy at the wall.

It will be remembered that thin film gauges were used to obtain the measurements on the leeward surface. These gauges are calibrated, and therefore the error bars shown represent the overall accuracy of the measurements.

The results in figure 8 were taken at widely differing stagnation enthalpies and incidence, but they show the strong increase in heat transfer with increasing Reynolds number which has been identified with transition.

Data obtained at a stagnation enthalpy of 2.4 MJ/kg and an incidence of 30° in the Calspan 96 inch shock tunnel[10] are also presented in figure 8(c), for comparison with present high enthalpy results. The Calspan data exhibits similar trends to the T4 data, with a comparable relative change in the heat transfer associated with transition, but with lower heat transfer levels. When the stagnation enthalpy was reduced to 2.9 MJ/kg in the present tests, the turbulent heat transfer levels obtained were in agreement with the Calspan data. Unfortunately no low enthalpy tests were made in which the Reynolds number was low enough to produce laminar leeward flow.

The results also serve as a reminder of the difficulty of using tunnel data to predict transition in flight. Bertin and Goodrich[10] use data similar to the Calspan data in Figure 8(c) to indicate a tunnel transition Reynolds number of $0.2\times10^5$ , which is more than an order of magnitude less than the value of $4\times10^5$ obtained in flight (albeit at an increased incidence of 40°). The comparisons presented by Throckmorton and Zoby[9] indicate that conventional hypersonic tunnels are no better, maintaining turbulent levels of heat transfer rate at Reynolds numbers down to $0.4\times10^5$ . The present tests yield approximate values of transition Reynolds number of $0.8\times10^5$ at a stagnation enthalpy of 23.2 MJ/kg and $2\times10^5$ at 40° for a stagnation enthalpy of 2.4 MJ/kg. Whilst these values represent some improvement on previous tunnel results, they remain at half an order of magnitude less than the flight values.

For further consideration of the leeward heat transfer rates, the method of converting the results to non-dimensional form requires more discussion. The approach used above focuses on the flow field transverse to the body, and implies a flow in which the leeside vortex motion leads to a surface flow rather like that of a swept cylinder[12]. The heat transfer results therefore are correlated in terms of a stagnation point heat transfer model. However, it is equally valid to focus on the strong streamwise component of flow[9] and to seek to correlate the results in terms of Reynolds number effects associated with a zero pressure gradient boundary layer model. Bearing in mind that, unlike equation (8), the Reynolds numbers used

explicitly involve the post shock viscosity, it follows that the two models will not be expected to yield exactly the same correlations.

For laminar flow, both forms of data presentation are used. In one, equation (8) is used as above in order to supply the normalising variable and in the other, noting that zero pressure gradient laminar heat transfer varies as the square root of the Reynolds number, the data is plotted as $St\sqrt{Re_{ns}}$ versus $Re_{ns}$.

For turbulent flow, it is necessary to introduce a partial Reynolds number dependence in employing equation (8). Helms[12] noted that, with a given flow structure, $\dot{q}$ may be expected to be proportional to $Re_{ns}^{-0.2}$, whilst the laminar stagnation point heating is proportional to $Re_{ns}^{-0.5}$. Therefore the ratio will be proportional to $Re_{ns}^{-0.3}$. Thus, following Helms, the stagnation heat transfer based correlation is employed by plotting $q/(q_r Re_{ns}^{0.3})$. The Reynolds number based correlation is employed by noting that, for turbulent heat transfer, the Stanton number is proportional to $Re_{ns}^{-0.2}$, and thus the turbulent data is plotted as $StRe_{ns}^{0.2}$ versus $Re_{ns}$ .

6.2.2. Comparison with Flight Data

The tunnel tests indicate that, for flight to tunnel comparisons with a turbulent boundary layer, nearly the same value of stagnation enthalpy is required. Flight data[9] was available at stagnation enthalpies of 9.9 MJ/kg and 6.5 MJ/kg, and, in figure 9(a), this is compared with measurements made in the present tests with a stagnation enthalpy of 8.1 MJ/kg, using the first correlation method. It can be seen that the tunnel and the flight data appear to be consistent.

However using the Reynolds number method to present the turbulent data figure 10(b), it can be seen that $StRe_{ns}^{0.2}$ for the present tests tends to be a little higher than the flight data[9] at comparable values of $Re_{ns}$, and that the apparent consistency noted above is due to a difference in Reynolds number. The present data is comparable with conventional hypersonic wind tunnel tests for a turbulent flow and appears to follow the trend with $Re_{ns}$ of

those tests. For reasons which are briefly discussed in reference 9, the Calspan shock tunnel data is not consistent with this trend.

Considering a laminar flow, the heat transfer is firstly plotted as $q/q_r$ in figure 9(b). As foreshadowed above, the flight laminar data is only available at high stagnation enthalpies but is seen to be consistent with tunnel data with stagnation enthalpies of 6 MJ/kg and lower; excepting, of course, the downstream station, where transition may be beginning. The high enthalpy condition at 22.5 MJ/kg, overpredicts the flight data by a factor of 2.

If the laminar data is plotted as $St\sqrt{Re_{n_s}}$ versus $Re_{n_s}$, as shown in figure 11, it can be seen that again the data at stagnation enthalpies of 6 MJ/kg and less are consistent with the flight data, at comparable normal shock Reynolds numbers. The flight data exhibits a trend of increasing $St\sqrt{Re_{n_s}}$ with decreasing $Re_{n_s}$ at the lower $Re_{n_s}$ values and the present tests continue this trend down to the lower Reynolds numbers. The discrepancy between tunnel and flight which was seen in figure 9(b) now appears as a Reynolds number effect. The trend of the data indicates that, if the tunnel Reynolds number could be increased to flight values without causing transition, similar values of $q/q_r$ would be obtained.

6.2.3. Effect of Stagnation Enthalpy

Examining the laminar case in figure 11, it can be seen that the data at $Re_{n_s} = 6.6\times10^4$ may appear to suggest a substantial effect of stagnation enthalpy at the two downstream stations. However, the value of $Re_{n_s}$ is then so high that the possibility of the early development of transition cannot be discounted, and so this data should be ignored. Therefore there is no evidence of stagnation enthalpy effects on leeward laminar heat transfer.

It will be recalled that, in section 3.1.2, the question was raised of the possible influence of freestream chemical freezing on the leeward flow. Such an influence would be connected with stagnation enthalpy effects which are absent in the present data, as well as in the leeward pressure distributions in figure 5. They are also absent in other leeward laminar heat

transfer data obtained at $\alpha$ = 50°, which, at stagnation enthalpies of 5-8 MJ/kg and 20-24 MJ/kg respectively, and nearly identical Reynolds numbers, displayed essentially identical levels of heat transfer along the fuselage. Therefore it is concluded that freestream freezing has no significant effect on the leeward flow.

The turbulent flow case is considered in figure 10. Referring to $\alpha$ = 50° & 40°, it is seen that $StRe_{ns}^{0.2}$ is weakly sensitive to $Re_{ns}$, and that this is true for most stagnation enthalpies, except at 22 MJ/kg. $StRe_{ns}^{0.2}$ is then higher than the other hypersonic wind tunnel data, particularly if the Calspan results are set aside for the purpose of this comparison.

It might be noted in figure 10(a) that these high enthalpy results are well in excess of results obtained at nearly the same Reynolds number, but a lower stagnation enthalpy, suggesting that they do indeed represent a high enthalpy effect. It is possible that they may be associated with chemically induced changes in the vorticity generated by the curved shock wave about the leading edge of the windward surface. Work is in progress to test this hypothesis through a study of leeward flow on cones at incidence.

Referring to the $\alpha$ = 30° case, only a little data is available, and no discernible stagnation enthalpy effects can be noticed.. The flow structure on the leeward surface is thought to be different to that at $\alpha$ = 40° and 50°, since there are indications that the trends with $Re_{ns}$ may be different for all the stations down the leeward surface.

### 6.2.4. Effect of Incidence

Considering the laminar flow case first, only limited data was obtained at $\alpha$ = 50° & 30°, and so no attempt was made to determine the effect of $Re_{ns}$ at these two conditions (Although, there was limited evidence that the sensitivity to $Re_{ns}$ seen at $\alpha$ = 40° was not experienced at $\alpha$ = 30° ). However, it can be seen from figure 8 that, when some allowance is made for the trends with $Re_{ns}$ in figure 11, the heat transfer increases as the incidence is reduced from 50° to 40°. This is taken as evidence of a changing flow pattern.

Returning to figure 10, in order to consider the turbulent data, it is see that the $\alpha$ = 50° & 40° measurements show similar trends with $Re_{ns}$, but the 30° results, although limited, indicate a changed heat transfer distribution along the model. For the low and medium enthalpy conditions, it is found that for stations x/L = 0.38 & 0.48, the heat transfer at $\alpha$ = 30° is higher than at the other two incidences. As in the laminar case, this is taken as evidence of a changed flow pattern. The high enthalpy data for turbulent flows does not exhibit substantial changes in heat transfer distribution with changing incidence, indicating a stable flow pattern in contrast to the flow patterns experienced at low enthalpy.

### 6.2.5. Effect of Mach Number

One shot was conducted at $\alpha$ = 40° with a hypersonic nozzle with a nominal Mach number of 9. The stagnation enthalpy was about 18 MJ/kg and it can be seen from figure 11 that $St\sqrt{Re_{ns}}$ was similar to the 19 MJ/kg, Mach number = 5 case at the same Reynolds number. This result confirms the application of the Mach number independence principle to the present results.

## 7. CONCLUSIONS

The experiments showed that, as with the other shock tunnels referred to here, the test times available in a free piston shock tunnel are more than adequate to establish steady conditions in the three dimensional, separated, leeward flow about a re-entry glider configuration. This was verified by pressure and heat transfer measurements.

The leeward pressure results were broadly consistent with equilibrium flow calculations and flight data, and were insensitive to changing stagnation enthalpy and Reynolds number.

Boundary layer transition on the windward centreline occurred at a Reynolds number which varied from 0.5 - $1\times10^6$, depending on the incidence. As with other hypersonic wind tunnels,

this is considerably lower than flight values. The point of transition moved further down the model as the incidence was increased. Poll's theory[18] indicated that transition was dependent on freestream disturbances, as the roughness of the model (3 μm) was too small to trigger transition. High stagnation enthalpies resulted in a lower transition Reynolds number. Whilst this suggests a high enthalpy effect on transition, the possibility of a change in freestream turbulence at high enthalpy cannot be discounted at this stage.

The leeward heat transfer measurements covered both laminar and turbulent flow regimes. Once again, the transition Reynolds number was half an order of magnitude less than the flight transition Reynolds number, but was closer to the flight values than transition Reynolds numbers obtained in other hypersonic wind tunnel facilities.

The leeward laminar heat transfer at an incidence of 40° was subject to a Reynolds number effect. When this was taken into account, the tunnel measurements were found to be consistent with flight values. Some data taken at the other two angles of incidence suggested that the flow patterns was sensitive to incidence, and that the Reynolds number dependence would not be the same at other incidences. There was no evidence of a stagnation enthalpy effect.

The leeward turbulent results at an incidence of 40° were subject to a weak Reynolds number effect, and when this was taken into account the heat transfer was seen to be a little in excess of flight values, but was consistent with results obtained with conventional hypersonic wind tunnels. There was evidence that the flow pattern changed in passing from 40° to 30° incidence. For the leeward turbulent flows, high stagnation enthalpies resulted in a considerable increase in heat transfer.

The experiments showed that valid flight vehicle testing could be conducted in a free piston shock tunnel. Where the test regimes coincided, results were generally consistent with those obtained in conventional hypersonic tunnels, and apart from leeward turbulent heat transfer at

low Reynolds numbers, with those in a conventional shock tunnel. They were also consistent with flight measurements, with the exception that, as with the other wind tunnel facilities, transition occurred at a lower Reynolds number. The leeward flow was seen to depend on the state of the boundary layer, the Reynolds number, the angle of incidence, and, for turbulent flow, the stagnation enthalpy, indicating that leeward flow testing on re-entry gliders will generally require attention to all these parameters.

## ACKNOWLEDGEMENTS

The authors wish to thank British Aerospace PLC, for supplying the original model of the United States Space Shuttle Orbiter, G. Dick for the manufacture of moulded copies, and the Australian Research Council for partial support of this project. One of the authors (R.J.S.) would like to express thanks to British Aerospace for a period spent at the College of Aeronautics, Cranfield, during which the initial analysis of test results was conducted.

## REFERENCES


1. Stalker, R.J., *Development of a Hypervelocity Wind Tunnel.*,1972, Aero. Journ. Vol. 76., pp 374-384.
2. Stalker, R.J., *Hypervelocity Aerodynamics with Chemical Nonequilibrium.*, 1989, Ann. Rev. Fluid Mech., Vol. 21, pp 37-60.
3. Hornung, H.G., and Stalker, R.J., *Studies of Relaxation Gas Dynamics in the Free Piston Shock Tunnel.*, 1978, Applied Mechanics. Ed. H. Oertel, Jr., Universität Karlsruke., pp 19-28.
4. Stalker, R.J., *Shock Tunnels for Real Gas Hypersonics.*, 1987, Agard Conference Proc. No. 428. - Aerodynamics of Hypersonic Lifting Vehicles. pp 4-1, 4-10. AGARD CP428.
5. Stalker, R.J., and Morgan, R.G., *The University of Queensland Free Piston Shock Tunnel T4 - Inital Operation and Preliminary Calibration.*, 4th National Space Engineering Symposium, Adelaide, 1988.
6. McIntosh, M.K., *Computer Program for the Numerical Calculation of Frozen and Equilibrium Conditions in Shock Tunnels.*, Report, Dept of Physics, ANU, 1968.
7. Lordi, J.A., Mates, R.E., and Moselle, J.R., *Computer Program for the Numerical Solution of Nonequilibrium Expansions of Reacting Gas Mixtures.*, NASA CR-472, 1966.
8. Hayes, W.D., and Probstein, R.F., *Hypersonic Flow Theory.*, Vol. 1, *Inviscid Flows.* 1966, Academic Press, INC., London.
9. Throckmorton, D.A., and Zoby, E.V., *Orbiter Entry Leeside Heat-Transfer Data Analysis.*, J. Spacecraft and Rockets., 1983, Vol 20, No. 6, pp 524-530.
10. Bertin, J.J., and Goodrich, W.D., *Effects of Surface Temperature and Reynolds Number on Leeward Shuttle Heating.*, J. Spacecraft and Rockets, 1976, Vol. 13, No. 8, pp 473-480.
11. Stalker, R.J., *Nonequilibrium Flow over Delta Wings with Detached Shock Waves.*, 1982, AIAA Journ., Vol. 20. pp 1633-1639.

12. Helms III, V.T., *An Empirical Method for Computing Leeside Centerline Heating on the Space Shuttle Orbiter.*, J. Spacecraft and Rockets., 1983, Vol. 20, No. 3, pp225-231.

13. Stalker, R.J., and Crane, K.C.A., *Driver Gas Contamination in a High Enthalpy Reflected Shock Tunnel.*, 1978, AIAA Journ., Vol. 16., pp 277-278.

14. Knight, D.D., *Calculation of 3-Dimensional Shock/Turbulent Boundary Layer Interaction Generated by a Sharp Fin.*, 1985, AIAA Journ., Vol. 23., pp 1885-1891.

15. Schultz, D.L., and Jones, T.V., *Heat Transfer Measurements in Short Duration Hypersonic Facilities.*, 1973, AGARDoGRAPH No. 165.

16. Gai, S.L., Sanderman, R.J., Lyons, P., and Kilpin, D. *Shock Shape over a Sphere Cone in Hypersonic High Enthalpy Flow.* 1984, AIAA Journ., Vol. 22, No. 7, pp 1007-1010.

17. Prabhu, D.K., and Tannehill, J.C., *Numerical Solutions of Space Shuttle Orbiter Flowfield Including Real Gas Effects.*, J. Spacecraft and Rockets., 1986, Vol. 23, No. 3, pp 264-272.

18. East, R.A., Stalker, R.J, and Baird, J.P., *Laminar Flat Plate Heat Transfer Measurements from a Dissociated High Enthalpy Hypersonics Air Flow.*, 1977, AASU Report no. 338.

19. Poll, D.I.A., *A New Hypothesis for Transition on Windward Face of the Space Shuttle.*, J. Spacecraft and Rockets, 1986, Vol. 23, No. 6, pp 605-611.

20. Yaping He., *Transition and Heat Transfer in the Compressible Boundary Layer over a Flat Plate.*, 1991, Submitted for PhD. University of Qld.

21. Henderson, A. Jr., *Hypersonic Viscous Flows.*, 1969, Chapter 3 of Modern Development in Gas Dynamics., Plenum Press.

22. Miller, C.G., *Experimental Investigation of Gamma Effects on Heat Transfer to a 0.006 Scale Shuttle Orbiter at Mach 6.*, AIAA Paper No. 82-0826, 1982.

23. Sutton, J., and Graves, R.A., *A General Stagnation Point Convective Heating Equation for Arbitrary Gas Mixtures.* NASA TR, R-376, 1972.

| Condition | $P_o$ MPa | $H_o$ MJ/kg | $T_\infty$ K | $P_\infty$ kPa | $\rho_\infty$ kg/m³ | $U_\infty$ m/s | $M_\infty$ | $\gamma$ | $Re_\infty$ ×10⁶ |
|---|---|---|---|---|---|---|---|---|---|
| 1 | 28.7 | 21.6 | 2540 | 12.9 | 1.51E-2 | 5400 | 5.14 | 1.35 | 0.122 |
| 2 | 14.2 | 23.8 | 2660 | 7.10 | 7.56E-3 | 5540 | 4.99 | 1.37 | 0.062 |
| 3 | 9.3 | 22.5 | 2390 | 4.70 | 5.62E-3 | 5390 | 5.10 | 1.38 | 0.046 |
| 4 | 3.9 | 19.5 | 1690 | 1.54 | 2.59E-3 | 5030 | 5.59 | 1.39 | 0.020 |
| 5* | 52.4 | 17.8 | 790 | 0.64 | 2.51E-3 | 5340 | 8.96 | 1.40 | 0.021 |
| 6 | 26.3 | 15.2 | 1890 | 11.0 | 1.84E-2 | 4660 | 5.32 | 1.34 | 0.135 |
| 7 | 48.1 | 8.3 | 1160 | 20.7 | 6.20E-2 | 3640 | 5.49 | 1.33 | 0.420 |
| 8 | 28.0 | 7.9 | 1220 | 10.6 | 3.47E-2 | 3570 | 5.61 | 1.34 | 0.240 |
| 9 | 6.1 | 11.7 | 1230 | 2.36 | 6.11E-3 | 4070 | 5.65 | 1.36 | 0.042 |
| 10 | 6.3 | 8.6 | 990 | 2.36 | 7.96E-3 | 3610 | 5.73 | 1.35 | 0.054 |
| 11 | 6.8 | 7.3 | 870 | 2.54 | 1.00E-2 | 3390 | 5.79 | 1.36 | 0.068 |
| 12 | 6.7 | 5.7 | 630 | 2.40 | 1.33E-2 | 2940 | 5.9 | 1.38 | 0.083 |
| 13 | 39.6 | 2.4 | 270 | 10.3 | 1.30E-1 | 2190 | 6.59 | 1.41 | 0.810 |
| 14 | 21.0 | 2.9 | 320 | 5.36 | 5.58E-2 | 2390 | 6.56 | 1.40 | 0.345 |
| 15 | 24.4 | 2.1 | 230 | 6.38 | 9.37E-2 | 2060 | 6.58 | 1.44 | 0.582 |
| 16 | 13.2 | 2.9 | 330 | 3.49 | 3.56E-2 | 2400 | 6.49 | 1.40 | 0.210 |
| 17 | 6.6 | 2.7 | 310 | 1.61 | 1.83E-2 | 2320 | 6.61 | 1.40 | 0.114 |
| 18 | 7.5 | 2.4 | 270 | 1.98 | 2.49E-2 | 2190 | 6.59 | 1.40 | 0.153 |

* This condition used a nozzle with a nominal Mach number of 10.

**Table 1. Test Conditions.**

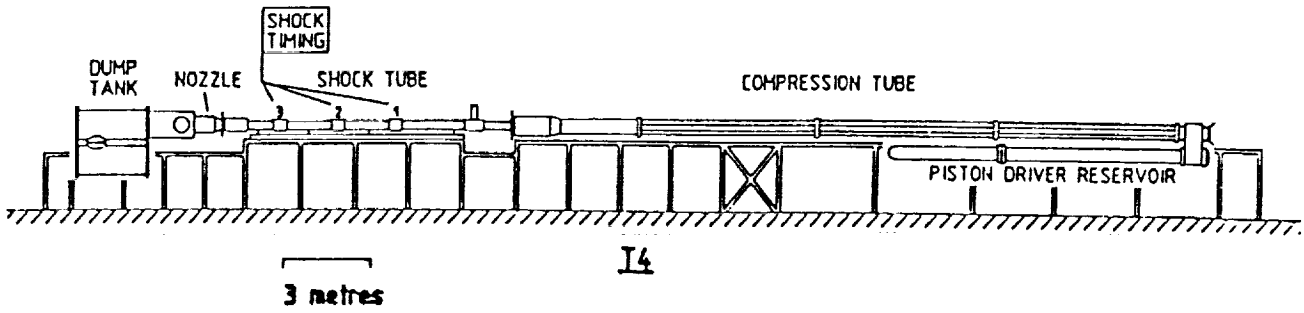


Figure 1. Sketch of the T4 Shock Tunnel Facility

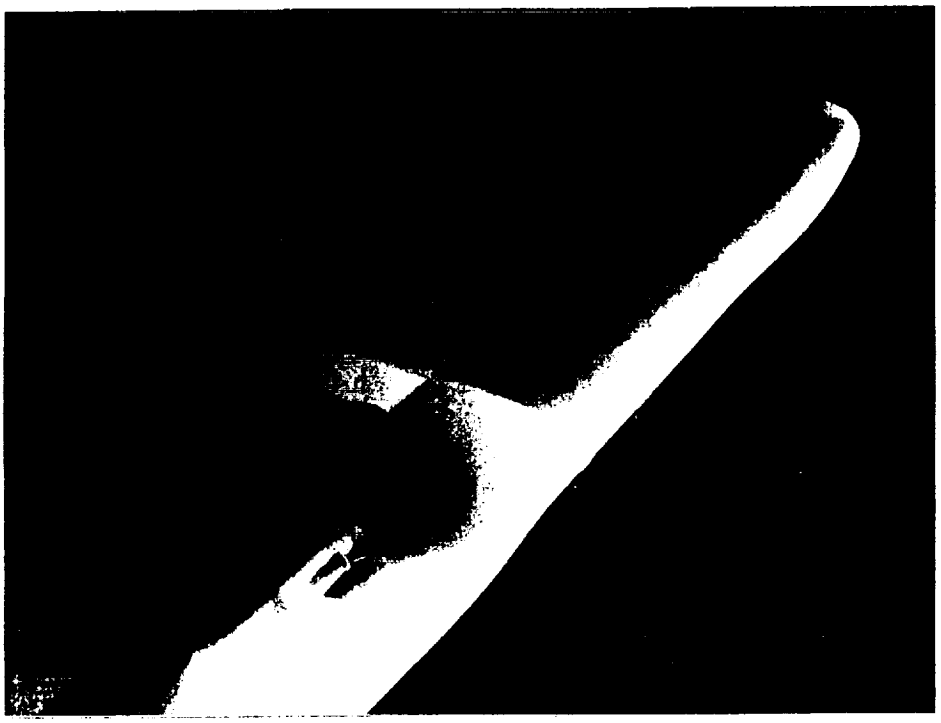

Flow

(a)

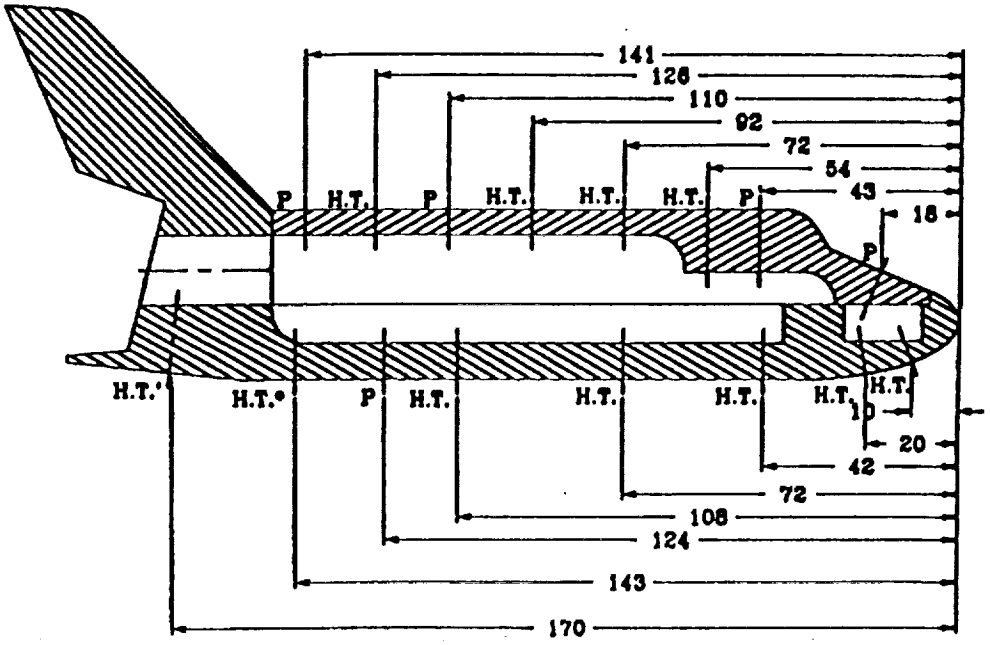


(b)

NOTES:

Dimensions in mm.
Pressure measurements taken only on original model.
H.T.' – Measured on original model only.
H.T.* – Measured on Aluminium epoxy model only.

Figure 2. a) Time integrated luminosity photograph of flow about shuttle orbiter model. $\alpha = 40°$, Condition 2. b) Sketch of the measuring stations on the shuttle model.

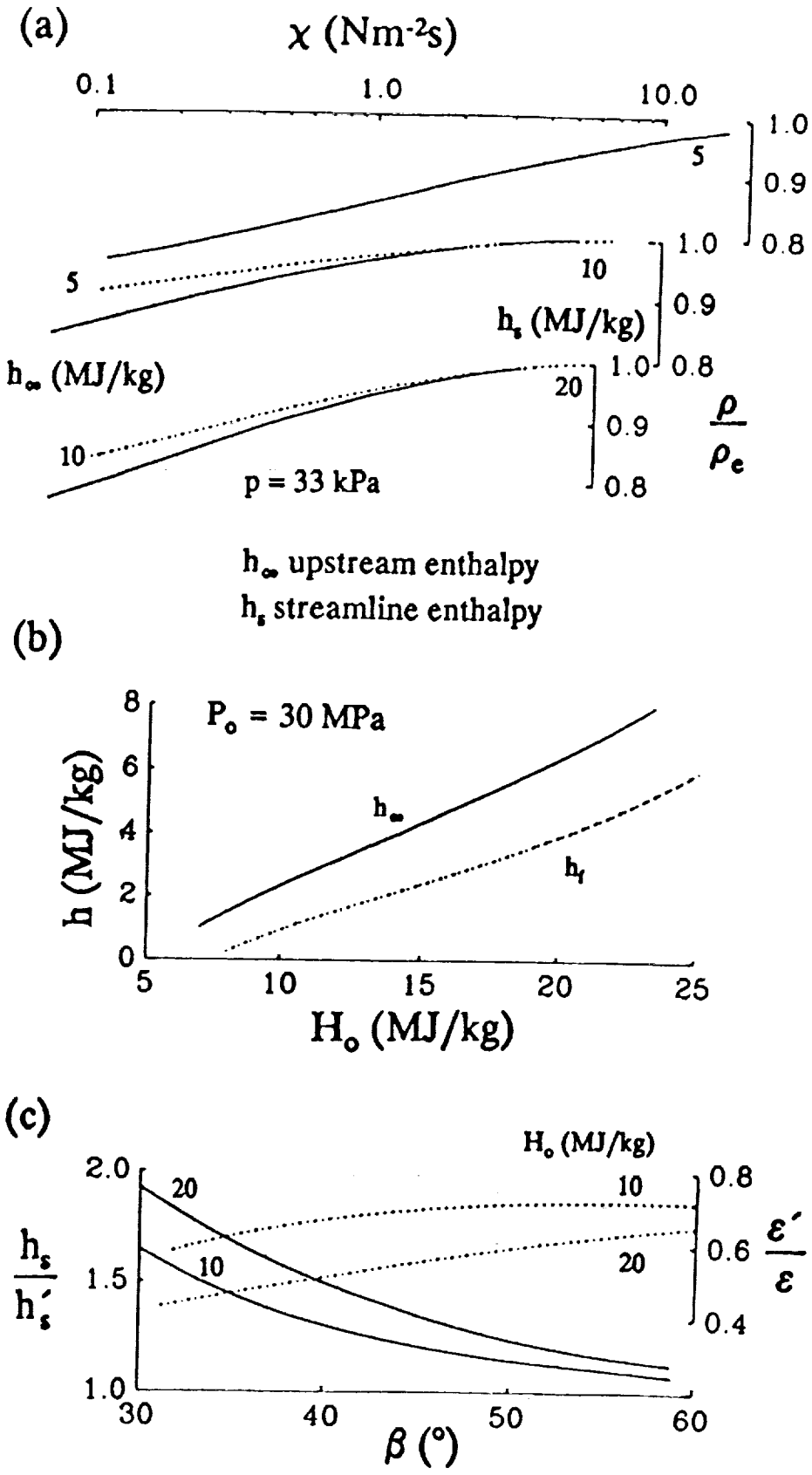


Figure 3. a) Constant pressure reaction after shock in air. b) Freestream enthalpy, $P_o$ = 30 MPa, A/A* = 100, throat dia = 25mm. c) Shock layer enthalpy and density ratio.

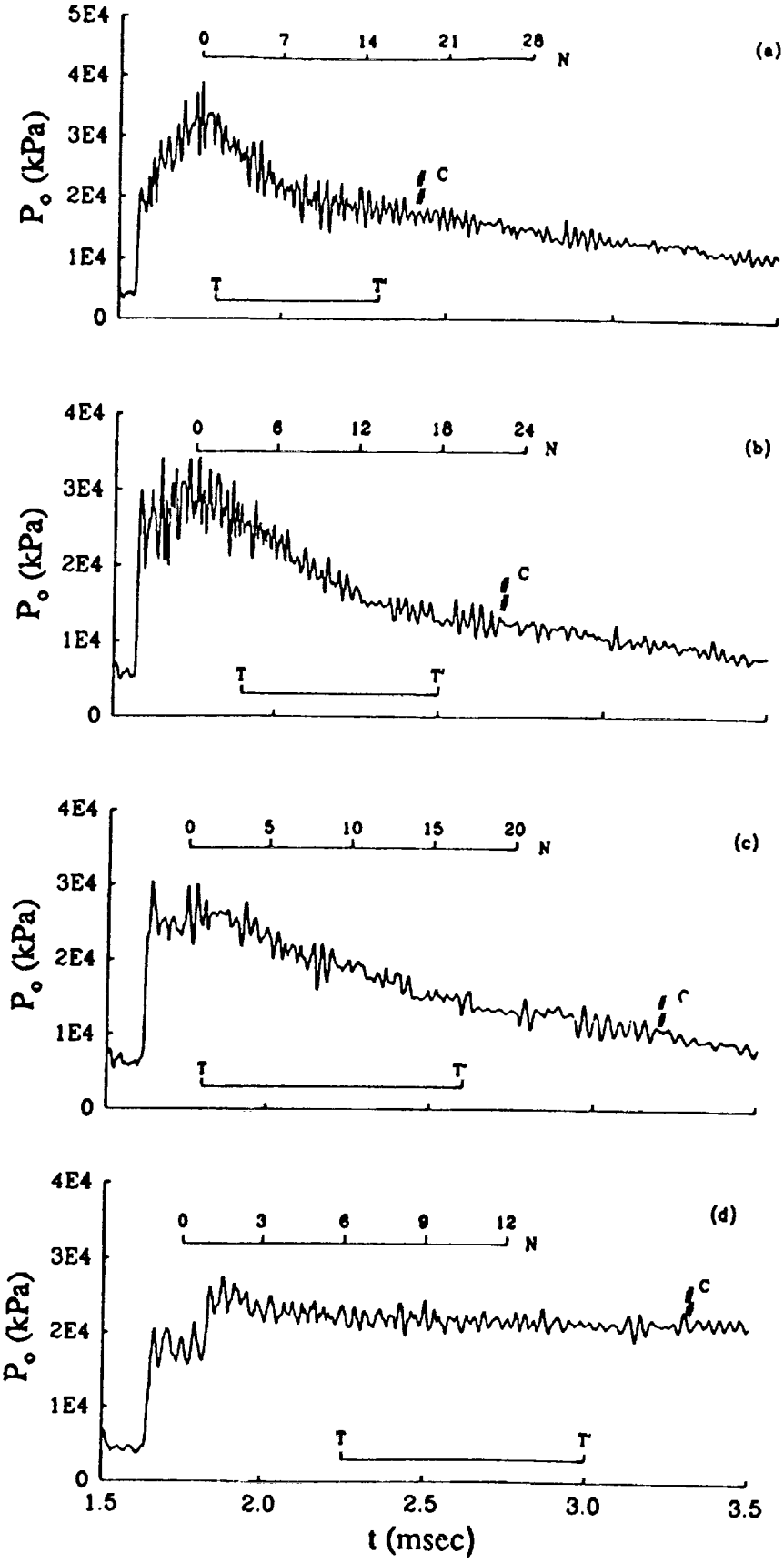


Figure 4. Stagnation Pressure Plots. N - Number of model passes flow makes. T-T' - Test Time. C - Contamination by driver gas.

a) Condition 1. b) Condition 6. c) Condition 8. d) Condition 14.

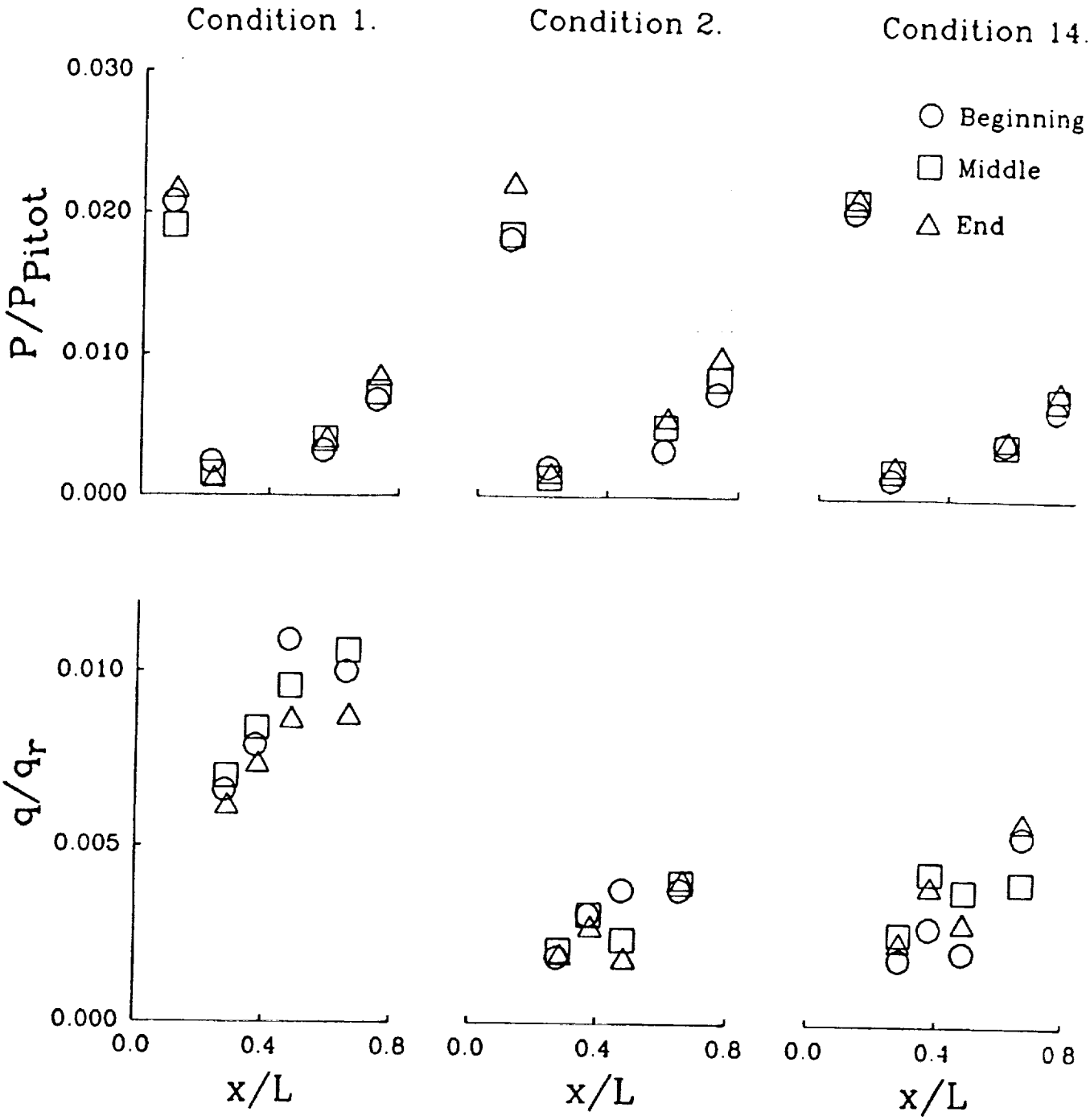


Figure 5. Leeward Steady Flow Check. $\alpha = 50°$. Pressure and heat transfer at the beginning, middle and end of the test time.

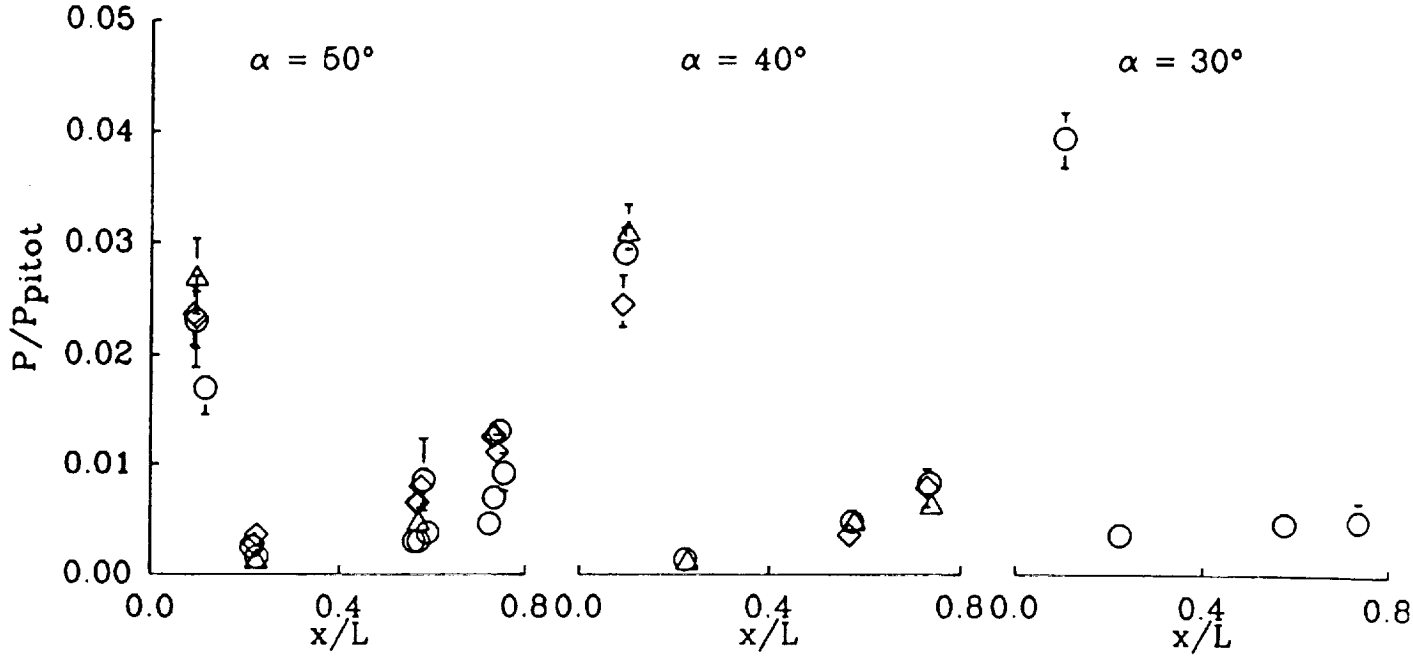


(a) Effect of Incidence

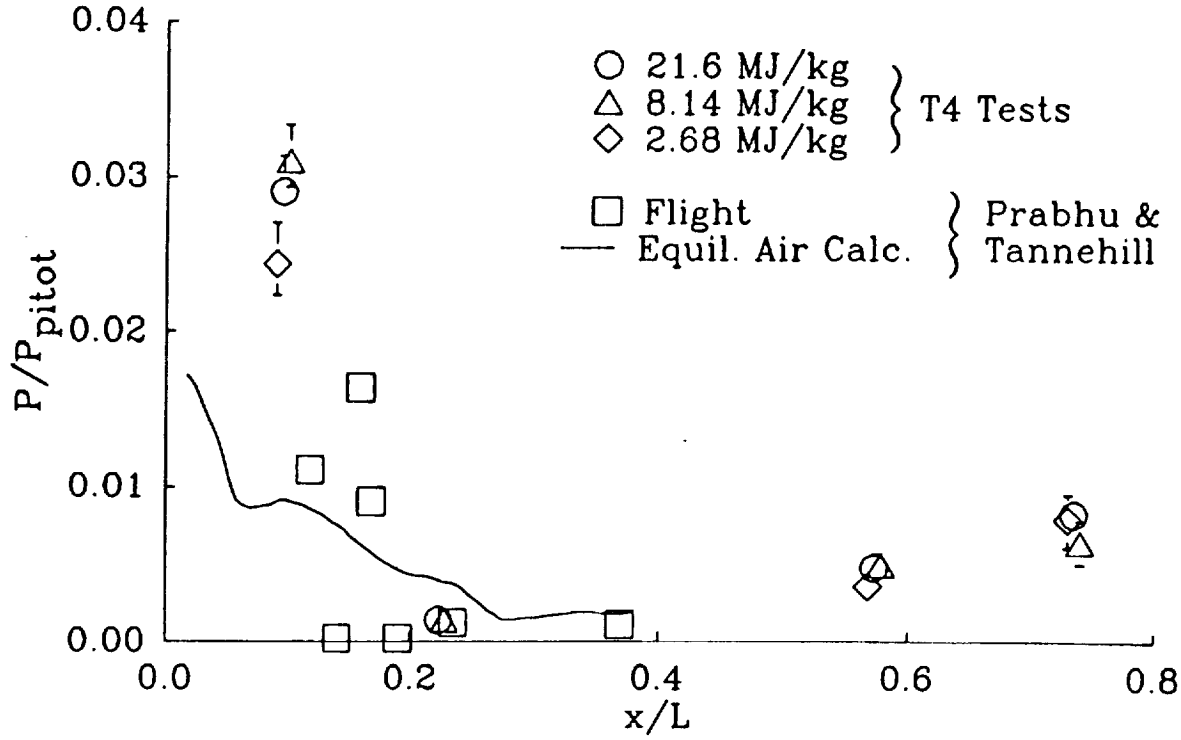


(b) Comparison with Flight

**Figure 6. Leeward Pressure Plots. a) Effect of Incidence. b) Comparison with Flight.**

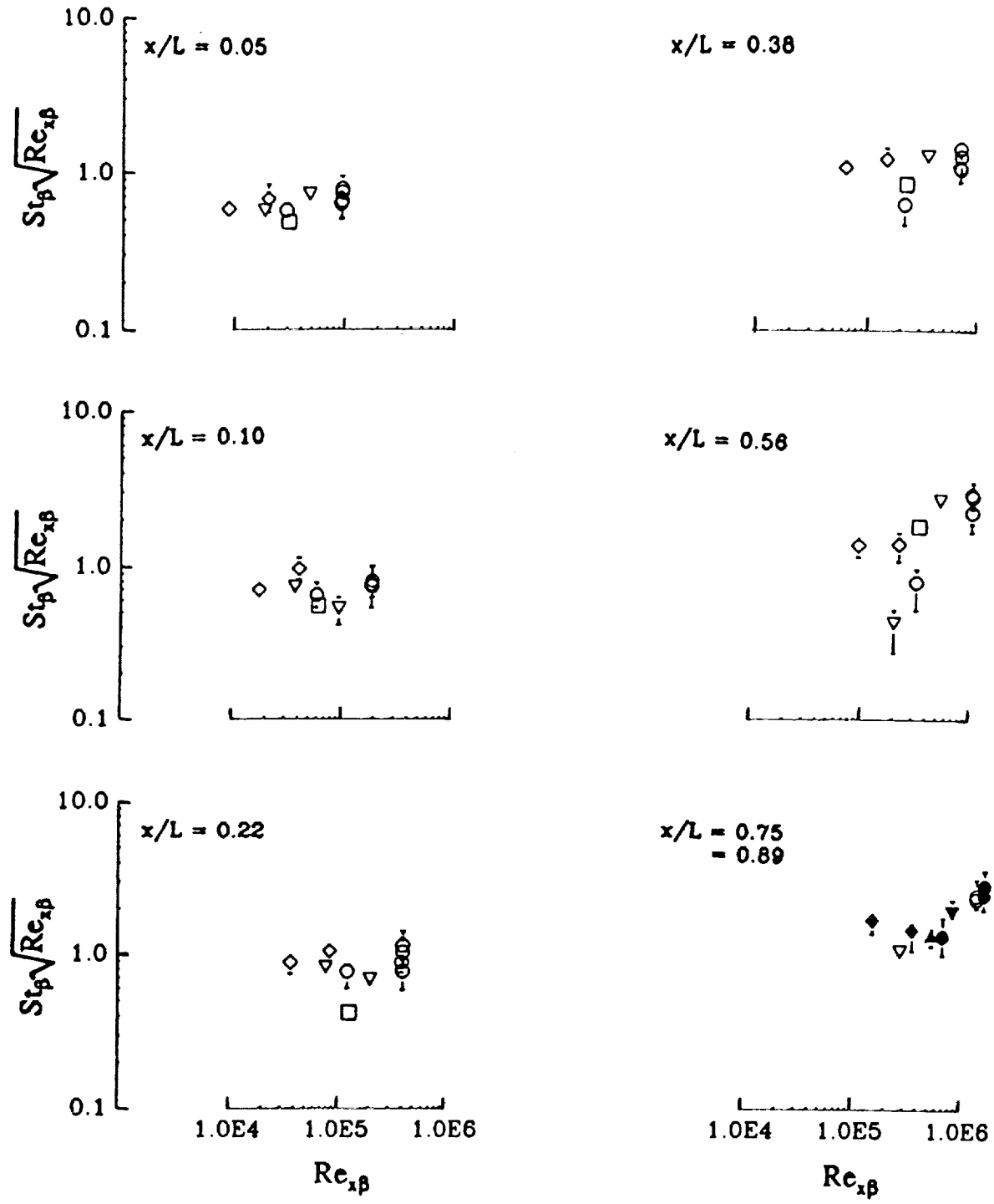


◇ 20 – 24 MJ/kg
□ 12 – 15 MJ/kg
▽ 5 – 8 MJ/kg
○ 2 – 3 MJ/kg
Filled symbols: x/L = 0.89, Steel model

Figure 7(a). Windward Heat Transfer. $St_\beta \sqrt{Re_{x\beta}}$ versus $Re_{x\beta}$, $\alpha = 50°$.

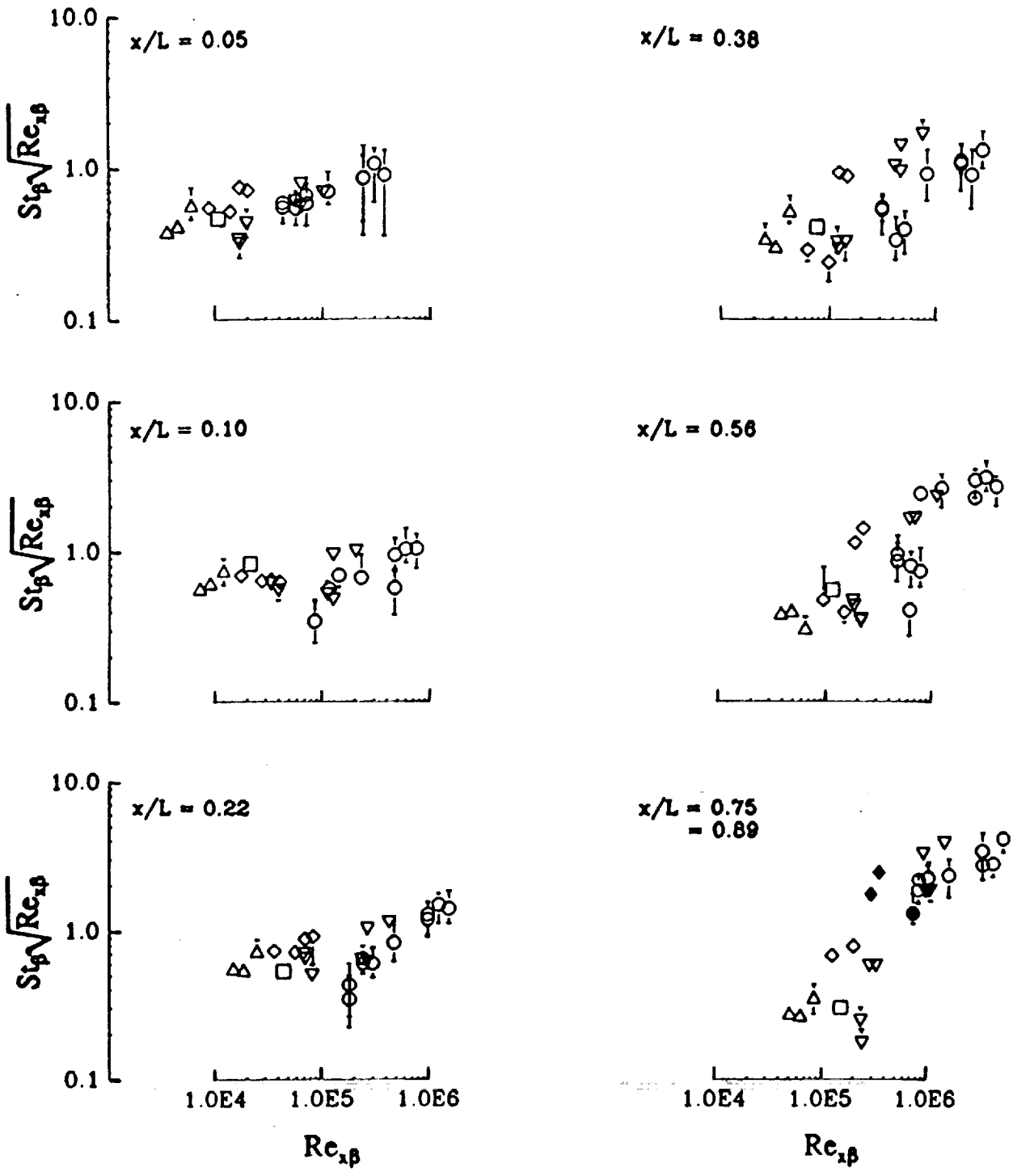


◇ 20 – 24 MJ/kg
△ 19 MJ/kg
□ 12 – 15 MJ/kg
▽ 5 – 8 MJ/kg
○ 2 – 3 MJ/kg
Filled symbols: x/L = 0.89, Steel model

Figure 7(b). Windward Heat Transfer. $St_\beta\sqrt{Re_{x\beta}}$ versus $Re_{x\beta}$, $\alpha = 40°$.

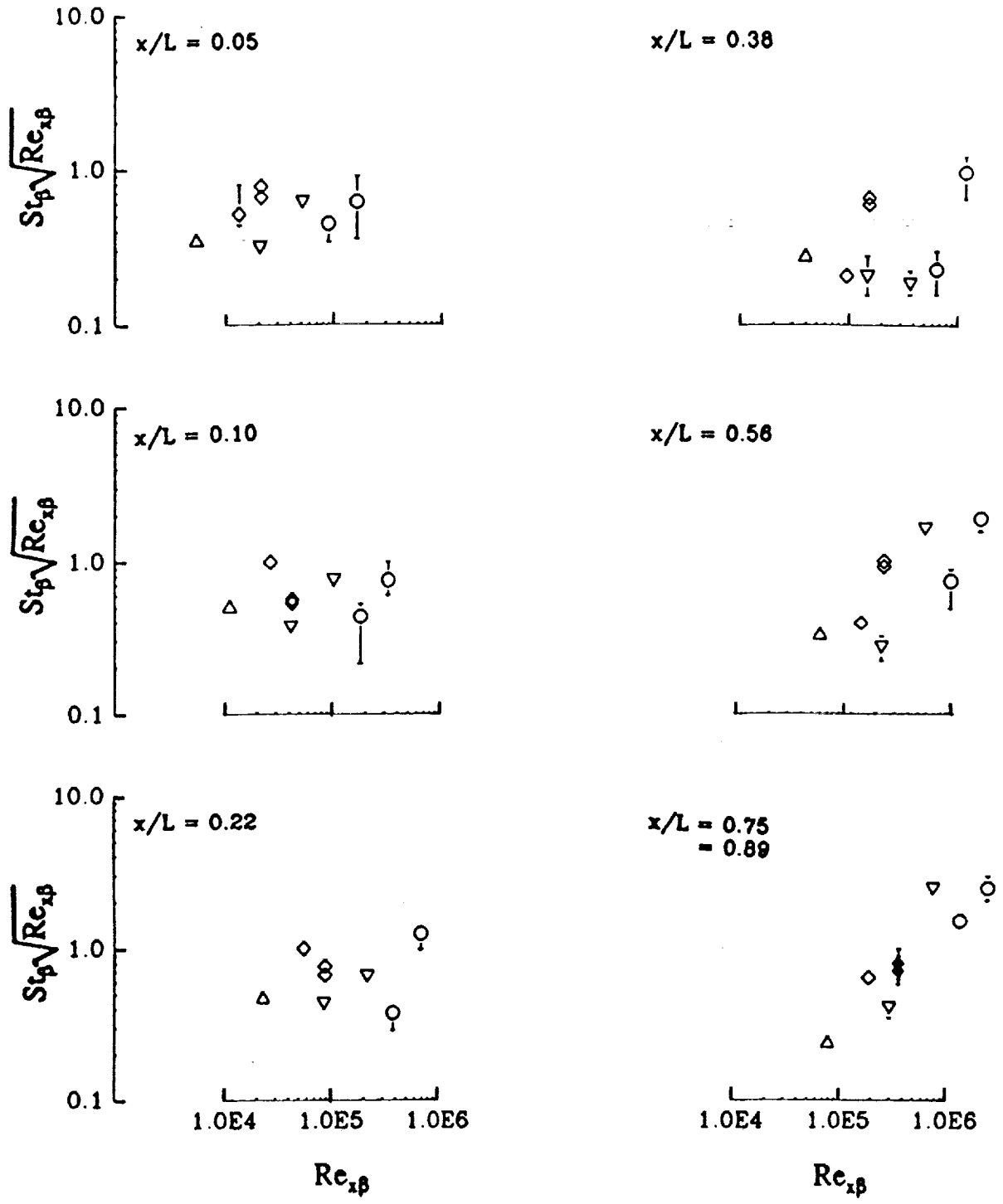


◇ 20 – 24 MJ/kg
△ 19 MJ/kg
▽ 5 – 8 MJ/kg
○ 2 – 3 MJ/kg
Filled symbols: x/L = 0.89, Steel model

Figure 7(c). Windward Heat Transfer. $St_\beta\sqrt{Re_{x\beta}}$ versus $Re_{x\beta}$, $\alpha = 30°$.

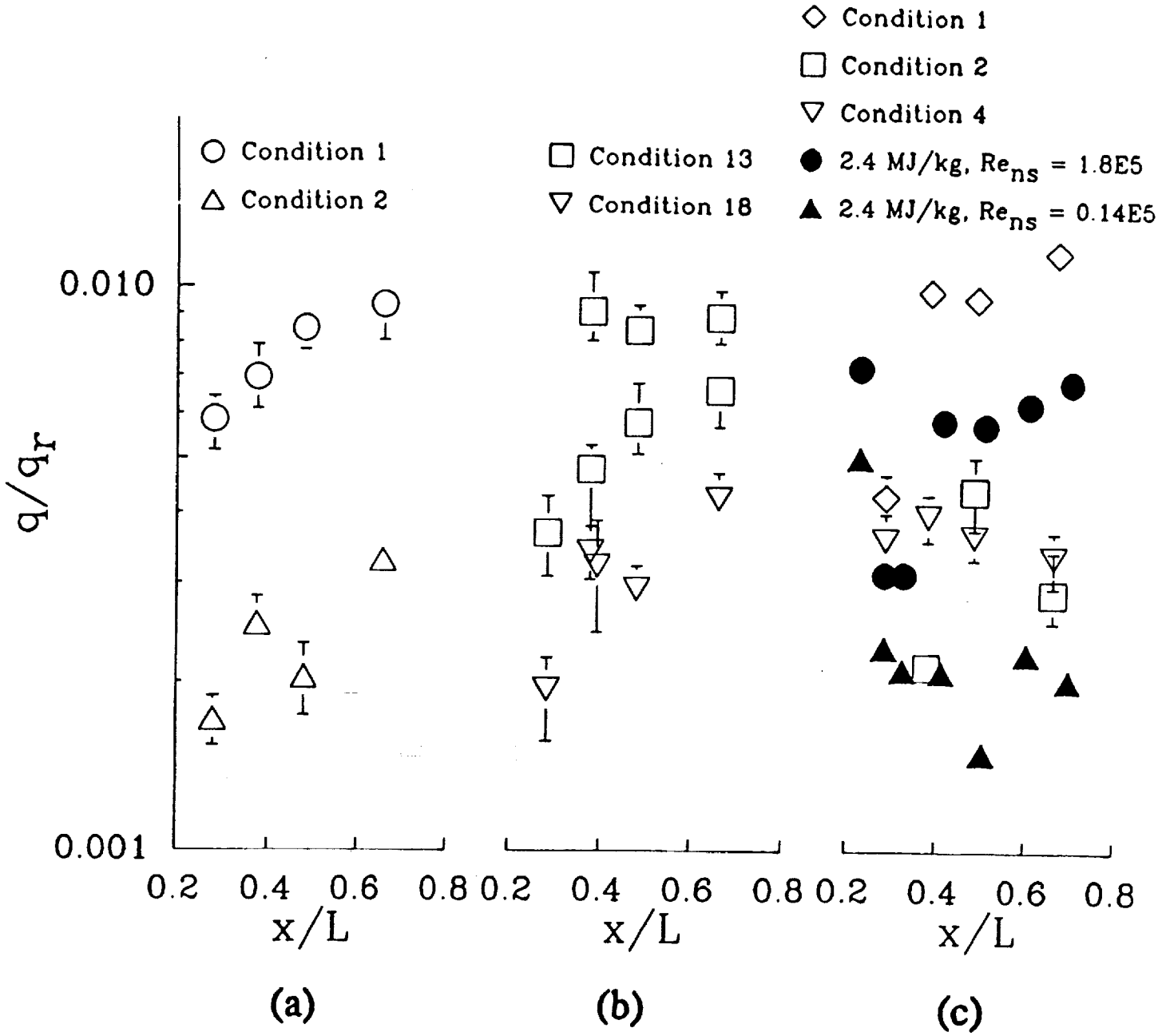


Figure 8. Leeward Heat Transfer - Effect of Transition. a) $\alpha = 50^{\circ}$. b) $\alpha = 40^{\circ}$. c) $\alpha = 30^{\circ}$. Filled symbols - Calspan data.

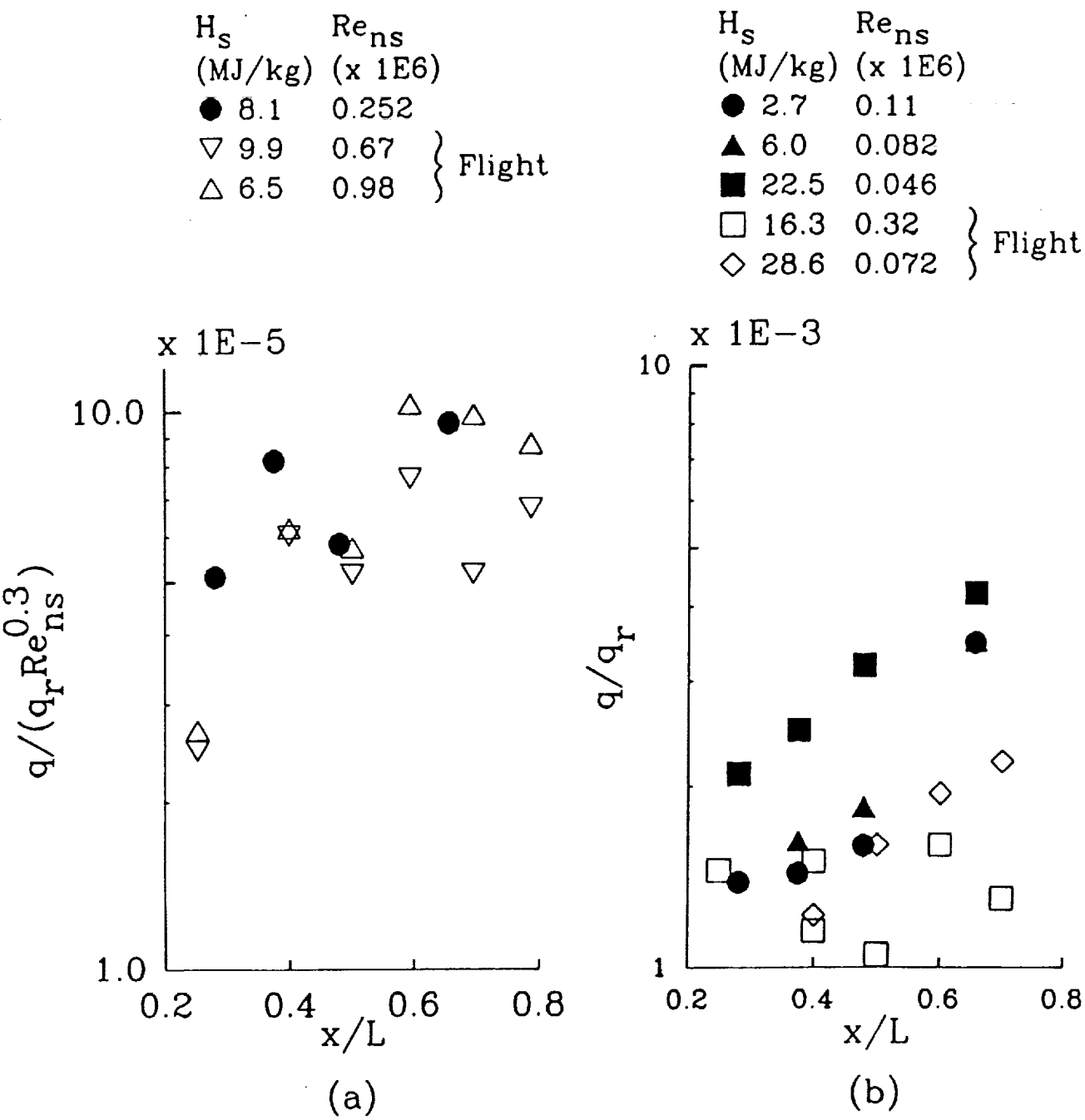


Figure 9. Leeward Heat Transfer - Comparison with Flight ($\alpha$ = 40°).

(a) Turbulent. (b) Laminar.

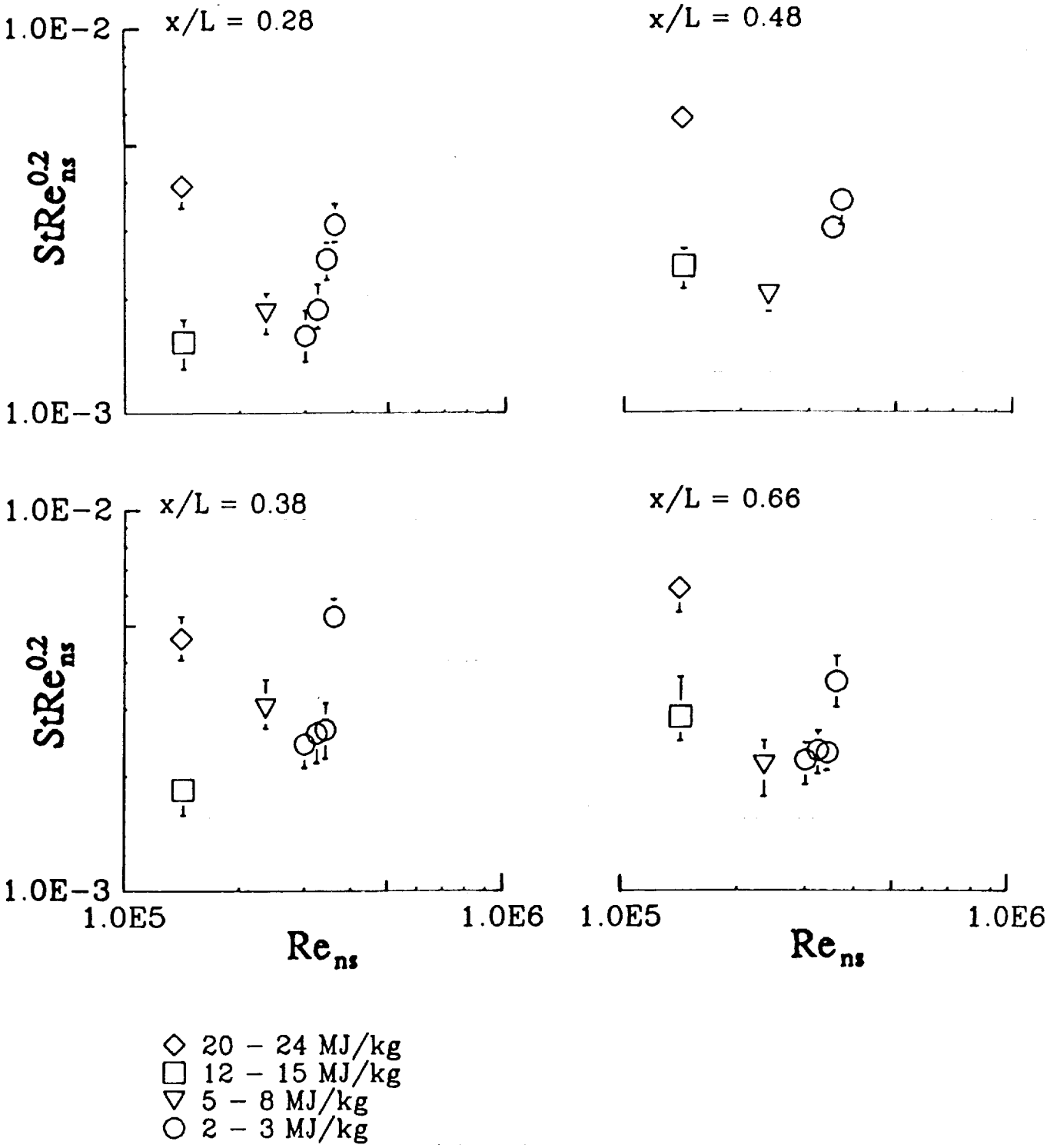


Figure 10(a). Leeward Turbulent Heat Transfer. $StRe_{ns}^{0.2}$ versus $Re_{ns}$, $\alpha = 50°$.

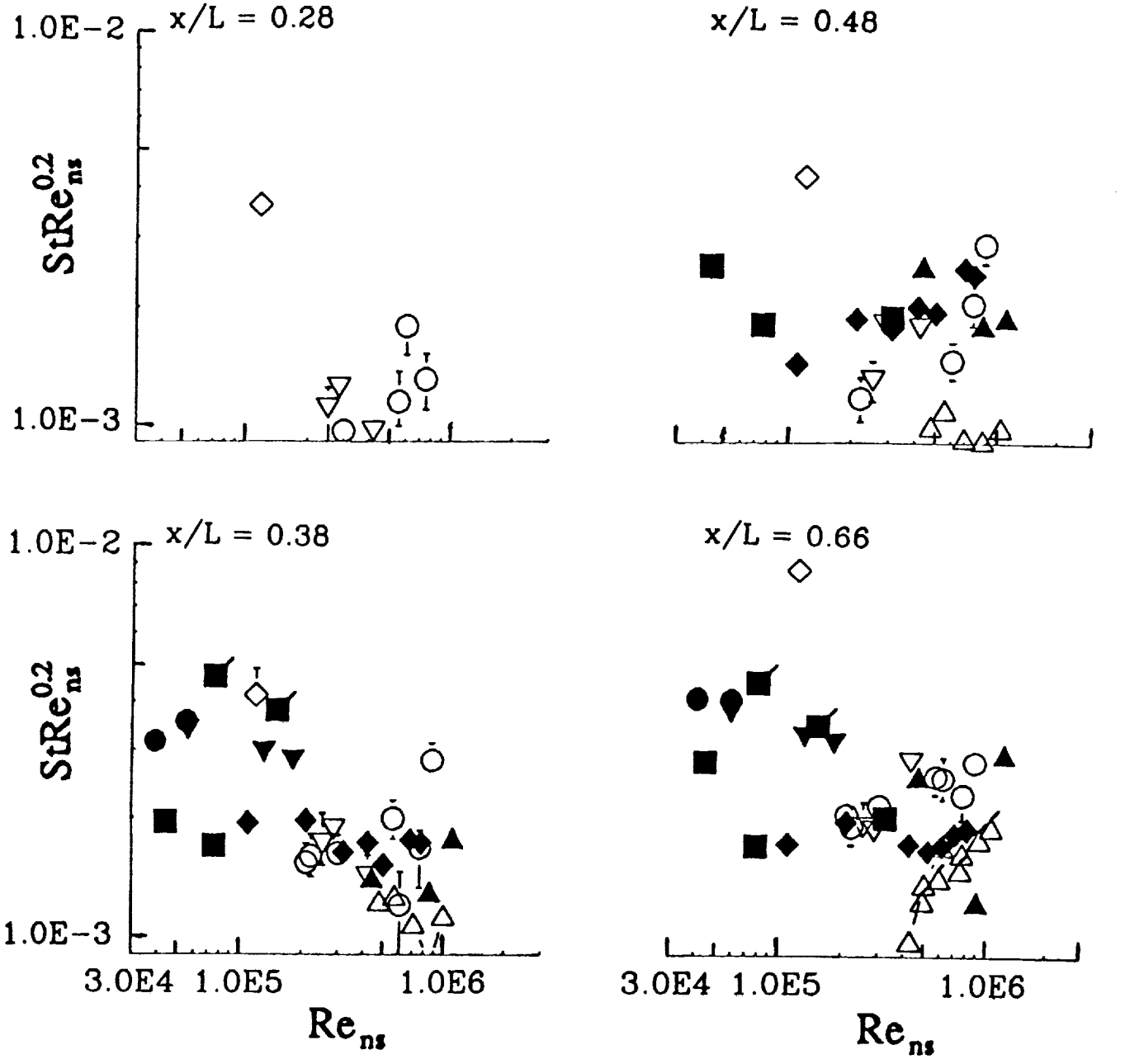


Figure 10(b). Leeward Turbulent Heat Transfer. $StRe_{\infty}^{0.2}$ versus $Re_{\infty}$, $\alpha = 40°$.

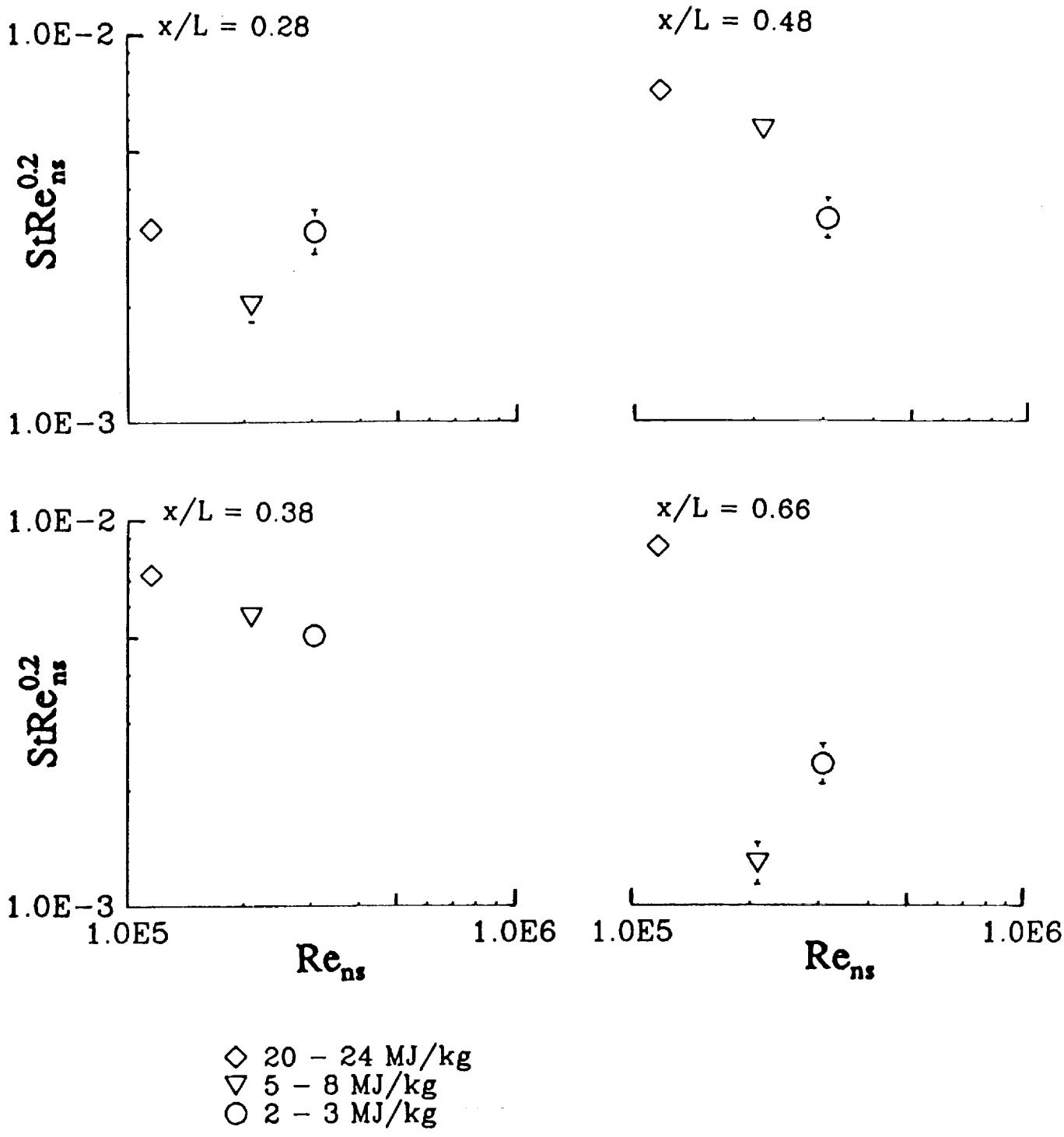


Figure 10(c). Leeward Turbulent Heat Transfer. $StRe_{ns}^{0.2}$ versus $Re_{ns}$, $\alpha = 30°$.

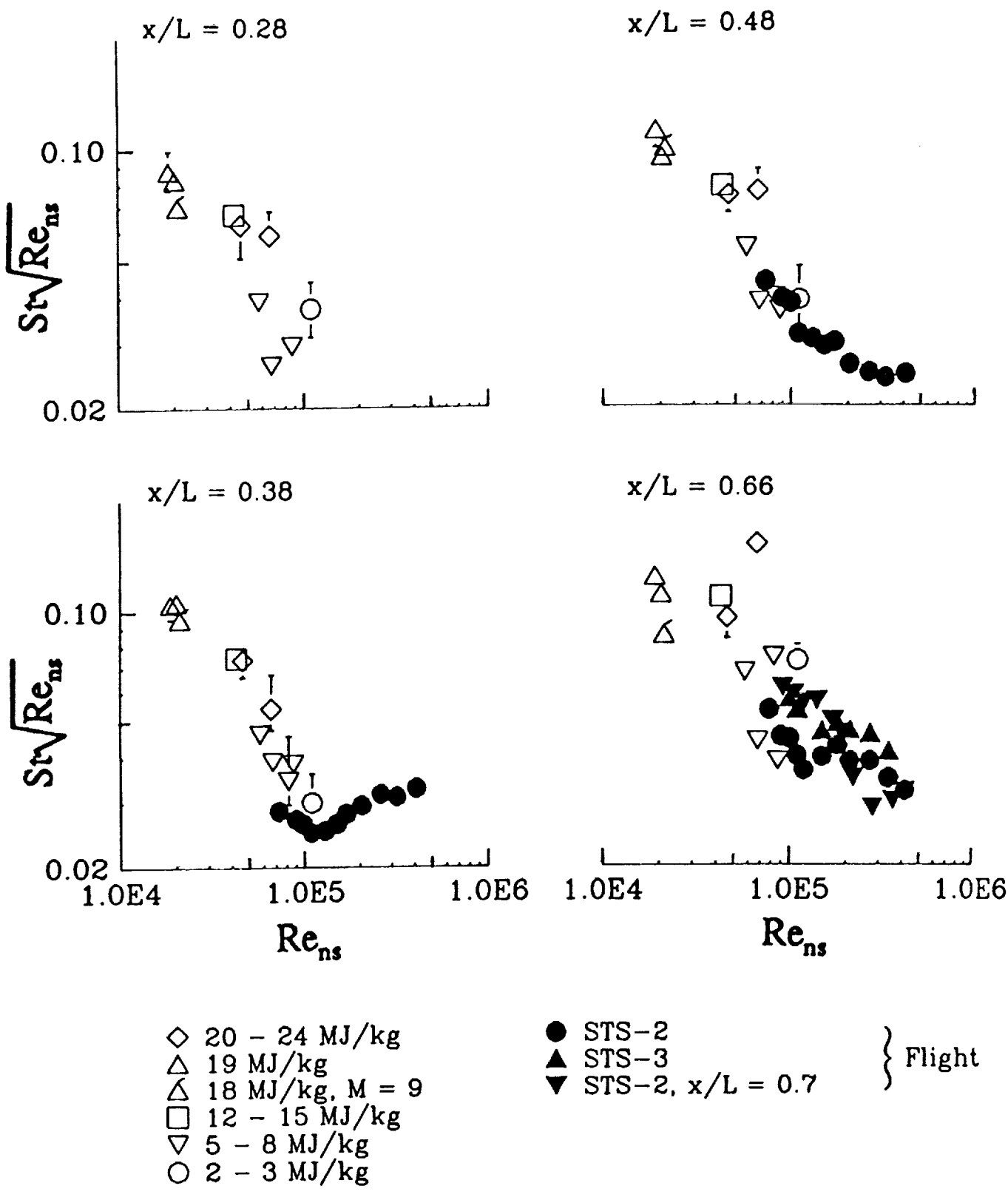


Figure 11. Leeward Laminar Heat Transfer. $St\sqrt{Re_{ns}}$ versus $Re_{ns}$, $\alpha = 40^{\circ}$.

# REPORT DOCUMENTATION PAGE

*Form Approved*
*OMB No. 0704-0188*



| 1. AGENCY USE ONLY *(Leave blank)* | 2. REPORT DATE | 3. REPORT TYPE AND DATES COVERED |
|---|---|---|
| | December 1993 | Contractor Report, CY 1991 |

**4. TITLE AND SUBTITLE**
Shock Tunnel Studies of Scramjet Phenomena, Supplement 7

**5. FUNDING NUMBERS**
505-70-62-02
NAGW-674

**6. AUTHOR(S)**
R. J. Bakos, R. G. Morgan, S. L. Tuttle, G. M. Kelly, A. Paull, J. M. Simmons, R. J. Stalker, M. V. Pulsonetti, D. Buttsworth, G. A. Allen, Jr., N. Ward, K. Skinner, A. J. Neely, R. M. Krek

**7. PERFORMING ORGANIZATION NAME(S) AND ADDRESS(ES)**
University of Queensland
Department of Mechanical Engineering
St. Lucia, Queensland
AUSTRALIA

**8. PERFORMING ORGANIZATION REPORT NUMBER**

**9. SPONSORING / MONITORING AGENCY NAME(S) AND ADDRESS(ES)**
National Aeronautics and Space Administration
Langley Research Center
Hampton, VA 23681-0001

**10. SPONSORING / MONITORING AGENCY REPORT NUMBER**
NASA CR-191572

**11. SUPPLEMENTARY NOTES**
Langley Technical Monitor: R. Clayton Rogers
Interim Report 0 Supplement 7, NAGW-674

**12a. DISTRIBUTION / AVAILABILITY STATEMENT**
Unclassified - Unlimited

Subject Category 34

**12b. DISTRIBUTION CODE**

**13. ABSTRACT** *(Maximum 200 words)*

Reports by the staff of the University of Queensland on various research studies related to the advancement of scramjet technology are presented. These reports document the tests conducted in the reflected shock tunnel T4 and supporting research facilities that have been used to study the injection, mixing, and combustion of hydrogen fuel in generic scramjets at flow conditions typical of hypersonic flight. In addition, topics include the development of instrumentation and measurement technology, such as combustor wall shear and stream composition in pulse facilities, and numerical studies and analyses of the scramjet combustor process and the test facility operation. This research activity is Supplement 7 under NASA Grant NAGW-674.

| 14. SUBJECT TERMS | 15. NUMBER OF PAGES |
|---|---|
| Scramjets, pulse facilities, hypersonic, hypervelocity, shock waves, combustion, shock tubes | 147 |
| | 16. PRICE CODE: A07 |

| 17. SECURITY CLASSIFICATION OF REPORT | 18. SECURITY CLASSIFICATION OF THIS PAGE | 19. SECURITY CLASSIFICATION OF ABSTRACT | 20. LIMITATION OF ABSTRACT |
|---|---|---|---|
| Unclassified | Unclassified | Unclassified | |